2023

Novel mechanistic insight into ciliary regulation: old pathways yield new mechanisms

Larissa L. Dougherty
Dartmouth College, larissa.l.dougherty.gr@dartmouth.edu

“Novel mechanistic insight into ciliary regulation: old pathways yield new mechanisms”

A Thesis
Submitted to the Faculty
in partial fulfillment of the requirements for the
degree of

Doctor of Philosophy

in
Biochemistry and Cell Biology

by Larissa L. Dougherty

Guarini School of Graduate and Advanced Studies
Dartmouth College
Hanover, New Hampshire

June 2023

Examining Committee:

(chair) ***Prachee Avasthi, PhD***

Arminja Kettenbach, PhD

Wei-Lih Lee, PhD

Pamela Tran, PhD

F. Jon Kull, Ph.D.
Dean of the Guarini School of Graduate and Advanced Studies

ABSTRACT

Cilia are structures present on most eukaryotic cells which provide important signaling and motile components to cells from early development to fully differentiated and matured cells. Regulation of these structures is critical to proper functioning of the cell and is known to be tied to the cell cycle. Preparation for ciliary assembly following cell cycle exit and ciliary disassembly following cell cycle reentry requires components throughout the cell body and within the cilium to facilitate this process. Here I identify how the cell adapts to ensure modifications to cilia occur for assembly or disassembly using the model organism *Chlamydomonas reinhardtii.* By chemically and genetically inhibiting map kinase phosphatases in *Chlamydomonas* which most closely match mammalian DUSP6, the phosphatase for ERK1/2 in the canonical cell cycle control ERK pathway, cilia shorten and fail to assemble. We find that DUSP6 inhibition also results in inhibited ciliary protein entry, altered protein localization to the transition zone, inhibited membrane trafficking or through inhibited cytoskeletal microtubule reorganization. Additionally, we find that maintaining cytoplasmic microtubules and short tracks of cilia can allow for cilia to immediately assemble within 5 minutes post deciliation. Together, this data provides a comprehensive view of how the cell induces changes outside of the cilium to regulate this critical signaling organelle.

ACKNOWLEDGMENTS

To Prachee: You have been an incredible role model and mentor. Thank you for teaching me SO many things, especially about persistence in going after what you want whether that's a career change or changing the way people do science. You have so much passion and enthusiasm which has only grown over my time in the lab. Thank you for helping me find that excitement in the science even when it got frustrating. Thank you for opening up so many doors and providing so many opportunities for me to grow. Most of all, thank you for always believing in me and motivating me to be a better scientist. I will forever be grateful for your mentorship and guidance.

To the faculty and staff at Dartmouth: I want to thank everyone for their kindness and support since moving to Dartmouth. Even during the pandemic, everyone was as friendly and as helpful as they could be. All of the smiles, check-ins, and friendly banter kept me spirited and excited for work every day. I especially want to thank Dr. Charlie Barlowe both for welcoming our lab to the department and then ultimately including me in his group during this final year. I am so grateful for gaining the opportunity to spend time with your lab, become acquainted with cool science outside of my expertise, and share ideas. I also want to thank everyone in the BCB office: Jenni Hinsley, Sam Schmidt, Ashley Cleary, and Emily Clough for always reaching out, having friendly faces, being incredibly on top of their jobs, and also helping me during my times of need. This department and program is truly fantastic beyond the science because of the people.

To my committee: Dr. Arminja Kettenbach, Dr. Wei-Lih Lee, and my outside examiner Dr. Pam Tran, thank you for taking interest in my project and supporting the science in the various directions it went. You have been extremely valuable and have asked some of the neatest questions which helped me to critically think about the science that I was doing. A special thank you to Dr. Pam Tran for agreeing to revisit my thesis work in its final years to provide helpful feedback and your interesting ideas!

To the students at Dartmouth: Thank you so much for your friendship and support throughout my time at Dartmouth, and especially during my final year. Each of you contribute to an incredible community in the MCB program and I am forever grateful for the memories made. Thank you Ao for always saying hi in the hallways; your energy is

contagious and always brings a smile to my face. Thank you Abubakar for always being a friendly face and ready to help us find resources and people along with keeping us in the loop on cool events. Thank you Adam, Jerry, Sarvesh and Zack for introducing me to other graduate students, providing critical feedback on science, and being incredible friends. You have made this last year so much fun and so memorable and have also made it hard for me to leave. I appreciate each of you.

To the faculty and staff at KUMC: Thank you for your initial investment in me as a student in my earlier years. You provided a foundation for me to grow upon and become the scientist that I am today. Thank you to my KUMC committee, Dr. Pamela Tran, Dr. Andras Czirok, Dr. Jim Calvet, and Dr. Sarah Zanders who were the early thinkers with me in my project and helped me move forward with the intial phases.

To the past members of the Avasthi Lab: Thank you for your brains, friendship and the memories. I had so much fun when I first joined the lab. We were a big group in a small area with all of the personalities. I'm grateful for getting to move up to Dartmouth from KUMC with Nick Rosenthal and Brae Bigge, and for getting to spend some time learning from Beth Bauerly and Cameron MacQuarrie. Most of all, I am thankful for my close friendship with Brae. She taught me the ropes when I rotated and first joined the lab, came with me to my first big conference, and then became one of my closest friends from there on out.

To my family: You have been my endless support from the very beginning. Thank you for always being there, being understanding about moving across the country, and never forgetting to ask when I'll finally be home. Moving away from home was one of the hardest things I've emotionally had to do but knowing that I'm coming back to a supportive family eager for my success and return has been very motivating. I am especially grateful for my fiancé, Jason Spengel, who has been the most involved in communication about the nitty gritty details of graduate school. You have been the most supportive of all. Thank you for always listening, having endless patience, never giving up on me, and staying steady through the long distance.

TABLE OF CONTENTS

LIST OF TABLES

LIST OF FIGURES

LIST OF ABBREVIATIONS

AURKA……..Aurora Kinase A

BFA……..…….…….Brefeldin A

BCI…….…….....…(E)-2-benzylidine-3-(cyclohexylamino)-2,3-dihydro-1H-inden-1-one

CHX……..…….……Cycloheximide

CMTs……...…..……..Cytoplasmic Microtubules

DIC……..…….Differential Interference Contrast

DUSP…….…..…..Dual Specificity Phosphatase

DMSO…….……...…....Dimethyl Sulfoxide

ERK1/2…….……..…..……..…Extracellular signal-Regulated Kinase

FGF……..……..…Fibroblast Growth Factor

HDAC6……..Histone Deacetylase 6

IBMX……...……3-isobutyl-1-methylxanthine

IFT……..…..…….Intraflagellar Transport

KAP…….……..…..…Kinesin Accessory Protein

LiCl……...…….…….....Lithium Chloride

MAPK…….Mitogen-Activated Protein Kinase

MAK……..…….Male germ cell-Associated Kinase

MEK1/2……..…..……Mitogen-Activated Protein Kinase Kinase 1/2

MG132…….…..…..……..…carbobenzoxy-Leu-Leu-leucinal

MKP……..…...…..……...……...……..Map Kinase Phosphatase

MKS…….……..…..……Meckel Grubert Syndrome

MOK …….…..…….MAPK/MAK/MRK Overlapping Kinase

MS……...…….….Mechanical Shear or Mass Spectrometry

NaPPi…….…...……...……..Sodium Pyrophosphate

NEK…….…….……NIMA-Related Kinase

NIMA….…….…….……..……Never in Mitosis gene A

NPHP…….…….……..Nephronophthisis

pMAPK…….…..……..phosphorylated MAPK

PTX……..……..…..……...Paclitaxel

RPE1…….…..……...…….…Retinal Pigment Epithelial cells

TAP…….……..Tris Acetate Phosphate

TZ……..…….…..……Transition Zone

WT……...……...…wild-type

CHAPTER 1:

INTRODUCTION

Cilia Function

Since their discovery as "little feet" by Antonie van Leeuwenhoek ~1674 (Lane, 2015), cilia have become established as very important organelles for facilitating cell signaling ("primary cilia") and sometimes for also facilitating motility ("motile cilia") to either the cell or components that come in contact with the cell. These antenna-like structures protrude from the plasma membrane to provide the cell with a platform that can send and receive intracellular and extracellular cues that have been found to aid in cell development (Goetz & Anderson, 2010; Park et al., 2019), cell proliferation through transducing environmental cues (Yeh et al., 2013), and migration and cell polarity (Veland et al., 2014).

Cilia can be found on most cells in the human body. For example, some places primary cilia are present in the human body include on photoreceptor cells in the eye to aid in phototransduction (Khanna, 2015), on neurons to regulate neuronal connectivity (Tereshko et al., 2021), in the kidney to detect movement of fluids (Yoder, 2007), and in the nose to detect smell (Kulaga et al., 2004). Motile cilia can be found on cells including on sperm (Inaba & Mizuno, 2016), in the respiratory tract to aid in movement of mucus (Shah et al., 2009), on the oviducts to transfer oocytes to the fallopian tube (Yuan et al., 2021), and on ependymal cells in the brain to move fluids (Ji et al., 2022). Because cilia are found on most cells, defects in cilia can cause diseases throughout the whole body termed "ciliopathies" including polydactyly, retinal dystrophy, polycystic kidney disease, and various cancers among many other diseases (Korobeynikov et al., 2017; Reiter & Leroux, 2017) (**Fig. 1.1**). In addition to cilia being present on most cells, there are an increasing number of proteins being identified that have some role in regulating cilia across cell types which increases the complexity of these diseases.

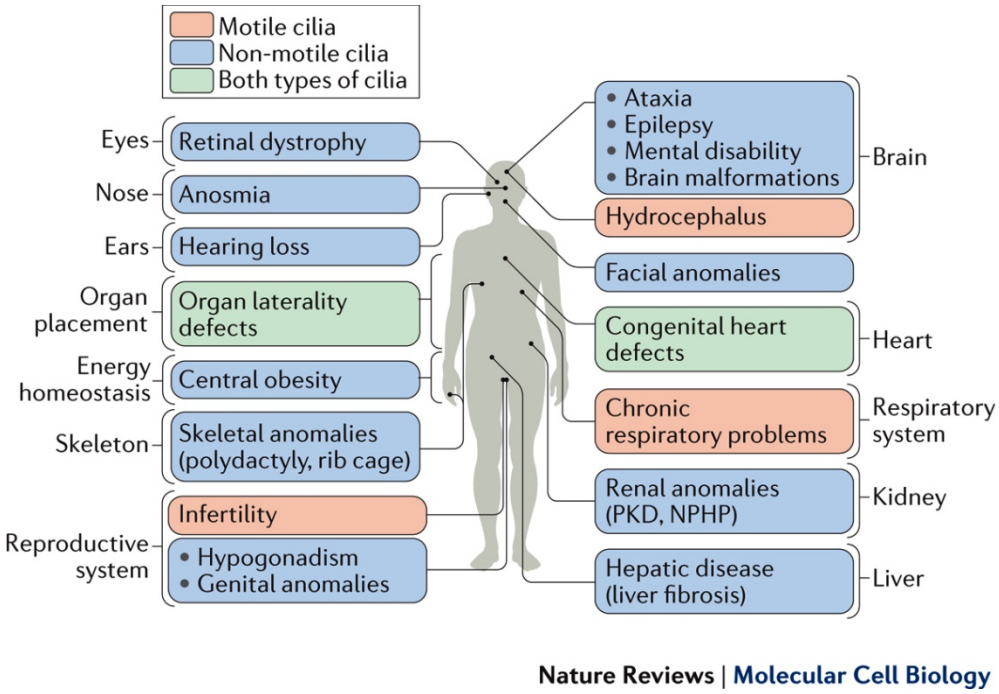

Figure 1.1. Ciliopathies in the human body. Ciliopathies affecting different organ systems are listed. Orange indicates defects in motile cilia, blue indicates defects in primary cilia, and green indicates defects in both. From (Reiter & Leroux, 2017).

Cilia Structure and Formation

Cilia are typically formed following exit from the cell cycle and entry into cellular quiescence at G0/G1. During this time, centrioles will take on a new role as basal bodies where they will either dock to vesicles which fuse with the membrane at the site of ciliogenesis, or they will directly dock to the site of ciliogenesis at the membrane both with the aid of distal appendage proteins (Kobayashi & Dynlacht, 2011). Upon reaching the site of ciliogenesis, the mother centriole in cells with primary cilia or multiple centrioles become the basal body which will nucleate cilia with microtubules that will make up the core of the cilium: the axoneme (Avasthi & Marshall, 2012; Avidor-Reiss & Leroux, 2015) (**Fig. 1.2**). This process can only occur with the aid of distal appendage proteins and removal of the capping protein CP110 (Kuhns et al., 2013). The microtubule axoneme extends to a defined steady state length and typically consists of 9 acetylated microtubule doublets arranged in a circle extending from the cilium base to the tip. In the case of most motile cilia specifically, microtubule axonemes contain a central pair of singlet microtubules in addition to axonemal dynein arms and radial spoke proteins that allow for their motility (Nechipurenko, 2020) (**Fig. 1.3**).

On the growing end of basal bodies forms the transition zone early in ciliogenesis which acts as a ciliary gate for protein entry (Reiter et al., 2012). Transition zones contain 3 major complexes of proteins including the NPHP module implicated in Nephronophthisis, the MKS complex implicated in Meckel-Gruber Syndrome, and the CEP290 module (Gonçalves & Pelletier, 2017) which aid in selectivity of protein entry. The transition zone and basal bodies are also held in place by transition fibers, a ciliary necklace, and y-linkers (Garcia-Gonzalo & Reiter, 2017).

For efficient ciliary elongation and maintenance, transport proteins pass through the transition zone with cargo in a directional manner through a process called Intraflagellar Transport (IFT) (Rosenbaum & Witman, 2002). At the transition zone, groups of proteins participating in ciliary transport begin to assemble. The IFT-B complex first begins assembling “trains” or links of IFT-B complex proteins. From this backbone formation, the other IFT complex, IFT-A, will load in addition to the motor

proteins cytoplasmic dynein-2 and kinesin-2 which will ultimately be responsible for moving the IFT complexes and ciliary cargo along the B tubules of the axoneme (Lacey et al., 2023; Van Den Hoek et al., 2022) (**Fig. 1.4**). At the ciliary tip, cytoplasmic dynein-2 will provide retrograde transport of cargo to the base of the cilium along A tubules (Lechtreck et al., 2017). All of these components work together to regulate ciliary growth, maintenance, and function.

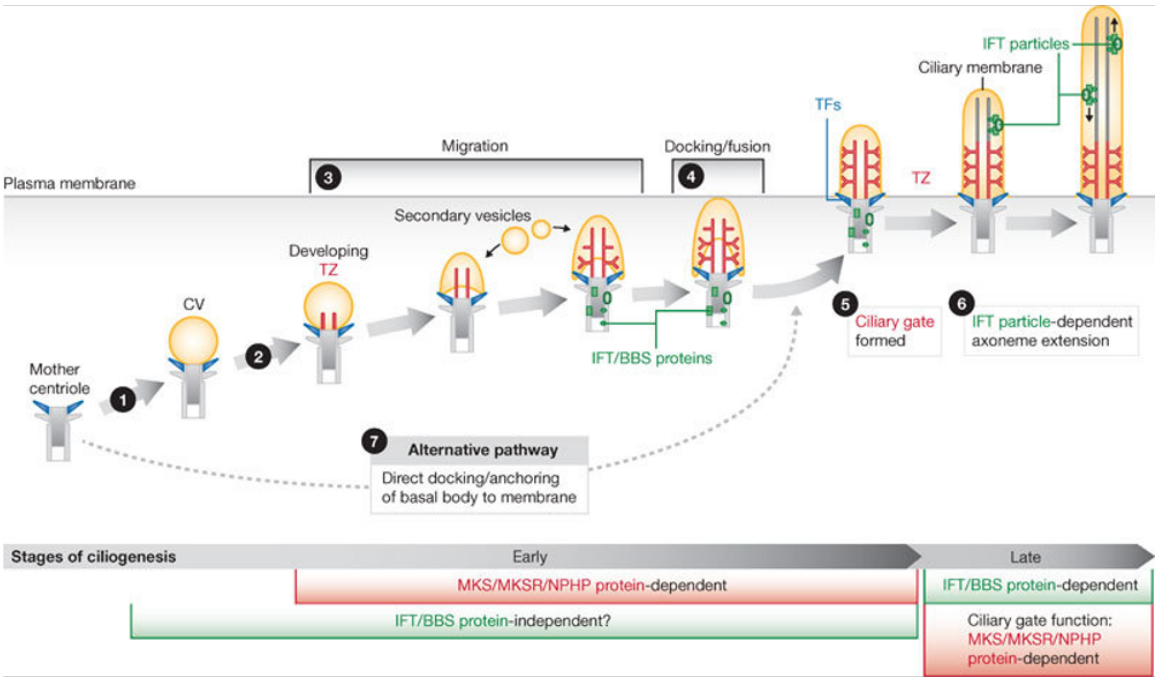

Figure 1.2. Stages of ciliogenesis in primary cilia. Following mitosis, the mother centriole will dock to a ciliary vesicle (CV), begin developing a transition zone, dock to the plasma membrane and continue elongating an axoneme. From (Reiter et al., 2012).

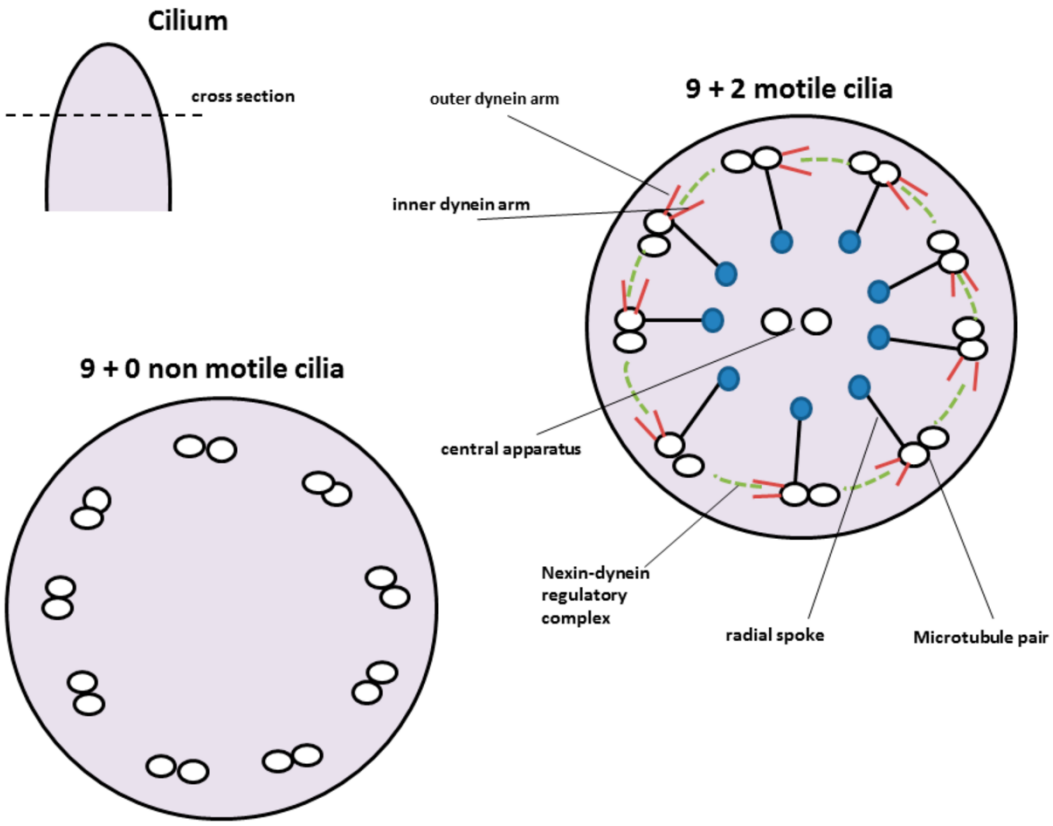

Fig. 1.3. Comparisons of cross sections for axonemes of nonmotile (primary) cilia and motile cilia. Though some cilia exist which do not follow these exact patterns, it is commonly seen that motile cilia contain inner and outer dynein arms, radio spoke proteins, and a central pair of microtubules which all aid in giving range of motion to motile cilia. From (Gänger & Schindowski, 2018).

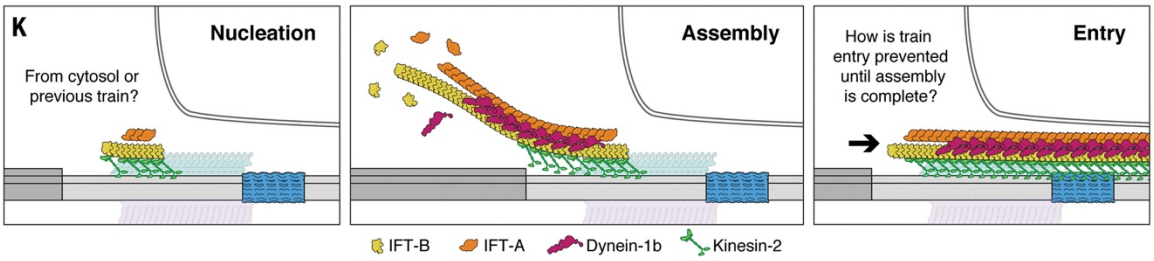

Figure 1.4. Consensus model of IFT components docking to tubulin. During nucleation, IFT components will add to the back of the train starting with IFT-B, then IFT-A, dynein-1b, and kinesin-2 last. Upon completion of the train, all components will enter the cilium. Adapted from (Van Den Hoek et al., 2022).

Cilia Regulation

Cilia disassemble during cell cycle reentry and are completely resorbed by the time the cell must divide (Izawa et al., 2015). This process is known to be regulated through different signaling pathways including the Hippo pathway (M. Kim et al., 2014), Wnt signaling (Wheway et al., 2018), the ubiquitin proteasome system (Kasahara et al., 2014), inositol signaling (Zhang et al., 2022), EGFR and Notch signaling (Zhu et al., 2019), GPCR signaling (Anvarian et al., 2019) and stressors such heat shock (Prodromou et al., 2012) which have been well reviewed (Avasthi & Marshall, 2012; Doornbos & Roepman, 2021; Halder et al., 2020; Korobeynikov et al., 2017; Mirvis et al., 2018; Patel & Tsiokas, 2021; Senatore et al., 2022; L. Wang & Dynlacht, 2018) (**Fig. 1.5**). These pathways ultimately lead to activation of the mitotic protein kinase Aurora Kinase A (AURKA) to induce ciliary resorption prior to cell division (Korobeynikov et al., 2017; Solc et al., 2012). Following autophosphorylation, this kinase will phosphorylate the microtubule deacetylase HDAC6 which removes acetylation from ciliary microtubules to decrease their stability and initiate resorption. In addition, the kinesin-13 family members, Kif2A and Kif24, will depolymerize the axoneme leading to ciliary disassembly (Korobeynikov et al., 2017; Miyamoto et al., 2015). In addition, it has been found that the canonical cell cycle control pathway, p38 MAP Kinase signaling, can also control ciliary length in C. elegans by regulating endocytosis and cross talks with another map kinase signaling pathway Ras/Raf/MEK/ERK through MEK-1 (van der Vaart et al., 2015). MEK-1 has previously been found to regulate ciliary length where inhibition through the MEK inhibitor, U0126, elongated cilia (S. Wang et al., 2013). Ras, which centrally acts downstream of various types of growth factor signaling, is also found to be amplified in various types of cancers and promotes ciliary shortening through ras activation (Liu et al., 2018).

Loss of critical cell cycle regulators specifically can regulate ciliogenesis. For example, the never in mitosis, gene A (NIMA) family kinases are known for their roles in cell cycle progression; however, mutational studies have also identified a role for some of these proteins in regulating cell cycle re-entry including the kif24-activator Nek2 (S. Kim

et al., 2015) and Nek8 (Zalli et al., 2012) in addition to related NIMA family kinase proteins Cnk2p (Bradley & Quarmby, 2005) and fa2p (Mahjoub et al., 2002) identified in *Chlamydomonas*. Opposing regulation has been seen with Nek1 where overexpression of its kinase domain has inhibited ciliogenesis indicating a role for promoting cell cycle exit (White & Quarmby, 2008). Upstream from this protein is activity of the E3 ubiquitin ligase anaphase-promoting complex (APC) and its coactivator Cdc20 which also regulate both cell cycle progression and ciliary disassembly and perform this function by targeting Nek1 for proteolysis (W. Wang et al., 2014). Other cell cycle regulatory proteins have been implicated as well in promoting cell cycle re-entry including the centrosomal protein highly expressed during mitosis, Nde1 (S. Kim et al., 2011), and Fibroblast Growth Factor Receptor 1 Oncogene Partner (FOP) which localizes to centriolar satellites (Jiang et al., 2020). Other cell cycle regulators also exist which regulate and promote cell cycle exit. The cyclin dependent kinase for cyclin E and A2, Cdk2, has also been found to work with cyclin A1 which is required during ciliogenesis (Vladar et al., 2018). In addition, Cdc14B phosphatase which counteracts Cdk1 phosphorylation to inhibit mitosis (Clement et al., 2012), the mitotic spindle checkpoint protein BubR1 (Miyamoto et al., 2011), and phosphorylation of the cytoplasmic dynein light chain Tctex-1 also contribute to directly promoting cell cycle entry and ciliary disassembly (Liu et al., 2018). These proteins and are typically hijacked in cancer where cells which are over-proliferating do not assemble cilia. For example, NEDD9 which acts as a scaffold for AURKA for proper stabilization is overexpressed in breast cancer cells, prostate tumors, and lung cancer (Nikonova et al., 2014). Understanding how these cell cycle regulatory proteins can be manipulated to prevent ciliogenesis and promote cell proliferation can provide new therapeutic targets for ciliopathies in addition to contributing to knowledge of how proteins can directly regulate cilia and the cell cycle.

While ciliary signaling requires very specific receptors for very specific signaling and sensory functions on different cell types, cilia are conserved in their structural characteristics. Changes to structural components within cilia have been found to regulate ciliogenesis. In the transition zone (TZ), defects to or loss of different components can change the physical TZ structure to prevent ciliogenesis such loss of TCTN1 (L. Wang et al., 2022). Loss of the anterograde motor protein, heterotrimeric kinesin-2, prevents

ciliogenesis in *Chlamydomonas* (Kozminski et al., 1995) in addition to loss of the IFT-B complex protein, IFT88, also prevents ciliogenesis (Kobayashi et al., 2021). Changes to the axonemal tubulin post-translational modifications, can also impact ciliogenesis. Inhibited glycylation, which stabilizes longer cilia when bound to axonemal tubulin, inhibits complete ciliary elongation (Gadadhar et al., 2017), and inhibited glutamylation inhibits ciliary shortening through altering protein localization and kinesin speed (O'Hagan et al., 2017). These are just a few of the many changes to the ciliary structure that participate in its regulation.

Additionally, cytoskeletal changes outside of the cilium have also been found to regulate ciliogenesis. Tubulin monomers are required for axonemal elongation as indicated by inability for ciliogenesis following strong binding through colchicine and other microtubule depolymerizing agents (Rosenbaum et al., 1969; Rosenbaum & Carlson, 1969; Sharma et al., 2011); however, I find conflicting evidence in chapter 4 for the need for drastic changes to the microtubule cytoskeleton for ciliary assembly as has previously been reported (Sharma et al., 2011; L. Wang et al., 2013). Actin remodeling keeps YAP/TAZ in the cytosol rather than translocating to the nucleus for gene expression which prevents ciliary shortening and vesicle trafficking. As soon as F-actin can predominantly polymerize, YAP/TAZ signaling can ultimately activate AURKA to induce ciliary disassembly (J. Kim et al., 2015). In primary cilia, cilia ectocytosis, or the excision of the ciliary tip, has been found to be required for ciliary disassembly (G. Wang et al., 2019). In addition, Arp2/3 complex-mediated actin remodeling has been found to also promote ciliogenesis through mediating endocytosis of ciliary proteins and membrane relocalization required for early ciliogenesis to contribute to the plasma membrane covering the growing cilium (Bigge et al., 2023). These membrane sources come from Golgi (Dentler, 2013) as well as from recycling of the plasma membrane (J. Kim et al., 2010). Actin dynamics also allow for proper basal body migration to promote ciliogenesis (Miyatake et al., 2015).

Cilia can also be severed as opposed to resorbed and also severed following resorption. All of these events occur in the case of mouse inner medullary collecting duct (IMCD3) cells where the cell can decide whether cilia are resorbed or severed based on

the signaling pathway upregulated (Mirvis et al., 2019). In addition, severing events have been noted in various other cell lines including in kidney epithelial cells when treated with cisplatin (Kong et al., 2019) and Madin-Darby Canine Kidney (MDCK) cells following changes to cell junctions and membrane domains (Overgaard et al., 2009). In *Chlamydomonas reinhardtii,* this event typically happens following cell stressors including low pH (Lewin et al., 1982), dibucaine (Witman et al., 1978), and altered tonicity (Solter & Gibor, 1978) which cause a buildup of calcium near the ciliary base (L. Quarmby & Hartzell, 1994; L. M. Quarmby, 1996; Wheeler et al., 2007). This ultimately activates the microtubule-severing ATPase, katanin, which severs the cilium between the axoneme and transition zone (Lohret et al., 1998; Mahjoub et al., 2002). Similar modes of ciliary severing have also been noted in tetrahymena (Rosenbaum & Carlson, 1969), IMCD-3 and HBECs (Overgaard et al., 2009) and sea urchin embryos (Auclair & Siegel, 1966). Ciliary severing has also been recently seen in paramecium where RNAi-mediated depletion of TZ components induced shedding which is the first documented structurally induced-severing event independent from cell stressors (Gogendeau et al., 2020).

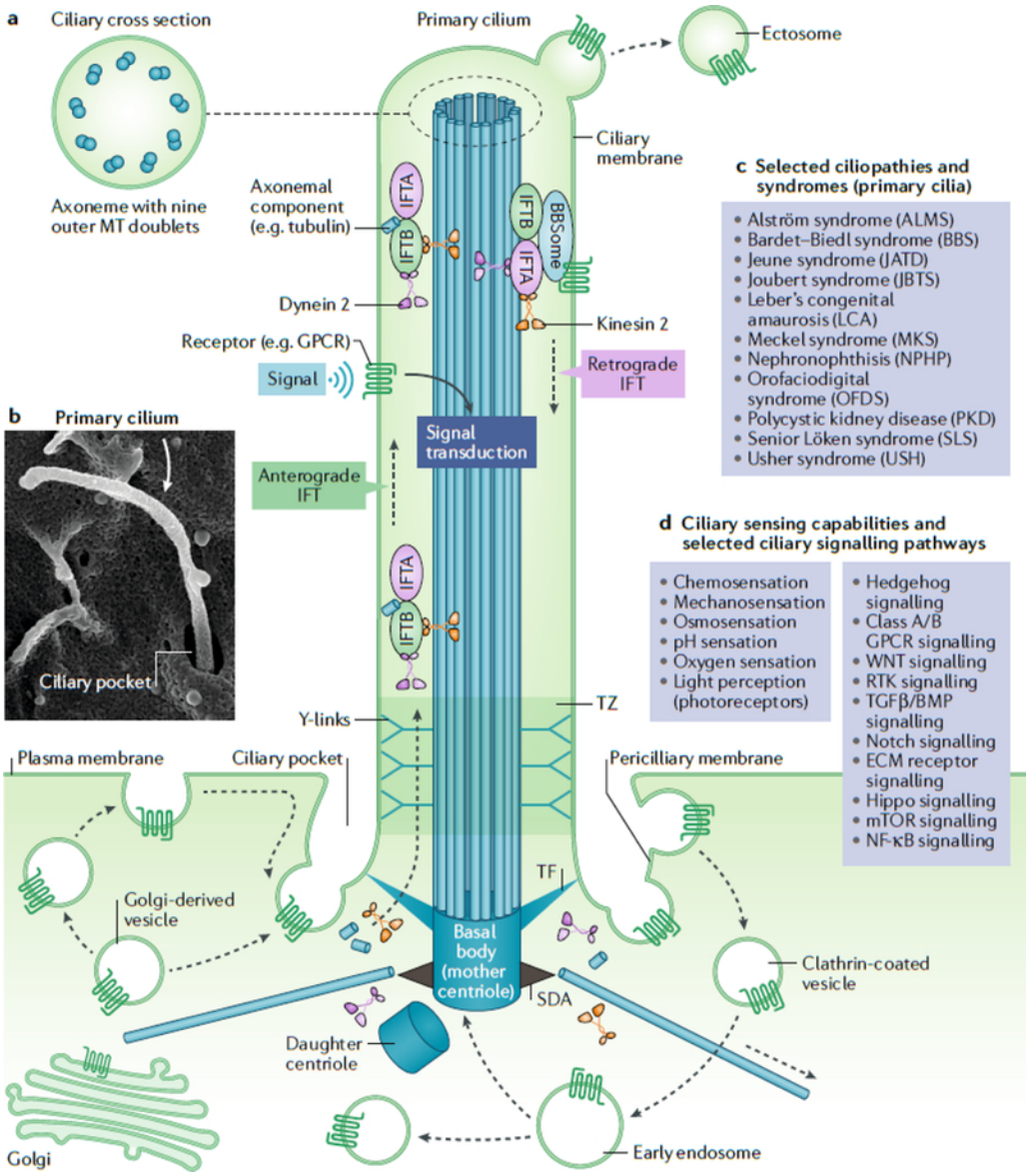

Figure 1.5. Overview of ciliary signaling. Many signaling pathways occur in the cilium and outside of the cilium to regulate this structure and cellular processes. Within the cilium, signaling pathways work to provide sensory functions as well as to regulate the cilium. The dynamic cilium is constantly undergoing maintenance including assembling and disassembling tubulin and axonemal proteins as well as recycling membrane from Golgi and plasma membrane as ectosomes containing important signaling components are released from the tips of cilia. From (Anvarian et al., 2019).

Chlamydomonas is a model organism for ciliary studies

Cilia have been studied in a wide range of different models, including in human cells, *Drosophila*, *C. elegans*, *Tetrahymena*, mouse oocytes, *Xenopus* and sea urchin embryos. Here, I use the unicellular green alga *Chlamydomonas reinhardtii* as a model organism for ciliary studies (**Fig. 1.6)**. This organism has been extensively studied to provide abundant fundamental information about ciliary mechanisms and regulation because of its 2 motile cilia with highly conserved components to mammalian cilia (O'Toole et al., 2012). These cells have a doubling time of 8 hours and exist on plate and in suspension as haploid cells (Sasso et al., 2018). In addition, *Chlamydomonas* cilia are easy to manipulate. Ciliary abscission can easily be induced with various perturbations. In this work, I focus primarily on either the use of acetic acid-induced pH shock to drop the pH of the suspended cells to 4.5 for 45s (Hartzell et al., 1993; Lewin et al., 1982), high concentrations of calcium chloride (L. Quarmby & Hartzell, 1994), or mechanical perturbations to induce ciliary shedding. Following all methods, cilia can regenerate completely within ~2 hours in wild-type cells which allows for quick studies of ciliary processes.

Chlamydomonas maintain cilia in nondividing cells similar to human cells. These cilia contain a 9+2 organization of the microtubule axoneme including radial spoke proteins and dynein arms to facilitate ciliary beating motility. These cilia, used to propagate the single cell, are similar to motile cilia found on terminally differentiated epithelial airway cells, fallopian tubes, and ependymal cells in the ventricle of the brain (Mitchison & Valente, 2017). These cilia also share conserved components and regulatory mechanisms to primary cilia (O'Toole & Dutcher, 2014). Because of these similarities and ease of ciliary manipulation, *Chlamydomonas* is an ideal model organism for these studies and is used throughout this work to understand ciliary regulation.

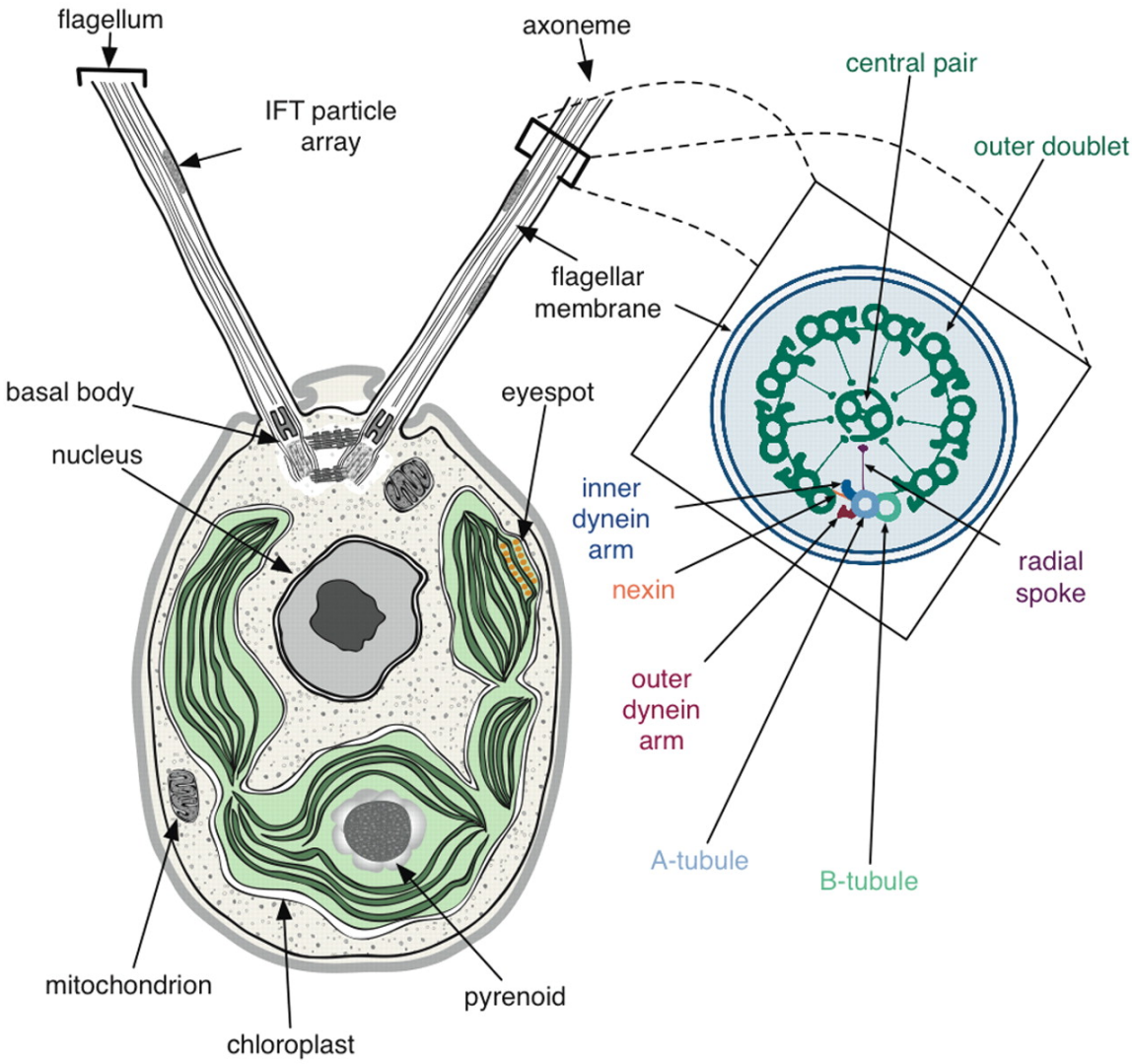

Figure 1.6. Inside *Chlamydomonas reinhardtii*. *C. reinhardtii* is a single-celled green alga with two motile cilia protruding from the plasma membrane which contain a 9+2 axonemal arrangement and include inner and outer dynein arms in addition to radial spoke proteins. From (Merchant et al., 2007).

4. Research Objectives

In this work, my goal is to understand how the cell becomes tuned for ciliary regulation following cell cycle re-entry. Extensive research has been completed to identify which factors are regulating cilia with the cell cycle on the molecular level. Here, I identify more broadly how the cell can tune multiple cellular systems to facilitate ciliary disassembly through both extraciliary and intraciliary components in *Chlamydomonas*. I investigate structural changes due to cytoplasmic microtubule manipulation and ERK pathway activation which is commonly upregulated in cancers on cells that exhibit a loss of cilia. Until this point, ERK signaling has been found to regulate ciliogenesis through ciliary elongation through MEK1/2 inhibition (S. Wang et al., 2013). MEK1/2 has been found to be activated at the basal bodies to promote genes that increase cell proliferation in cancerous cells (Schneider et al., 2005). ERK has been found in ~85% of cancers and MEK1/2-ERK1/2 signaling is commonly found to have aberrant activation in most cancer types with resistance to drug treatments (Song et al., 2023).

First, I look at changes to the cell following cell cycle entry using chemical and genetic perturbations. I find that combinations of double mutant map kinase phosphatases mkp2, 3 and 5 in *Chlamydomonas* immediately inhibits ciliogenesis and induces ciliary resorption over time consistent with cell cycle entry. Looking at factors required for ciliogenesis, I find substantial alterations to kinesin-2 entry into cilia, membrane trafficking to cilia, localization of the transition zone protein NPHP4, and reorganization of cytoplasmic microtubules. This work identifies a more comprehensive and mechanistic view of cellular changes at the onset of assembly inhibition and establishes a role for Ras/Raf/MEK/ERK signaling in regulating ciliogenesis alongside its well-known role in regulating cell cycle progression.

Following this work, I investigate changes to the proteome during ciliary shortening using the DUSP6 inhibitor (E)-2-benzylidine-3-(cyclohexylamino)-2,3-dihydro-1H-inden-1-one ("BCI"). Here I find that in ciliary proteomics, BCI most drastically changes regulation to flagellar associated proteins which have functions specific to the ERK pathway. In addition, I find proteins involved in the ubiquitination pathway upregulated. Following this observation, I find that BCI-treated cells have

increased ubiquitination of proteins in the cell body overall compared to other ciliary resorption agents which highlights a potential for investigation into map kinase crosstalk for regulating ciliary dynamics.

In our final work, I take a deeper look at how the cell utilizes microtubule dynamics during ciliogenesis. It has previously been shown that inhibiting microtubule dynamics either through taxol stabilization or colchicine-induced destabilization attenuates ciliary assembly and acute needs for tubulin induce whole cell microtubule depolymerization. I find that ciliogenesis occurs despite cytoplasmic microtubule stabilization with minimal concentrations of taxol, and cytoplasmic microtubules are not grossly restructured following mechanical shearing. This work identifies a defect in microtubule reorganization specific to pH shock and calcium induced signaling that also affects acetylated tubulin stability. These findings also suggest that large scale cytoplasmic microtubule dynamics are not required for ciliogenesis which contrasts previous data identifying a need for cytoplasmic microtubule depolymerization (L. Wang et al., 2013) with respect to freeing up tubulin monomers for axonemal elongation or allowing access to ciliary proteins for ciliogenesis.

CHAPTER 2:

The ERK activator, BCI, inhibits ciliogenesis and causes defects in motor behavior, ciliary gating, and cytoskeletal rearrangement

Larissa L Dougherty[1,2], Soumita Dutta[2,3], Prachee Avasthi[1,2,§,*]

[1]Biochemistry and Cell Biology Department, Geisel School of Medicine at Dartmouth College, Hanover, New Hampshire

[2]Anatomy and Cell Biology Department, University of Kansas Medical Center, Kansas City, Kansas

[3]Department of Microbiology and Molecular Genetics, University of Texas Health Science Center at Houston, Texas

[§]Address correspondence to prachee.avasthi@dartmouth.edu at Geisel School of Medicine at Dartmouth College

[*]Prachee Avasthi is a paid consultant for Arcadia Science

The text and figures from chapter 2 represent a paper published in Life Science Alliance (**doi**: 10.26508/lsa.202301899). Larissa L Dougherty performed conceptualization, data curation, formal analysis, investigation, methodology, project administration, validation, visualization, writing – original draft, and writing – review and editing. Soumita Dutta performed conceptualization, data curation, investigation, methodology, and writing – review and editing. Prachee Avasthi performed conceptualization, formal analysis, funding acquisition, investigation, project administration, resources, software, supervision, visualization, and writing – review and editing.

We are grateful for Chris Shoemaker and his lab for providing hTERT-RPE1 cells, methods, and guidance on related procedures to facilitate this work. We thank the reviewers for their careful reading which greatly improved the manuscript. We would also like to thank Ann Lavanway at the Dartmouth Imaging Facility for helping with immunofluorescence imaging, Radu Stan for preparing and imaging cells for electron microscopy, the BioMT Core at Dartmouth (funded by NIH NIGMS grant P20-GM113132) and Genomics and Molecular Biology Shared Resources Core at Dartmouth (funded by NCI Cancer Center Support grant 5P30CA023108-37) for use of equipment, the Department of Anatomy and Cell Biology at the University of Kansas Medical Center where this work was started, and our funding source NIH MIRA R35GM128702(PA).

ABSTRACT

Mitogen-activated protein kinase (MAPK) pathways are well known regulators of the cell cycle but they have also been found to control ciliary length in a wide variety of organisms and cell types from *Caenorhabditis elegans* neurons to mammalian photoreceptors through unknown mechanisms. ERK1/2 is a MAP kinase in human cells that is predominantly phosphorylated by MEK1/2 and dephosphorylated by the phosphatase DUSP6. We have found that the ERK1/2 activator/DUSP6 inhibitor, (E)-2-benzylidine-3-(cyclohexylamino)-2,3-dihydro-1H-inden-1-one (BCI), inhibits ciliary maintenance in *Chlamydomonas* and hTERT-RPE1 cells and assembly in *Chlamydomonas*. These effects involve inhibition of total protein synthesis, microtubule organization, membrane trafficking, and KAP-GFP motor dynamics. Our data provide evidence for various avenues for BCI-induced ciliary shortening and impaired ciliogenesis that gives mechanistic insight into how MAP kinases can regulate ciliary length.

INTRODUCTION

The cell cycle and ciliogenesis utilize centrioles at different times. Proper ciliary function is important for cellular signaling and development in most mammalian cells (Reiter & Leroux, 2017). Dysregulation of these antenna-like microtubule signaling/motile hubs can result in problems ranging from polydactyly to retinal dystrophy (Reiter & Leroux, 2017). Ciliary assembly and maintenance is regulated by intraflagellar transport (IFT) which controls the movement of materials into and out of the cilium (Ishikawa & Marshall, 2017).

Ciliogenesis occurs when cells exit the cell cycle (Kasahara & Inagaki, 2021). After cell division and during quiescence, the centrosome takes on a new role from serving as spindle poles for chromosome segregation to serving as basal bodies at the base of the cilium (Lattao et al., 2017). One of the two centrioles in the centrosome, the mother centriole, docks to the plasma membrane during G1/G0 to nucleate the cilium and recruit proteins involved in ciliogenesis (Azimzadeh & Marshall, 2010). In *Chlamydomonas*, two cilia begin to assemble from microtubule growth pushing from the basal bodies into the plasma membrane. This creates a protrusion which ultimately becomes a cilium. As the cell reenters the cell cycle, the cilium will disassemble either through shedding or axonemal disassembly before entering cell division (Patel & Tsiokas, 2021).

The ERK pathway is tightly regulated to control the cell cycle. MAPK pathways regulate cellular stress responses, developmental phases of cells, and cell proliferation (Zhang & Liu, 2002). The Ras/Raf/MEK/ERK pathway is one of the central/core signaling pathways that has been well characterized for incorporating extracellular signals into the cell to promote cell proliferation and differentiation (Shaul & Seger, 2007). At its most basic regulation in human cells, it involves the balance of ERK1/2 phosphorylation by the kinase MEK1/2, and the phosphatase DUSP6/MKP3 (Lake et al., 2016), though there is extensive crosstalk, other proteins, and feedback loops also involved in regulation of this phosphorylation cascade.

Various MAPKs have been found to regulate ciliary structure. Prior work has shown that mutants for MAPKs can alter cilium length. For example, a type of MAPK in *Chlamydomonas*, LF4 which is a MAPK/MAK/MRK Overlapping Kinase (MOK), leads to longer cilia when mutated (Berman et al., 2003) as well as mutated MPK9 in *Leishmania Mexicana* (Bengs et al., 2005). In photoreceptor cells, male germ cell-associated kinase (MAK) negatively regulates ciliary length to prevent degeneration (Kazatskaya et al., 2017). In *C. elegans*, MAPK15 directly regulates primary cilium formation and localization of the ciliary proteins BBS7 and other proteins involved in cilia formation and maintenance. More recently, ERK7, another MAPK, has been found to regulate an actin regulating protein, CAP Zip, which is necessary for ciliary length maintenance in conjunction with other signaling pathways (Miyatake et al., 2015). In addition, it is known that ERK1/2 suppression with 1,4-diamino-2,3-dicyano-1,4-bis[2-aminophenylthio]butadiene, or U0126 , can elongate cilia as well as decrease apoptosis in kidney cells (S. Wang et al., 2013). Our goal in this work is to understand how the central signaling MAPK pathway can regulate ciliogenesis in addition to its role in regulating the cell cycle (Wortzel & Seger, 2011).

BCI induces ERK1/2 activation through DUSP6 inhibition. In this study, we utilize the small molecule inhibitor (E)-2-benzylidine-3-(cyclohexylamino)-2,3-dihydro-1H-inden-1-one ("BCI"). BCI has previously been found to allosterically inhibit the dual specificity phosphatase DUSP6 in zebrafish. Following DUSP6 inhibition, phosphorylated ERK1/2 (pERK1/2) cannot be dephosphorylated leading to accumulation of pERK1/2 which permits Fibroblast Growth Factor (FGF) signaling (Molina et al., 2009). Since this characterization, BCI has been utilized as an ERK activator to study oncogenic signaling in various cancer cell lines including in mouse pro-B cells (Chan et al., 2020), ovarian cancer cells (James et al., 2019), and in an undifferentiated sarcoma cell line among others (Lin et al., 2020).

Here we use *Chlamydomonas reinhardtii,* a unicellular green alga which is an extensively used ciliary model organism with well conserved ciliary proteins, structure, and function to humans (O'Toole et al., 2012). By BCI, inducing ERK1/2 activation through BCI-induced DUSP6 inhibition, we ultimately find multiple pathways altered

that are important for ciliogenesis and ciliary maintenance. This pathway has been previously manipulated through the MEK1/2 inhibitor U0126 to prevent MAPK activation as well as lengthen cilia (Avasthi et al., 2012). To understand why this process occurs, we looked at various processes that are involved in ciliary length maintenance and assembly.

RESULTS

BCI-induced MAP kinase phosphorylation disrupts ciliary maintenance and assembly in Chlamydomonas reinhardtii.

Given the lengthening effects of ERK inhibition on ciliary length through U0126 (Avasthi et al., 2012), we wanted to test specificity of the pathway in ciliary regulation through activation of the pathway. BCI has previously been found to activate ERK1/2 upon inhibiting the dual specificity phosphatase/MAP kinase phosphatase, DUSP6/MKP3 in addition to DUSP1 (**Fig 2.1A**). BCI was selected as a tool due to the dramatic phenotype of completely blocked ciliary growth. BCI does not inhibit various other FGF inhibitors or related phosphatases including Cdc25B, PTP1B, and Dusp3/VHR in zebrafish (Molina et al., 2009; Shojaee et al., 2015). To test if this intended effect occurs in *Chlamydomonas*, we checked MAPK phosphorylation following 15 minute intervals of treatment with BCI for up to 1 hour using an antibody for human ERK 1/2. Phosphorylation increased within 15 minutes and then decreased by 60 minutes, indicating that BCI activates phosphorylation of MAP Kinases in *Chlamydomonas* **(Fig 2.1B**). For data throughout this study, $p < 0.05$ is considered significant.

To determine if ERK1/2 activation through BCI treatment can shorten cilia, we tested a range of BCI concentrations and measured cilia after a 2 hour treatment when length changes are typically apparent. We saw a dose-dependent effect on cilia length where increasing BCI concentrations decreased cilia length up to 45 μM BCI where cilia were completely resorbed (**Fig 2.1C-D**). This decreased length could be a result of reduced assembly or increased disassembly (Marshall et al., 2005). To test assembly, we severed cilia with low pH and tested ciliary reassembly (Lefebvre, 1995). In the presence of BCI, cilia could not regenerate at all (**Fig 2.1E)** confirming that there is a strong assembly defect when MAPK is activated through inhibition of its dephosphorylating enzyme despite the presence of excess ciliary protein available for ciliogenesis (Rosenbaum et al., 1969).

We repeated these experiments in hTERT-RPE1 cells to see if this was a *Chlamydomonas*-specific effect. Like *Chlamydomonas*, RPE1 cells showed a dose-dependent effect on ciliary shortening (**Fig 2.S1A-B**). In addition, BCI induces ERK1/2 phosphorylation in RPE1 cells within 15 minutes of treatment (**Fig 2.S1C**). Together, this data shows that BCI induces phosphorylation of MAP kinases during short treatments, prevents ciliary assembly in *Chlamydomonas* and prevents ciliary growth in RPE1 cells.

Map kinase phosphatases regulate ciliary length

To determine if ciliary shortening is due to inhibitor targeting of DUSP6 in *Chlamydomonas*, we used genetic mutants of potential *Chlamydomonas* DUSP6 orthologs. To identify the *Chlamydomonas* DUSP6, we compared the zebrafish DUSP6 protein to the *Chlamydomonas* genome and took the top 3 most similar proteins to investigate which will be referred to here on as the putative DUSP6 ortholog mutants (**Fig 2.S1D-E**). We first compared their BCI binding pockets. BCI is predicted to interact with human Trp 262, Asn 335, and Phe 336 as well as the general acid loop backbone according to docking studies (Molina et al., 2009). The predicted zebrafish BCI binding pocket was partially conserved to the putative DUSP6 *Chlamydomonas* ortholog mutants (**Fig 2.S1D-1E**). We acquired these single mutants from the *Chlamydomonas* Resource Center and confirmed their mutation through PCR confirmation of a cassette insertion within the gene (**Fig 2.S1F**). This cassette insertion in the target protein gene knocks out that protein. Following this confirmation, these mutants were then crossed to generate double mutants. We tested both their ability to induce pMAPK expression upon treatment with BCI (**Fig 2.1F**) and their ciliary phenotypes (**Fig 2.1G-H**). Comparing steady state ciliary lengths showed that the DUSP6 ortholog mutant *mkp2* had significantly shorter ciliary lengths when compared to wild type (**Fig 2.1G**) and half as many ciliated cells (**Fig 2.S1G**), though it was able to reciliate and regenerate back to previous lengths within 2 hours. The *mkp3* and *mkp5* single mutant regenerations did not significantly differ from wild type and cells were nearly fully reciliated within 2 hours (**Fig 2.1G, Fig 2.S1G**). In addition, the single mutants increased pMAPK expression following 15 minutes of BCI treatment (**Fig 2.1F**). Because the dusp6 ortholog single mutants could

still express pMAPK and regenerate cilia, it was possible that these phosphatases could compensate for loss of function of one phosphatase. Thus, we crossed the dusp6 ortholog single mutants together and found that not only was pMAPK signal attenuated in each double mutant and almost completely abolished in *mkp2 x mkp3* and *mkp3 x mkp5* mutants (**Fig 2.1F**), but *mkp2 x mkp3* and *mkp3 x mkp5* mutants could not regenerate their cilia to normal or mutant lengths in 2 hours (**Fig 2.1H and Fig 2.S1H**). Because *mkp2 x mkp3* and *mkp3 x mkp5* mutants recapitulated the BCI phenotype, we chose to focus on these double mutants in comparison to BCI for the rest of this study. This data supports that there may be redundant functions for these MKPs in *Chlamydomonas* that can compensate for loss of function of one map kinase phosphatase, that map kinase phosphatases play a role in regulating ciliary length, and that BCI potentially targets more than one MKP in *Chlamydomonas*.

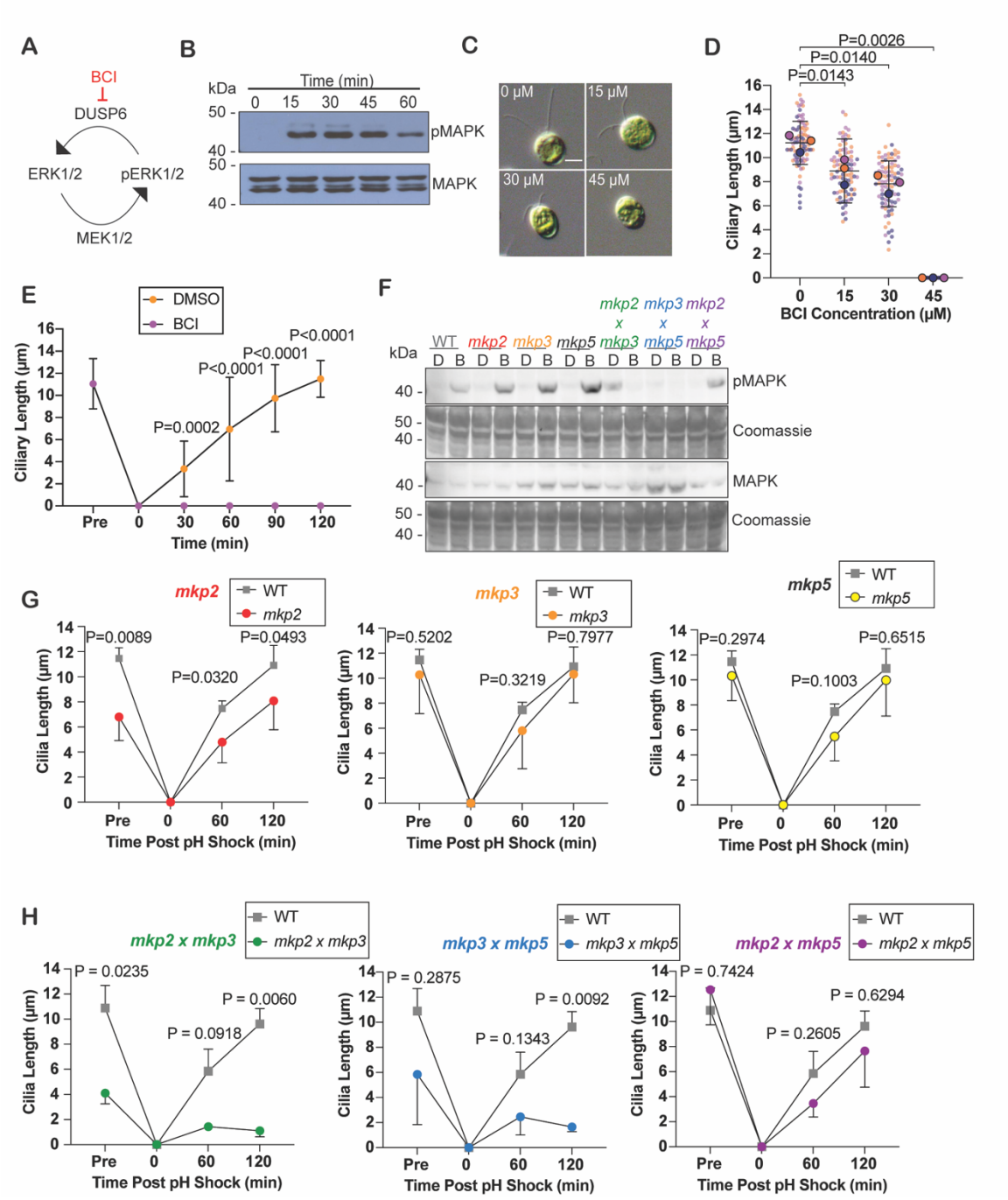

Figure 2.1. BCI activates the MAPK pathway in *Chlamydomonas reinhardtii* and inhibits ciliogenesis. **(A)** The MAP kinase ERK1/2 is phosphorylated by MEK1/2 and dephosphorylated by DUSP6. **(B)** Western blot comparing MAPK and pMAPK protein expression following a 2 hr treatment with 30 µM BCI for the indicated times in *Chlamydomonas*. **(C)** Representative images of steady state *Chlamydomonas* cilia length in 0 µM BCI to 45 µM BCI following a 2 hour treatment. Scale bar is 5 µm. **(D)** Quantification of ciliary

lengths in (**C**). Error bars show the mean with the 95% confidence interval for averages from each trial (n=30, N=3). The P value was calculated with a one-way ANOVA with Dunnett's multiple comparisons test. This super plot shows averages from each trial with larger circles plotted on top of the individual points. (**E**) Regenerating ciliary lengths following pH shock and regrowth in 30 μM BCI (purple) or 0.5% DMSO (orange) over 2 hours. Error bars are mean with 95% confidence of the means from each trial (n=30, N=3). The P values for the 120 minute time points were determined using a two-way ANOVA with Bonferroni's correction. (**F**) Western blots of protein from wild type (CC-5325) and DUSP6 ortholog single and double mutants. Cells were treated with DMSO or 30 μM BCI for 15 minutes before protein collection. PVDF membranes were probed for either p42/p44 pERK1/2 or p42/p44 ERK1/2 in *Chlamydomonas*. Total protein is shown below with Coomassie. **(G-H)** The mean ciliary length measurements with mean and 95% confidence intervals in regenerating DUSP6 ortholog single mutants and double mutants over 2 hours (n=30, N=3). P values compare the averages at each time point between wild type (gray squares) and the mutant in each case (circles) which were determine with a two-way ANOVA with Tukey's multiple comparisons test.

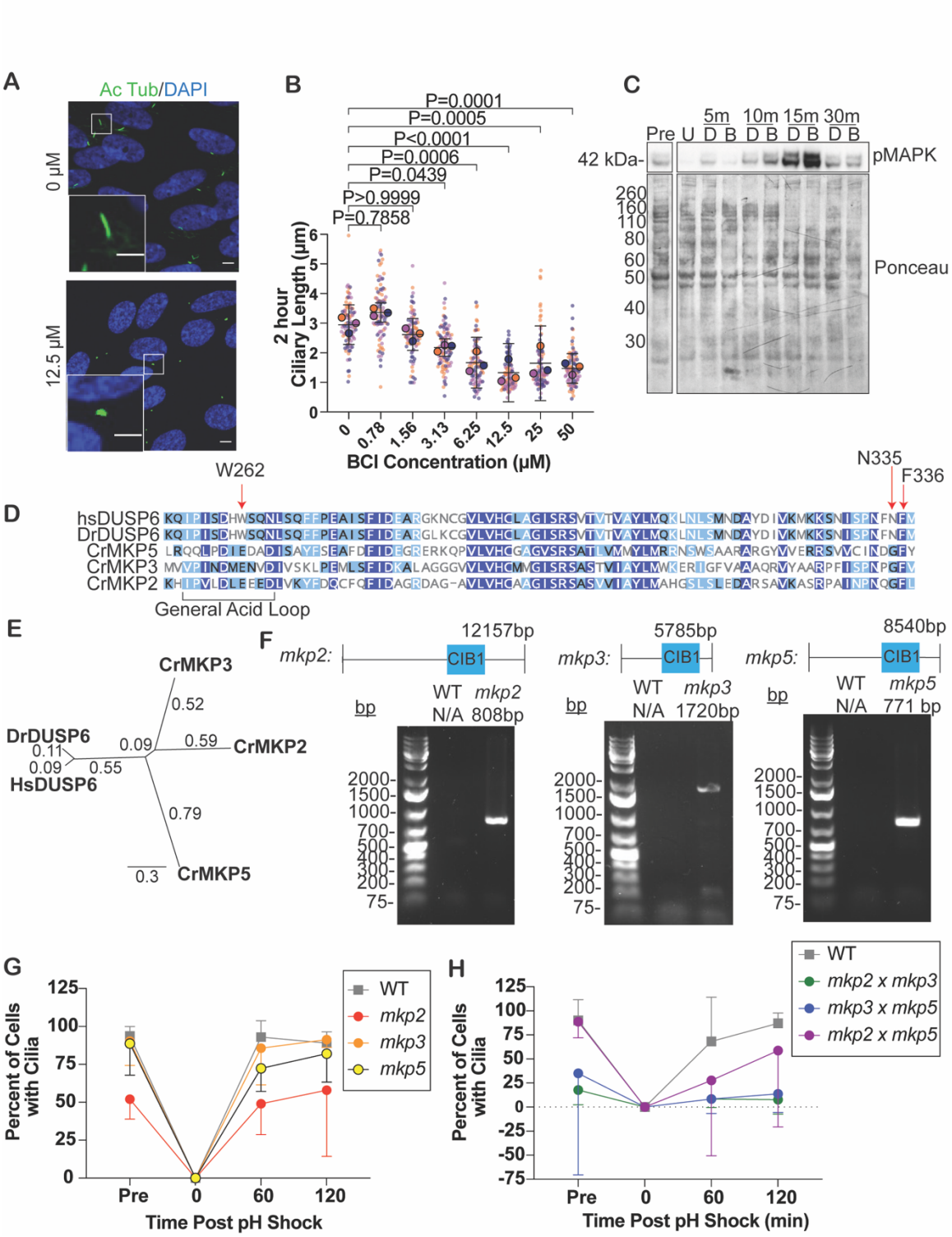

Figure 2.S1. *Chlamydomonas* DUSP6 ortholog mutants have ciliary length defects.

(A) Representative images of serum starved RPE1 control cells in DMSO ("0 µM") compared to the shortest cilium lengths measured following a 2 hour BCI treatment (12.5 µM BCI). Cells were

probed for acetylated tubulin (green) and DAPI (blue). Acetylated tubulin length was measured for the ciliary length. The scale bar in larger images is 5 μm, and in insets is 3 μm. (**B**) Ciliary lengths of serum starved RPE1 cells treated with the indicated concentrations of BCI for 2 hours. Error bars are mean with 95% confidence interval (n=30, N=3). The P values were calculated with an ordinary one-way ANOVA on the averages of the 3 trials with Bonferonni's multiple comparisons test. **(C)** Western blot showing that 6.25 μM BCI induces ERK1/2 phosphorylation in RPE1 cells. Cells were first incubated with the MEK1/2 inhibitor U0126 to completely inhibit pMAPK signal and then cells were treated with 6.25 μM BCI for the indicated times. Ponceau staining was used to measure total protein. U is U0126 (50 μM), D is DMSO, and B is BCI (6.25 μM). **(D)** Sequence alignment of predicted residues BCI interacts with (Molina et al., 2009). Dark blue regions indicate 100% similarity, light blue indicates 60-100% similarity, and white indicates less than 60% similarity. (**E)** Phylogenetic tree for the top 3 zebrafish DUSP6 hits in *Chlamydomonas*. The phylogenetic tree is a neighbor-joining tree. Numbers denote branch length. **(F)** Genotype results for the *Chlamydomonas* DUSP6 mutant ortholog cassette insertions acquired from the *Chlamydomonas* Resource Center for all single mutants. Primers were designed to amplify part of the wild type protein to part of the CIB1 insert. (**G-H**) Percent of cells ciliated in single DUSP6 ortholog mutants (**G**) and in double mutants (**H**). Error bars are mean with 95% confidence interval for the averages of 3 independent experiments (n=100, N=3).

BCI disrupts ciliary KAP-GFP dynamics

Ciliary entry of the anterograde motor, kinesin-2, is known to be required for ciliogenesis (Adams et al., 1982). It is possible that cilia shorten and cannot regenerate in the presence of BCI due to blocked kinesin-2 entry into cilia. To test this hypothesis, we first checked if kinesin-2 was present in the cilium and basal bodies of BCI treated *Chlamydomonas* cells using a GFP-tagged kinesin accessory protein on kinesin-2, also known as KAP-GFP, previously generated and validated by Mueller et al., 2004 (**Fig 2.2A**) (Joshua Mueller & Catherine A. Perrone, 2004). The KAP subunit is a cargo adaptor protein which is known to interact with IFT complexes and other cargoes for anterograde transport. Defects in this adaptor can have a wide range of implications for ciliogenesis. After a 2 hour treatment with BCI, cells with cilia maintained KAP-GFP fluorescence at their basal bodies regardless of BCI concentration (**Fig 2.2B**). However, at 30 μM BCI, total KAP-GFP fluorescence in the cilia decreased (**Fig 2.2C and D**). Interestingly, the normalized fluorescence per micrometer of cilia was not significantly different between DMSO and BCI treated cells (**Fig 2.2E**) suggesting that KAP-GFP fluorescence proportionally decreases with ciliary length.

To determine how KAP-GFP dynamics respond to BCI treatment, we used Total Internal Reflection Microscopy (TIRF) to measure KAP-GFP dynamics in real time (**Fig 2.2F**). Previous studies have shown that kinesin-2 expression and injection size are negatively correlated to ciliary length (Brown et al., 1999; Ludington et al., 2013). From kymographs of KAP-GFP movement in cilia using TIRF, we measured frequency (**Fig 2.2G**), velocity (**Fig 2.2H**), and train size (**Fig 2.2I**) between 60 minutes and 120 minutes. In opposition to Ludington et al., 2013, frequency continually decreased from 60 minutes to 120 minutes in BCI whereas velocity and train size decreased by 60 minutes and maintained that decrease even after 120 minutes in BCI-induced shortening cilia. Because we see a decrease in the frequency of KAP-GFP entering cilia, decreased velocity of KAP-GFP movement in cilia in addition to shortening cilia, this data suggests that KAP-GFP ciliary entry is disrupted and ciliary maintenance cannot be achieved to allow proper ciliogenesis to occur under MKP inhibited conditions.

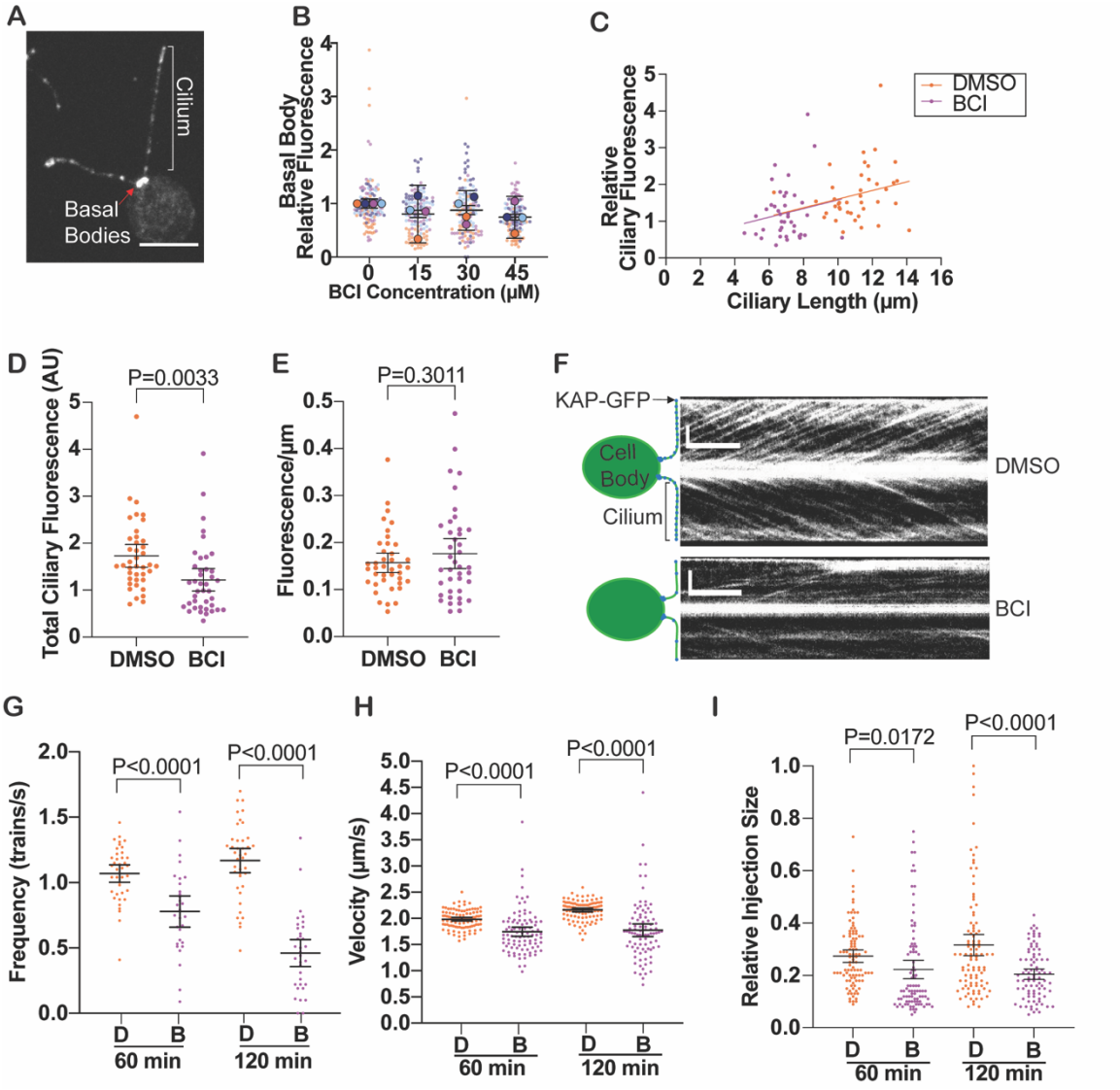

Figure 2.2. KAP-GFP dynamics are altered in the cilium of BCI treated cells. (A) *Chlamydomonas* expressing KAP-GFP. Indicated are the measured areas of KAP-GFP localization: the 2 basal bodies and cilia. Scale bar is 5 μm. (**B**) Super plot quantification of basal body fluorescence in (A) following a 2 hour treatment with BCI at the indicated concentrations. Error bars are mean with 95% confidence interval for the averages of the trials. P=0.5126 which was determined by an ordinary one-way ANOVA. (**C**) Ciliary length plotted against ciliary fluorescence for cells in DMSO (orange circles) or 30 μM BCI (purple) after a 2 hour treatment (n=40, N=1). Simple linear regression was used to generate linear regression lines and comparisons. For DMSO, y=0.1171x+0.4305 and r^2=0.05676. For BCI, y=0.1174x+0.4051 and r^2 = 0.2636. Comparing slopes, F=4.048e-006 (1,76) and P=0.9984. Comparing intercepts, F=0.005429 (1, 77) and P=0.9415. (**D**) Comparison of total ciliary fluorescence shown in (C). P

values were determined using a student's t-test. (**E**) Comparisons of ciliary fluorescence in DMSO or BCI per micrometer of cilia in (C). P values were determined using a student's t-test. (**F**) Example kymographs collected from total internal reflection fluorescent (TIRF) microscopy of KAP-GFP movement in cilia in cells treated with DMSO (top) or 30 μM BCI (bottom) for 2 hours. Vertical scale bars are 4 μm. Horizontal scale bars are 2 seconds. (**G-I**) KAP-GFP dynamics quantified from the kymographs (n=20, N=1). The error bars are mean with 95% confidence interval (n=20, N=1). P values were calculated from a two-tailed unpaired t-test for pairwise comparisons. (**G**) Frequency of KAP-GFP trains measured as the total amount of trains counted over the total amount of time the kymograph was collected. For DMSO, n=40 (1 hr and 2 hr). For BCI, n=30 (1 hr) and 34 (2 hr). (**H**) Velocity of KAP-GFP trains measured as the distance traveled in μm over time in seconds. For DMSO, n=100 (1 hr and 2 hr). For BCI, n=93 (1 hr) and 88 (2 hr). (**I**) Relative injection size KAP-GFP trains measured as relative total fluorescent intensity of each train relative to the maximum measurement. For DMSO, n=100 (1 hr and 2 hr). For BCI, n=93 (1 hr) and 88 (2 hr). P values were determined using a student's t-test.

BCI Inhibits KAP-GFP protein synthesis

Given KAP-GFP entry defects, we checked total KAP-GFP protein expression levels in regenerating cells in the presence of DMSO or BCI (**Fig 2.3A**). Interestingly, we found that total KAP-GFP protein expression in the cell was not replenished in BCI-treated cells after 2 hours (**Fig 2.3B-C**) which was not significantly rescued with the proteasome inhibitor MG132 (carbobenzoxy-Leu-Leu-leucinal) (**Fig 2.S2A-B**). We measured KAP-GFP intensity at the basal bodies during these time points and found that KAP-GFP fluorescent intensity at the basal bodies was not significantly altered (**Fig 2.3D**). This indicates that KAP-GFP can still be targeted to the basal bodies despite inability for cilia to assemble. This data indicates that BCI inhibits KAP-GFP protein expression in the cell but this expression defect is uncoupled to the ciliary entry defect given that recruitment is unaltered.

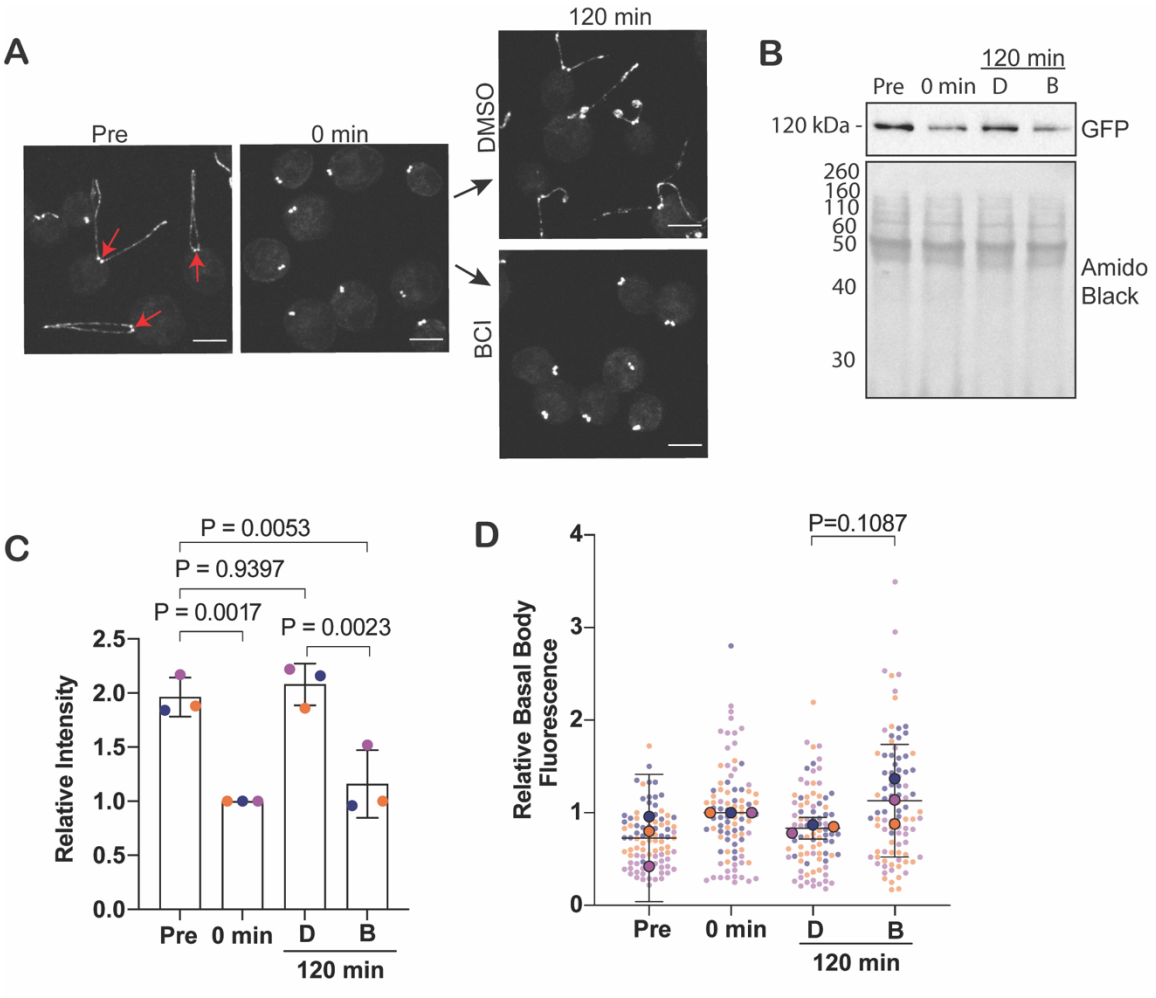

Figure 2.3. BCI decreases KAP-GFP protein expression without impacting its recruitment/targeting. (A) Immunofluorescent images of KAP-GFP cells during regeneration in either DMSO or 30 µM BCI. Scale bars are 5 µm. Red arrows point to basal bodies which are the object of quantification in (D). **(B)** Western blot for KAP-GFP expression in regenerating cells in either DMSO (D) or 30 µM BCI (B). Total protein was measured with amido black. **(C)** Quantification of (B). Error bars are mean with standard deviation for 3 independent experiments. P values were calculated using an ordinary one-way ANOVA with Dunnett's multiple comparisons test. **(D)** Quantification of KAP-GFP fluorescence at the basal bodies in (A). Error bars are mean with 95% confidence interval of the averages for 3 independent trials (n=30, N=3). The P value was calculated using an unpaired t-test with Welch's correction.

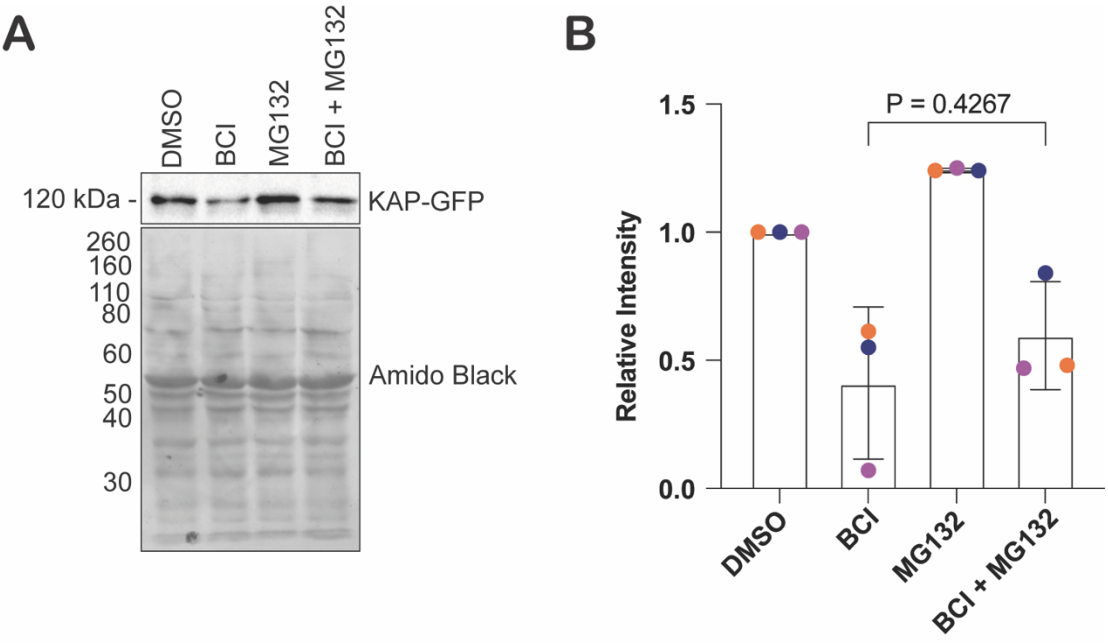

Figure 2.S2. BCI inhibits KAP-GFP protein synthesis. (**A**) Western blot of KAP-GFP expression compared to total protein shown with amido black. Cells were treated for 2 hours with either 0.5% DMSO, 20 µM BCI, 50 µM MG132, or both 50 µM MG132 and 20 µM BCI. (**B**) Quantification of (A). Error bars are standard deviation of the mean (N=3). The P value was determined by an unpaired t-test between BCI and BCI+MG132.

BCI has minor effects on a transition zone protein but not on gross transition zone structure

Given the role of NPHP4 function in the transition zone, we investigated the role of this protein in regulating ciliogenesis. The transition zone is the ciliary gate of the cell which works to regulate protein entry and exit at the cilium (Gonçalves & Pelletier, 2017). Unchanged KAP-GFP localization at the basal bodies but decreased frequency of KAP-GFP ciliary entry suggests that there could be a defect in the transition zone structure. To test this, we first looked at this structure with electron microscopy to identify visible structural defects. Cross sections of the transition zone in both untreated and BCI-treated cells appeared unaltered, noting the classical "H shape" and wedge connectors (Diener et al., 2015) (**Fig 2.4A**). We also checked a transition zone protein, NPHP4, in BCI-treated cells. Previous studies have found that altered NPHP4 expression decreases IFT velocity, changes protein composition in the cilium, and disrupts ciliary protein entry (Awata et al., 2014; L. Wang et al., 2022). In both steady state and regenerating cells with BCI, NPHP4 still localized as two puncta at the transition zone which supports the unaltered structure visualized with EM, though NPHP4 immunofluorescence was decreased (**Fig 2.4B-C**). Together, these data suggest that BCI does not grossly disrupt the transition zone as a mechanism for altering ciliogenesis, although it may inhibit localization of proteins at the transition zone that may ultimately affect trafficking into the cilium.

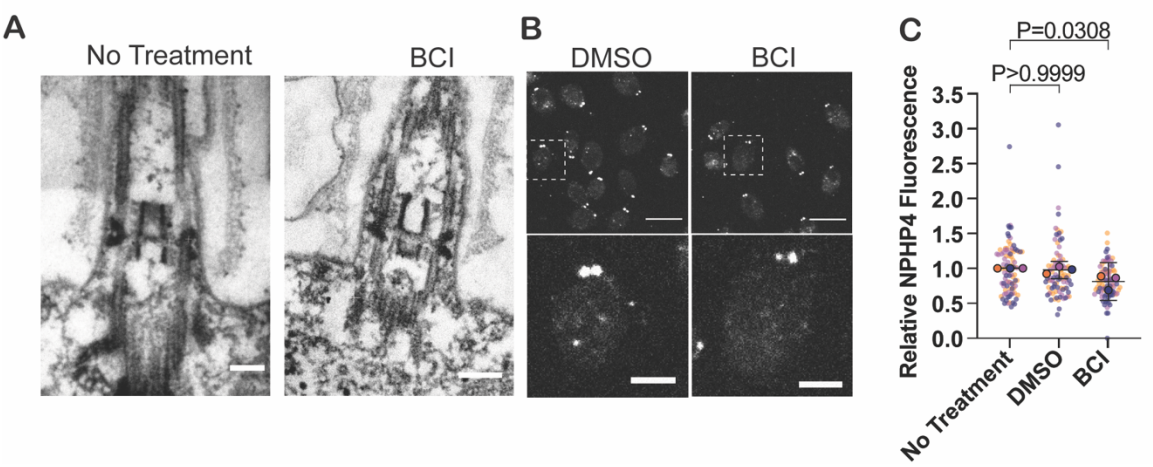

Figure 2.4. NPHP4 localization is altered at the transition zone with BCI treatment. (**A**) Electron microscopy images of the ciliary transition zone during a 2 hour steady state with or without 30 µM BCI. Scale bars are 100 nm. (**B**) Cells expressing HA-tagged NPHP4 were treated with either DMSO or 30 µM BCI for 2 hours and then stained for HA. Scale bars in top images are 5 µm. Scale bars in the bottom insets are 1.5 µm. (**C**) Fluorescent quantification of the NPHP4 signal. Error bars are mean with 95% confidence interval of the averages from each trial (n=30, N=3). The P values were determined with an ordinary one-way ANOVA with Bonferroni's multiple comparisons test on the means from each trial.

BCI disrupts membrane trafficking

The altered KAP-GFP trafficking in the cilium and decreased NPHP4 at the transition zone with a lack of visible structural changes made us curious if other trafficking defects were present in the cell. Membrane trafficking in *Chlamydomonas* has been found to be important for maintaining cilia length and for ciliary assembly. Previous studies have shown that Golgi-derived membrane is important for ciliary assembly and maintenance (Dentler, 2013), and inhibiting internalization through Arp2/3 complex perturbation also results in defective ciliary assembly and maintenance (Bigge et al., 2023). While EM of the Golgi showed no noticeable differences in Golgi structure (**Fig 2.S3A**), collapsing the Golgi with BFA (Brefeldin A) intensified ciliary shortening when paired with 20 μM BCI. This suggests that BCI excludes Golgi from potential membrane trafficking related targets of BCI (**Fig 2.5A**).

To investigate other indications of disrupted membrane trafficking, we checked the ability for cells to internalize extracellular material. Previously, Bigge et al. 2023 showed that actin puncta formation, reminiscent of endocytic pits seen in yeast and are found to increase in abundance immediately post ciliary shedding by pH shock, was absent in cells that could not regenerate cilia normally. They concluded that this is likely due to the inability for the cells to form these puncta to internalize and repurpose membrane for use in early ciliogenesis. In the presence of BCI, actin puncta increased both in steady state cells (**Fig 2.5B-C**) and in regenerating cells (**Fig 2.S3B**). However, in the steady state *Chlamydomonas* DUSP6 ortholog double mutants, *mkp3 x mkp5* mutants actin puncta did not significantly differ from untreated wild type whereas *mkp2 x mkp3* mutants had significantly more actin puncta (**Fig 2.S3C**). This data indicates a differential role for these phosphatases in regulating actin puncta formation. In addition, the data could also indicate that these puncta can form in BCI or *mkp2 x mkp3* mutants, but their lifetime is increased, perhaps due to incomplete endocytosis, and thereby preventing membrane to be repurposed from these sites for early ciliogenesis. We measured total internalization with membrane dye uptake and found that in steady state cells, membrane dye uptake did not differ significantly (**Fig 2.5D-E**), suggesting that BCI does not alter total internalization. Together, this data suggests that BCI disrupts ciliary membrane

trafficking independent of the Golgi. While endocytosis may be increased or slowed due to higher incidence of actin puncta detected, the overall internalization of membrane dye within the cell body is not dramatically affected. This is not wholly unexpected if the defects of plasma membrane internalization caused by BCI are preferentially impacting cilia.

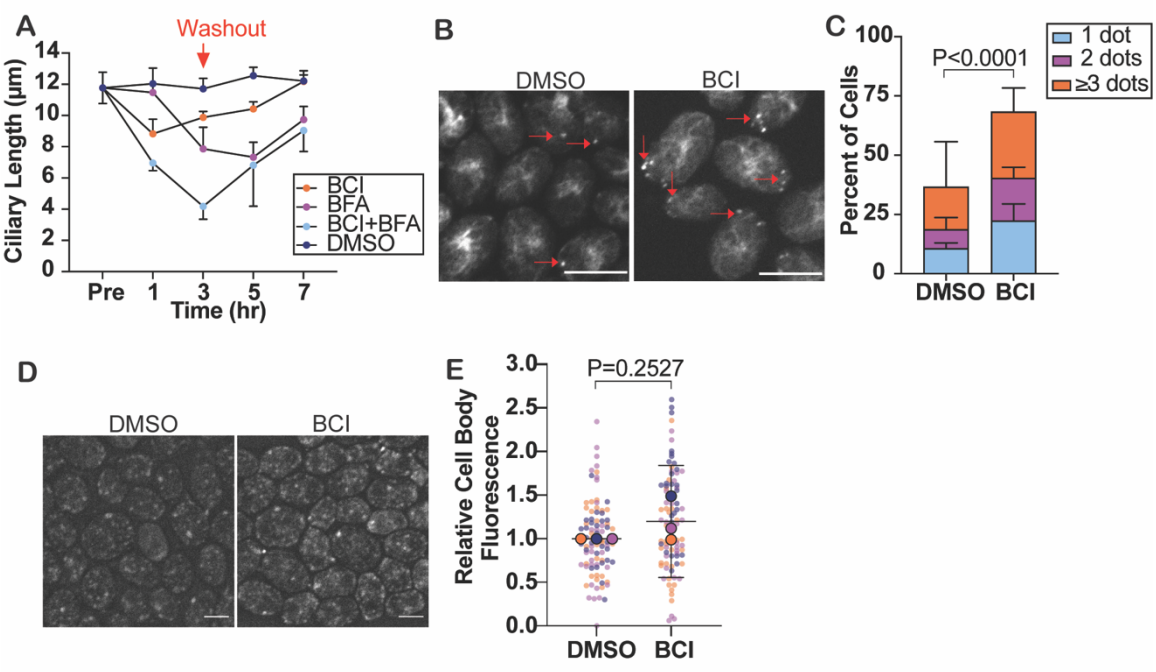

Figure 2.5. Membrane trafficking is altered in BCI treated cells. (A) Steady state cells treated with either 20 µM BCI (orange), 36 µM BFA (purple), both BCI and BFA (light blue), or DMSO (navy) for 3 hours before cells were washed out. Error bars are mean with 95% confidence interval for the averages each experiment (n=30, N=3). The P values compare BCI+BFA to the other treatments at 3 hours and were determined using a two-way ANOVA with Tukey's correction. Comparing to BCI+BFA at the 3 hour timepoint, P=0.0117 for BCI, P=0.2285 for BFA, and P=0.0301 for DMSO. **(B)** Immunofluorescent images of actin puncta visualized with phalloidin in cells treated with 30 µM BCI or DMSO for 2 hours. Red arrows indicate the actin puncta quantified. Scale bars are 5 µm. **(C)** Quantification of actin puncta. Error bars are mean with standard deviation (n=100, N=3). The P value was determined using a Chi-square test with a two-sided Fisher's exact test for cells with dots versus no dots. **(D)** Immunofluorescent images of membrane dye uptake. Scale bars are 5 µm. **(E)** Quantification of membrane dye uptake. Error bars are mean with the 95% confidence interval of the averages from each trail (n=30, N=3). The P value was determined with an unpaired t-test.

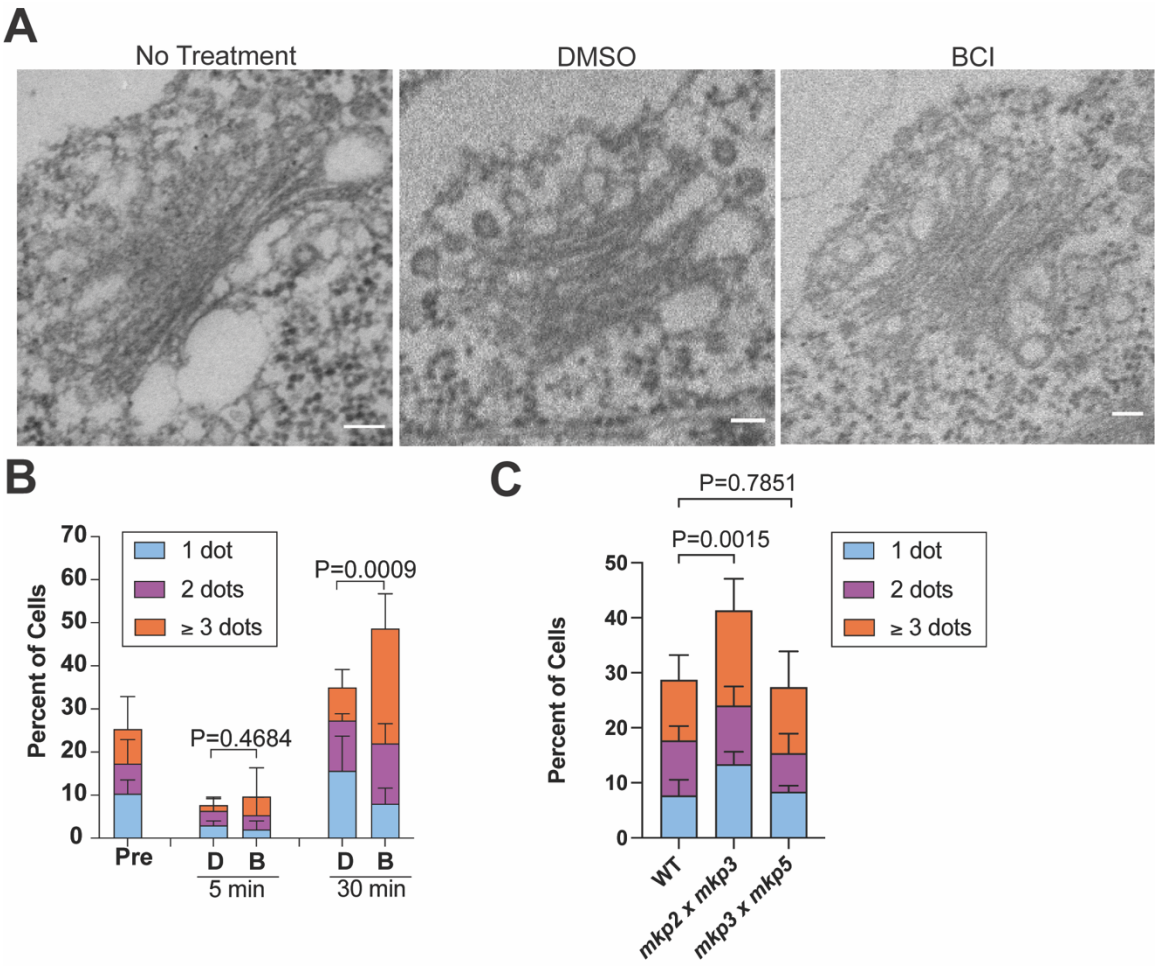

Figure 2.S3. *Chlamydomonas* DUSP6 ortholog double mutants show membrane trafficking defects. (**A**) Representative EM images of the Golgi apparatus in cells with no treatment, DMSO, or 30 µM BCI. Scale bars are 100 nm. (**B**) Quantification of actin puncta in regenerating wild type cells in either 30 µM BCI or DMSO. Error bars are mean with standard deviation (n=100, N=3). P values were determined using an unpaired t-test. (**C**) Quantification of actin puncta in steady state DUSP6 ortholog double mutants. Error bars are mean with standard deviation (n=100, N=3). P values were determined using a two-sided Fisher's exact test comparing no dots to total dots. Individual bars represent average percent of cells (n=100, N=3).

BCI disrupts cytoplasmic microtubule reorganization

Because membrane trafficking pathways are altered with BCI, we were curious if this defect could be due to disrupted intracellular trafficking through cytoskeleton rearrangement. We began by looking at cytoplasmic microtubule organization in regenerating cells. Upon deciliation, microtubules undergo large-scale reorganization (Wang et al., 2013). We looked at cells regenerating their cilia and found that cells in BCI could not fully reform their microtubule structure in the presence of BCI (**Fig 2.6A-B**). To see if cells could be forced to reorganize microtubules in the presence of BCI, we used paclitaxel (PTX) which stabilizes microtubules. In the presence of PTX and BCI, cells were able to reorganize their cytoplasmic microtubules in 60 minutes (**Fig 2.6A-B**), though paclitaxel stabilization could not rescue ciliary length in BCI-treated cells (**Fig 2.6C**). To rule out the possibility that BCI induces tubulin degradation, we used MG132 which inhibits the proteasome, therefore blocking protein degradation. Cytoplasmic microtubule reorganization was not significantly rescued with MG132 suggesting that tubulin is not degraded in the presence of BCI to prevent reorganization post regeneration (**Fig 2.6A-B**). These data suggest that BCI inhibits the mechanisms and proteins involved in cytoplasmic microtubule reorganization.

PTX-stabilized microtubules do not rescue BCI-defective ciliogenesis

To determine if the defect in microtubule reorganization after deciliation blocks regeneration in BCI, we stabilized cytoplasmic microtubules with PTX to see if the assembly defect could be rescued. After pretreating cells for 60 minutes with PTX to stabilize the microtubules prior to deciliation and then regenerating in PTX and BCI, ciliogenesis was not able to be rescued, though control cells in PTX were able to regenerate cilia normally (**Fig 2.6D-E**). This data suggests that though BCI prevents cytoplasmic reorganization, this is not the cause for immediate inhibition of ciliogenesis in regenerating cells. We checked microtubule reorganization in regenerating DUSP6 ortholog double mutants and found that *mkp2 x mkp3* and *mkp3 x mkp5* mutants had fewer cells overall which maintained full cytoplasmic microtubules arrays, though these cells were able to reorganize microtubules to previous amounts within 60 minutes. This

suggests a role for these ortholog mutants in regulating early cytoplasmic microtubule organization in the cell (**Fig 2.S4A-B**). This data further supports that BCI targets proteins involved in cytoplasmic microtubule organization, though this may not directly prevent ciliogenesis from occurring during MAPK activation.

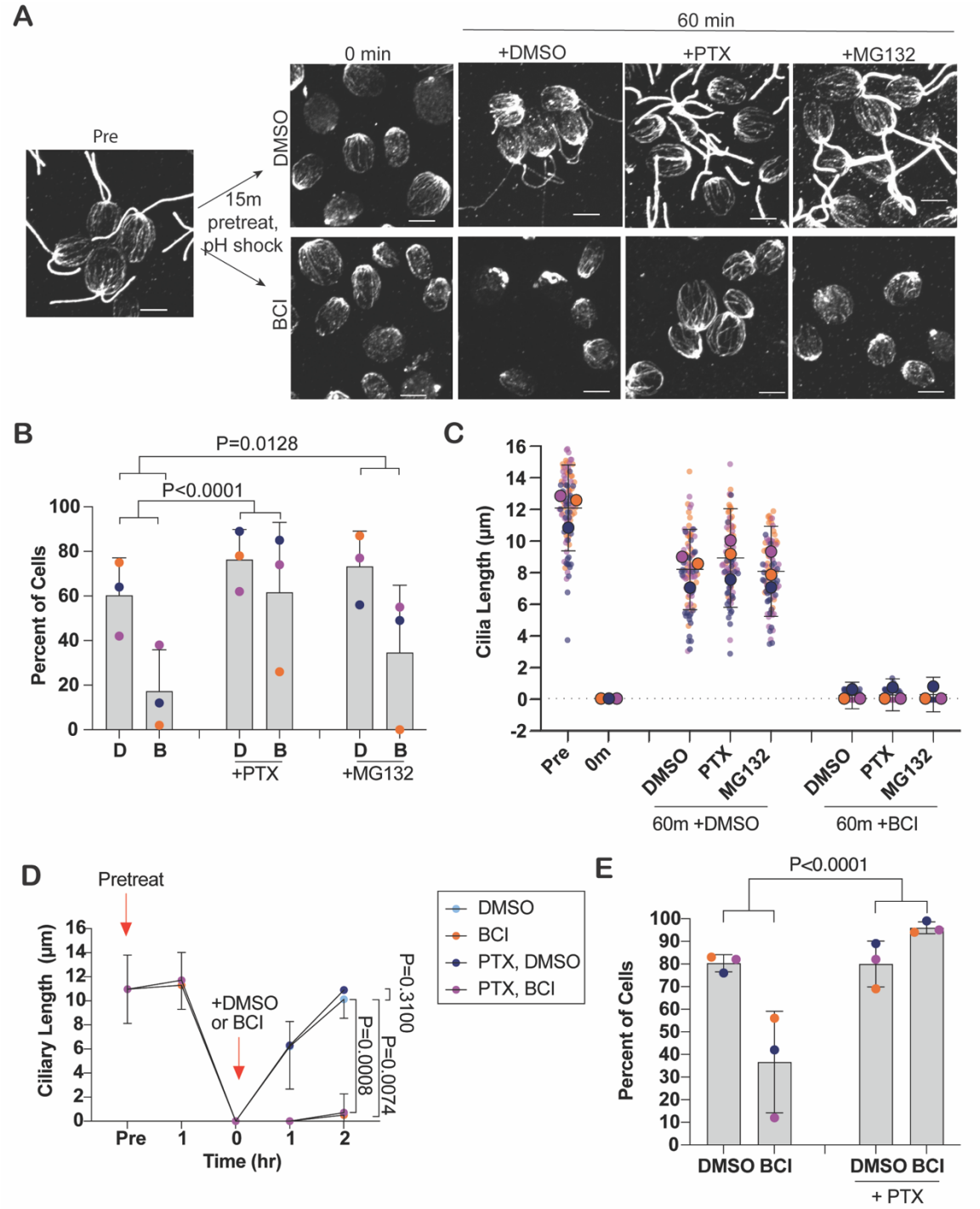

Figure 2.6. PTX-induced cytoplasmic microtubule stabilization does not rescue ciliogenesis in the presence of BCI. **(A)** Cells were pretreated with either DMSO or 20 µM BCI for 15 minutes and then regenerated in DMSO or 20 µM BCI with the addition of DMSO, 15 µM paclitaxel (PTX), or 50 µM MG132 for 60 minutes before fixing and staining for β-tubulin. Scale bars are 5 µm. **(B)** Quantification of fully reorganized microtubules in (A) at 60 minutes.

Bars represent the mean of the percent of cells with organized microtubules. Error bars are standard deviation (n=100, N=3). D is DMSO, B is BCI. P values were determined using a two-sided Fisher's exact test. **(C)** Quantification of ciliary lengths of cells in (A) pretreated with DMSO or 20 μM BCI. The averages from each trial are plotted on top of the individual data points. Error bars are mean with the 95% confidence interval for the mean from each trial (n=30, N=3). (**D**) Cells were pretreated with DMSO or 15 μM PTX for 60 minutes and then regenerated with or without PTX with the addition of either DMSO or 20 μM BCI for 2 hours. Graphed is the ciliary length quantification. Error bars are mean with 95% confidence for the averages from each trial (n=30, N=3). P values were determined for the 2 hour time points using a two-way ANOVA with Tukey's correction. **(E)** Quantification of recovered β-tubulin reorganization at 2 hours in DMSO or 20 μM BCI with or without 15 μM PTX. Error bars are mean with standard deviation (n=100, N=3). The P value was determined using a two-sided Fisher's exact test.

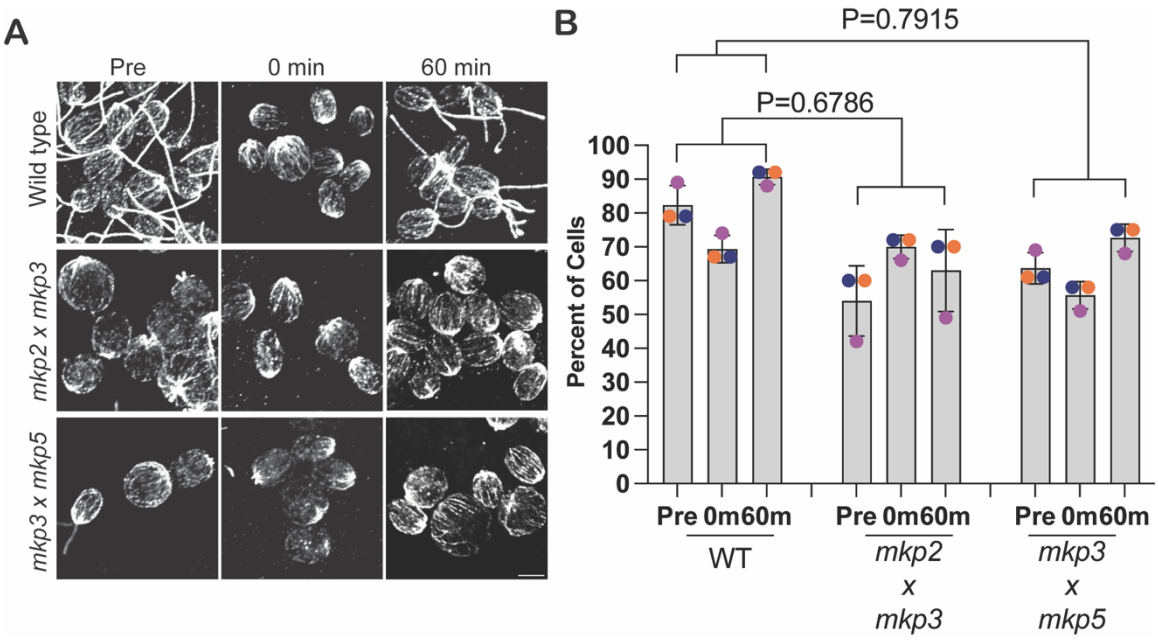

Figure 2.S4. *Chlamydomonas* DUSP6 ortholog double mutants do not exhibit microtubule polymerization defects. (**A**) *Chlamydomonas* DUSP6 ortholog double mutants were regenerated and stained for β-tubulin . Scale bar is 5 µm. (**B**) Quantification of (A). The mean number of cells over 3 trials is plotted with standard deviation (n=100, N=3). P values compare the pre and 60 minute full microtubule quantifications between wild type and each mutant. The P values were calculated using a two-sided Fisher's exact test.

DISCUSSION

In this study, we have explored mechanisms of action related to ciliogenesis for the DUSP6 inhibitor, BCI, in order to better understand how ERK can regulate ciliogenesis along with the cell cycle. Previous work has shown that silencing the MAPK pathway with MEK1/2 inhibitors can lengthen cilia (Avasthi et al., 2012; S. Wang et al., 2013), and here, we show that through inhibiting the pathway with DUSP6 inhibition, cilia cannot elongate. While effects on disassembly remain a possibility, the striking inability to increase from zero length upon deciliation and the effects on anterograde IFT through the TIRFM assays suggest a potent effect on assembly (**Fig 2.2**).

By dissecting various processes related to stages of ciliogenesis including ciliary protein synthesis, intracellular membrane and protein trafficking to basal bodies, ciliary gating, and IFT dynamics, we find it likely that activation of the ERK pathway via MKP inhibition has multiple touchpoints that ultimately affect ciliogenesis. The broad range of these effects is somewhat expected considering the quantity and diversity of known ERK targets within cells. We have several possible explanations based on the data to explain why cilia cannot grow in the presence of BCI (**Fig 2.7**). While KAP-GFP can still be recruited to the basal bodies, its entry is inhibited in regenerating cilia in the presence of BCI, and we have shown that its synthesis is significantly decreased. This data suggests that (1) there could be modifications to existing KAP-GFP in BCI treatment that prevent its entry in ciliogenesis and which slow its kinetics in the cilia and/or (2) the transition zone is altered to prevent KAP-GFP entry.

NPHP4, a protein with important function for ciliary gating, has decreased localization to the transition zone in the presence of BCI. While localization is altered at a concentration of BCI which shortens cilia partially, the physical structure is unaltered (**Fig 2.4**). The structure could be altered on a finer scale that is not detectable with the techniques employed in this work. The decrease in NPHP4 suggests that there are likely other proteins decreased at the transition zone in a BCI dependent manner such as proteins including NPHP1 with which it directly interacts (Gonçalves & Pelletier, 2017). These proteins may be involved in directly regulating which proteins can enter and exit

the cilium, and their absence may slow any movement of proteins into and out of the cilium. It is also possible that MAPK activation results in a phosphorylation cascade which regulates NPHP4 modification, such as through direct phosphorylation, to regulate its localization rather than its protein synthesis. Previous work has shown that phosphorylation of the transition zone protein Tctex1 can promote ciliary disassembly and cell cycle progression (Li et al., 2011). Expression or localization of other proteins in the transition zone may be altered under these conditions.

In addition, we found that ERK activation through BCI causes a membrane trafficking defect. Previous work has shown that inhibition of Golgi-derived membrane induces ciliary shortening through Golgi collapse (Dentler, 2013). The epistatic ciliary shortening in BFA and BCI together suggests that BCI may create an additive effect on the Golgi that may disrupt protein and membrane trafficking for ciliogenesis from a source separate from the Golgi which is supported by the defects in endocytosis as measured by actin puncta. While the electron microscopy images of the Golgi in BCI did not appear altered, there could be defects that are not visible with this method.

Our data also provides evidence that while BCI inhibits re-establishment of cytoplasmic microtubules that are typically disrupted upon ciliary regeneration, PTX stabilization of these microtubules does not rescue this defect suggesting that the BCI ciliogenesis defect is not caused by impaired intracellular trafficking on microtubules (**Fig 2.6**). Impaired microtubule re-establishment may reduce paths for KAP-GFP dissipation or cycling on microtubules, trapping it at basal bodies (**Fig 2.3A**). Altered cytoplasmic microtubule dynamics may similarly affect additional proteins needed for ciliary assembly, resulting in the ultimate ciliogenesis defect in BCI. Lack of these protein highways could also prevent mRNA from localizing to its intended area for adequate protein synthesis of precursor proteins required for ciliogenesis. Constitutive ERK activation could also induce negative feedback loops that prevent transcription as well which could inhibit mRNA formation.

Previous work has provided evidence that microtubule dynamics are required for ciliary assembly in *Chlamydomonas* and destabilization was proposed to be for the purpose of freeing up tubulin for ciliary assembly (Wang et al., 2013). However,

microtubule stabilization with paclitaxel before deciliation and the subsequent normal ciliary regrowth suggests that microtubule destabilization is not needed for ciliogenesis (**Fig 2.6D-E**). In this study, we used a concentration of paclitaxel (15 μM) that was just low enough to induce stabilized microtubules. It has been shown that lower concentrations of paclitaxel induce G1/G2 arrest whereas higher concentrations induce mitotic arrest (Giannakakou et al., 2001). Similarly, we could be seeing a differential effect for paclitaxel on ciliogenesis where lower concentrations allow ciliogenesis to continue despite the processes induced in parallel with microtubule stabilization. In addition, while the percentage of cells with intact microtubule arrays were reduced in double mutants ("pre" in wild type cells vs "pre" in double mutants) (**Fig 2.S4B**), microtubules in double mutants were able to reorganize to their pre-deciliation levels in double mutants. While microtubule integrity may be globally affected by impaired MKP function, cytoplasmic microtubule reorganization following deciliation is not affected to the degree seen for BCI treatment. This suggests the BCI has additional effects beyond what is recapitulated by these specific MKPs.

While BCI does not inhibit various other FGF inhibitors or related phosphatases including Cdc25B, PTP1B, and Dusp3/VHR in zebrafish, in *Chlamydomonas*, our various experiments identify effects of BCI not entirely recapitulated by single or even double MKP mutants. This suggests there are likely additional MKP or off-target effects of the drug.

Together, we have found mechanisms contributing to ciliary defects which could be the foundation of various ciliary diseases. The cilium acts as a major signaling hub in the cell to regulate cellular activities. When this structure cannot form and function properly, important signals cannot be transmitted throughout the cell. Cilia are normally resorbed for division and then reassembled during G1/G0. BCI could arrest cells at the interphase checkpoint or induce cell cycle arrest which could inhibit protein synthesis to shift ciliary assembly to disassembly. As shown in **Figure 1F**, the double ortholog mutants mkp2 x mkp3 and mkp3 x mkp5 do not respond to BCI with an increase in pMAPK expression unlike mkp2 x mkp5 and the ortholog single mutants. It has previously been shown that while pMAPK is not necessary for cell division in

Drosophila, it is required for cell growth (Majumdar et al., 2010). Without this signal being generated, these cells may be stuck in cell division which does not allow for ciliogenesis. Constant ERK activation can also lead to negative feedback to regulate this signal for cell cycle progression (Fritsche-Guenther et al., 2011). The ERK pathway has not been fully elucidated in *Chlamydomonas*, but it is possible that these similar mechanisms are in place for MAPKs. Further work is needed to identify the precise cause of completely inhibited cilium growth from zero length. Regardless, the insight provided here can help to provide a basis for understanding more broad mechanisms for how ciliopathies or manipulated cilia can drastically alter the fate of the cell.

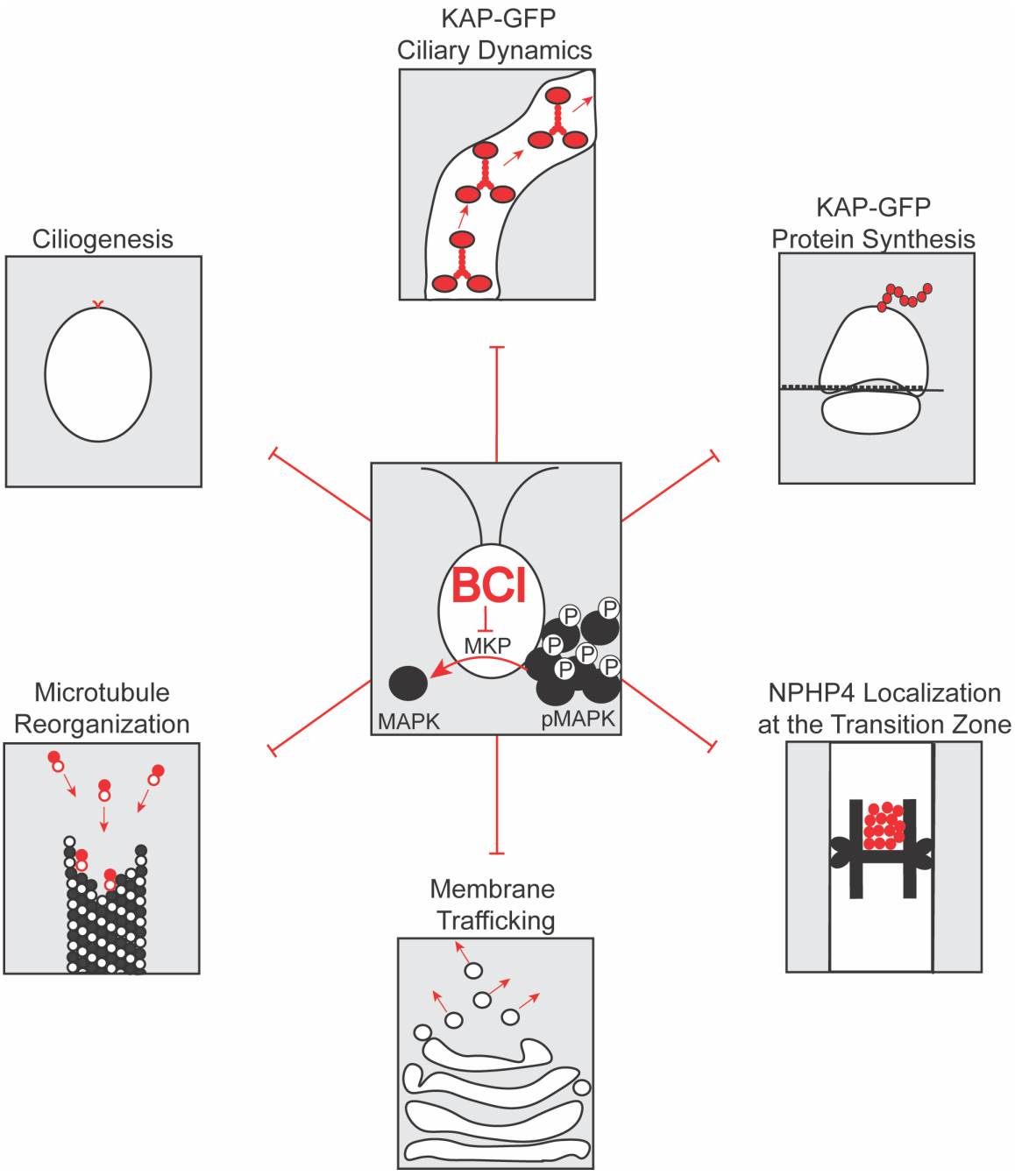

Figure 2.7. Summary of BCI effects in the cell. BCI inhibits phosphate removal from MAPK. This ultimately alters or inhibits ciliogenesis, KAP-GFP dynamics in cilia, KAP-GFP protein synthesis, NPHP4 protein localization at the transition zone, membrane trafficking, and microtubule organization.

MATERIALS AND METHODS

Strains and Maintenance:

The wild type strain (CC-5325), NPHP4-HAC, KAP-GFP, *mkp2* mutant (LMJ.RY0402.168348), *mkp3* mutant (LMJ.RY0402.191934), and *mkp5* mutant (LMJ.RY0402.083264), and Arl6 strain were acquired from the *Chlamydomonas* Resource Center (X. Li et al., 2019). *Chlamydomonas* cells were grown on 1.5% Tris-Acetate-Phosphate (TAP) agar plates in constant light (Helloify BR30 LED Plant Grow Light Bulb, 9W, 14umol/s blue and red light). Cells were inoculated in liquid TAP and grown in constant light and agitation 18 hours prior to experiments.

The human TERT-RPE1 cells were a gift from Chris Shoemaker at Dartmouth College, Hanover, NH. These cells were maintained in Dulbecco's Modified Eagle Medium (DMEM, Corning MT10013CV) with 10% fetal bovine serum (FBS) and 10 µg/mL Hygromycin B (InvivoGen) at 37˚C in 5% CO_2. To induce ciliogenesis, cells were grown to 80% confluency and then serum starved in DMEM with 0.5% FBS for 48 hours at 37˚C, 5% CO_2 prior to experiments.

Crosses:

Crossings were carried out according to (Tulin, 2019) with slight modifications. *Mkp2, mkp3*, and *mkp5* mutants were each mated with a mating-type positive KAP-GFP strain to generate positive mutants. Screened positive mutants were then crossed to the original single mutants. Briefly, strains were separately placed in M-N for 8 hours under constant illumination, combined and grown at a slant overnight under constant light. The pellicle was pipetted onto 4% agar plates, spread, and kept dark for at least 5 days. Zygospores were moved onto 1% TAP plates and let split into tetrads overnight before being split, grown, and screened for genotypes and ciliary phenotypes.

Genotyping:

A single colony of *Chlamydomonas* cells were placed in chelex beads, boiled at 90˚C, and then spun down at 550xg, 1min. This template was used along with 1x DreamTaq Buffer (Invitrogen), 2 mM dNTPs (NEB), 0.5 µM forward and reverse primers (IDT), and Dream Taq Polymerase (Invitrogen). PCR parameters were used according to the *Chlamydomonas* Resource Center. DNA was mixed with 6x loading dye to 1x (Invitrogen) and run on a 1% agarose gel in TBE with 1x SYBR Safe DNA Gel Stain (Invitrogen, S33102) and imaged on a Bio-Rad ChemiDoc MP.

Primers*:*

mkp2 mutant forward primer: CTGCGGACATCAGCTCAAT

mkp3 mutant forward primer: CAAGAGCACCTGGCACAGGAG

mkp5 mutant forward primer: TCGTGACAGACCTGCAGAG

CIB1 reverse primer: CCGAGGAGAAACTGGCCTTCT

Ciliary Length Experiments:

Steady state cells were grown in liquid TAP under constant light and agitation for 18 hours and then treated with >1% DMSO or BCI (Sigma, B4313-5MG) for 2 hours. Samples were collected in equal volumes of 2% glutaraldehyde and allowed to settle before imaging. To measure cilia, 3uL of settled cells were placed directly on a slide with a coverslip and imaged at 40x magnification with a Zeiss Axioscope 5 DIC and Zeiss Zen 3.1 software (blue edition). One cilium per cell was measured with the segmented line tool and fit spline for 30 cells per time point.

Regenerating cells were grown in liquid TAP under constant light and agitation for 18 hours and then pH shocked for 45 seconds with 0.5M acetic acid to bring the culture pH=4.5 and then brought back up to pH=7.0 with 0.5M potassium hydroxide. These cells were immediately centrifuged at 550xg for 1 minute and supplied new TAP

with or without drugs. Samples for DIC imaging were collected in equal volumes of 2% glutaraldehyde.

TIRF Microscopy and Quantification:

Cells were treated with 0.5% DMSO or 30 μM BCI for 2 hours, staggered to allow time for imaging at both 1 hour and 2 hours of treatment. KAP-GFP cells were placed on a poly-lysine treated coverslip and diluted 1:100 in TAP. Cells were imaged with a 100x oil immersion objective on a Nikon Eclipse Ti microscope with two Andor 897 EMCCD cameras suing the 499nm laser line. Data was collected and kymographs generated in NIS Elements Software.

Quantifications were carried out on the kymographs in FIJI. KAP-GFP trains (groups of KAP-GFP molecules) are indicated by the fluorescing slants in the kymograph. For frequency measurements Frequency = (number of trains)*(Frames per second/total frames measured). For velocity: Velocity = (tanθ in radians of train relative to the basal body)*(Frames per second)*(um/pixel conversion). For injection size (fluorescent intensity of a train), kymographs were background subtracted with rolling ball radius and a line thick enough to cover the largest GFP signal was drawn over each train from the basal bodies to the tip of the cilium and then normalized.

Immunofluorescence and Quantification:

KAP-GFP immunofluorescence and quantification: Cells were adhered to poly-lysine coated coverslips for 2 minutes and then permeabilized in cold (-20˚C) methanol for 10 minutes, replacing the methanol once after 5 minutes. Coverslips were allowed to dry and then mounted with Fluoromount G (Thermo Scientific) and imaged with 100x oil immersion objective on a spinning disk confocal microscope (Nikon Eclipse Ti-E with Yokogawa 2-camera CSU-W1 spinning disk system and Nikon LU-N4 laser launch) with the 488nm laser and collected with NIS Elements Software. To quantify basal body fluorescence and cilia fluorescence, summed slice projections were collected using FIJI

for each image stack and background subtracted with rolling ball radius. An equal size circle was drawn around the basal bodies across one trial and the area, mean gray value, and integrated density measurements were collected for each time point or treatment group. The total cell fluorescence was calculated using the calculation for corrected total cell fluorescence (CTCF=IntDen-([Area of selection]*[background mean grey value]). Background mean grey values were calculated by taking the average of 3 random background measurements per image. For cilia measurements, the selection area involved drawing a tight area around the cilia for one cilium per cell per time point or treatment. The length of the cilia was measured alongside the fluorescence measurements and plotted against each other (**Fig 2.2C**).

Microtubule immunofluorescence and quantification: Staining was performed similarly to Wang et. Al, 2013. Cells were adhered to poly-lysine coverslips, fixed in microtubule buffer (30 mM HEPES [pH=7.2], 3 mM EGTA, 1 mM $MgSO_4$, 25 mM KCl) containing fresh (<1 month opened) 4% PFA for 5 minutes, incubated in microtubule buffer with 0.5% NP-40 for 5 minutes, and then permeabilized in cold (-20˚C) methanol for 5 minutes. Coverslips were placed in a humidified chamber and blocked in 5% BSA and 1% fish gelatin for 30 minutes and 10% normal goat serum in block for 30 minutes. Coverslips were then incubated overnight at 4˚C with primary antibody (B-tubulin, CST 2146S, 1:100) in 20% block in 1x PBS. Washes were done with 1x PBS, 3x10 minutes and coverslips were placed back in humidified chamber with secondary antibody (Alexa Fluor 488 goat anti-rabbit IgG, Invitrogen A11008, 1:500) for 1 hour covered. Coverslips were washed 3x10 minutes covered and allowed to dry completely before mounting with Fluoromount G and imaging on a spinning disk confocal microscope. Microtubule quantification was performed as described in **Figure 6** where 100 cells total were counted and assigned to have either no microtubules, partially visible microtubules, or full microtubules according to the staining. Cells were counted using the cell counter plugin in FIJI.

Phalloidin Staining: Phalloidin staining was performed according to Craig and Avasthi, 2019. Cells adhered to coverslips for 2 minutes and were fixed with fresh 4% PFA in 7.5 mM HEPES in 1x PBS for 15 minutes, washed in 1x PBS for 3 minutes,

permeabilized in cold (-20˚C) 80% acetone for 5 minutes and then 100% cold acetone and allowed to air dry. Coverslips were rehydrated in 1x PBS for 5 minutes and incubated with Atto-488 Phalloidin (Sigma, 49409-10Nmol) for 16 minutes and then washed in 1x PBS for 5 minutes, covered (Craig & Avasthi, 2019). Coverslips were air dried, mounted in Fluoromount G, and imaged at 100x on the spinning disk confocal microscope. For dot quantification, max intensity projections were generated for each image stack and dots per cell counted using FIJI's cell counter plugin.

Membrane Staining: Membrane staining was performed according to Bigge et al., 2023. Cells were treated with 0.5% DMSO or 30 μM BCI for 2 hours and then adhered to coverslips for 2 minutes. Coverslips were moved to ice and 200 μg/mL membrane dye (FMTM 4-64FX, fixable; Thermo, F34653) for 1 minute covered, fixed with 4% PFA in 1x HBSS for 10 minutes, and washed 3x3 minutes in 1x PBS (Bigge et al., 2023). Coverslips were air dried and mounted to slides with Fluoromount G and imaged on the spinning disk confocal microscope. For quantification, summed slice projections were created and processed as described in KAP-GFP staining. The area selection measured encompassed an entire cell for 10 cells per image, 3 images per treatment and time point, across 3 trials.

RPE1 cilium staining: Staining was performed according to Alsolami et al., 2019. Cells were seeded on chamber slides and grown to 80% confluency before serum starving in DMEM with 0.5% FBS for 48 hours. Media was removed and cells were washed with 1x PBS, fixed in cold (-20˚C) methanol for 10 minutes and washed once more in 1x PBS for 5 minutes. Cells were blocked in 1x PBS with 0.2% Triton X-100 (PBX) at 37˚C for 5 minutes and then in PBX with 3% BSA for 30 minutes at 37˚C. Slides were moved to a humidified chamber with primary antibody (anti-acetyl-alpha tubulin, clone 6-11B-1, Sigma, MABT868) diluted in PBX (1:250) added for 1 hour at room temp. Slides were washed 3x5 minutes in PBS and placed back in a covered humidified chamber. Secondary antibody (Alexa Fluor 488 goat anti-mouse IgG, Invitrogen, A11001) was diluted in PBX (1:500) and added to coverslips for 1 hour at room temp. Slides were washed 3x5 minutes in PBS, mounted with Flouromount G, and imaged with 60x and 100x oil immersion objectives on the spinning disk confocal (Alsolami et al., 2019). Max

intensity projections were created in FIJI for each image, and primary cilia were measured using the segmented line tool for the acetylated tubulin staining.

SDS-PAGE and Immunoblotting:

RPE1 cells were washed with cold 1x HBSS and then placed on ice with RIPA buffer + 10x phosphatase inhibitors for 20 minutes with agitation after 10 minutes. Cells were scraped and placed into a tube and spun at 21,000xg, 10min, 4˚C. The lysate was mixed with 4x loading buffer (Invitrogen) and BME to 10%, boiled at 95˚C for 10 minutes, and run on a 10% bis-tris gel for 2 hours before transferring to a PVDF membrane and blocked for 1 hour in TBS-T and 5% BSA. The primary antibody (Phospho p44/42 MAPK (Erk1/2) (Thr202/Tyr204) Antibody #9101, CST) used for both RPE1 and *Chlamydomonas* was diluted 1:1000 in TBS-T and incubated with blots overnight at 4˚C. Blots were washed 3 times in TBS-T and incubated with secondary antibody (Goat anti-rabbit IgG HRP conjugate, Invitrogen, G21234) for 1 hour at room temp. Blots were washed 3x10 minutes in TBS-T and then incubated with pico chemiluminescent substrate (Invitrogen) and imaged on a Bio-Rad ChemiDoc MP.

Chlamydomonas cells were centrifuged at 550xg for 1 minute. The supernatant was removed and replaced with 100uL of glass beads (425-600 μm) and 100 μL lysis buffer (1% NP-40, 9% TAP, 5% glycerol, 1mM DTT, 1x protease and phosphatase inhibitors per 1mL of cells spun down. Cells were bead beated 3x1 minute with 1 minute breaks on ice and then centrifuged at 21,000xg for 15 minutes at 4˚C. The supernatant was collected and mixed with DTT and LDS Sample Buffer (Invitrogen), and boiled at 70˚C for 10 minutes. Protein was run on 10% Bis-tris gels (Invitrogen) at 150V and transferred onto a nitrocellulose or PVDF membrane.

To probe for KAP-GFP, blots were incubated with 5% milk and then probed with GFP antibody (CST, 1956S) in 1% milk +BSA overnight at 4˚C. Blots were washed 3x10 minutes in PBS-T and incubated with secondary antibody (goat anti-rabbit IgG HRP conjugate, Invitrogen, G21234) diluted in 1% milk +BSA (1:5000) for 1 hour at room

temp. Blots were washed 3x10 minutes in TBS-T and then incubated with pico chemiluminescent substrate (Thermo) and imaged on a Bio-Rad ChemiDoc MP.

Electron Microscopy:

Electron microscopy was performed by Radu Stan according to a protocol by Dentler and Adams 1992. Wild type cells were treated with 30 µM BCI or 0.5% DMSO for 2 hours and then diluted in equal volumes of fresh, EM-grade 2% glutaraldehyde diluted from 16% in water (Electron Microscopy Sciences). Cells settled at room temperature and the supernatant was removed and cells were resuspended with 1% glutaraldehyde with 50 mM sodium cacodylate overnight at 4˚C. The supernatant was removed and cells were spun 3x1 minute at 600xg with 50 mM sodium cacodylate washes and then fixed and imaged with a Helios Scanning Electron Microscope 5CX with a STEM3+ detector (Dentler & Adams, 1992).

Statistical Analysis:

Data collection and statistical calculations were completed in GraphPad Prism Version 9.2.0 (283). Super plots were generated according to (Lord et al., 2020). In figure legends, n refers to individual measurements made across one trial, and N refers to the number of trials performed. Geneious Prime 2022 was used to generate the phylogenetic tree and sequence alignment (**Fig 2.S1D-E**). *Chlamydomonas* sequences were generated from Phytozome 13 (Goodstein et al., 2012). To determine significance, values with $P<0.05$ are considered significant.

Data Availability:

This study includes no data deposited in external repositories

Table 2.1. Tools and Reagents

Reagent	**Source**	**Identifier**
Strains		
Wild type	*Chlamydomonas* Resource Center	CC-5325
mkp2	*Chlamydomonas* Resource Center	LMJ.RY0402.168348
mkp3	*Chlamydomonas* Resource Center	LMJ.RY0402.191934
mkp5	*Chlamydomonas* Resource Center	LMJ.RY0402.083264
NPHP4-HAC	*Chlamydomonas* Resource Center	CC-5115
KAP-GFP	*Chlamydomonas* Resource Center	CC-4296
RPE1 cells	Gift from Chris Shoemaker, ATCC	CRL-4000
Antibodies		
DAPI	Biotium	40043
Rat anti-HA (for NPHP4)	Sigma	11867423001
Atto-Phalloidin 499	Sigma	49409-10Nmol
Phospho p44/42 MAPK (Erk1/2) (Thr202/Tyr204)	Cell Signaling Technology	9101

p44/42 MAPK (Erk1/2)	Cell Signaling Technology	9102
Membrane Stain (FMTM 4-64FX, fixable)	ThermoFisher	F34653
β-Tubulin Antibody	Cell Signaling Technology	2146S
GFP (D5.1) Rabbit mAb	Cell Signaling Technology	2956S
SYBR-Safe DNA Gel Stain	Invitrogen	S33102
Alexa Fluor 488 goat anti-rat IgG	Invitrogen	A11006
Alexa Fluor 488 goat anti-rabbit IgG	Invitrogen	A11008
Alexa Fluor 488 goat anti-mouse IgG	Invitrogen	A11001
Goat anti-rabbit IgG HRP conjugate	Invitrogen	G21234
Oligonucleotides		
mkp2 mutant forward primer: CTGCGGACATCAGCTCAAT	This paper	N/A
mkp3 mutant forward primer: CAAGAGCACCTGGCACAGGAG	This paper	N/A
mkp5 mutant forward primer: TCGTGACAGACCTGCAGAG	This paper	N/A
CIB1 reverse primer: CCGAGGAGAAACTGGCCTTCT	This paper	N/A

CHAPTER 3:

BCI induces changes to the ciliary proteome and increases ubiquitination of cell body proteins in *Chlamydomonas reinhardtii*

This chapter has not been published. Arminja Kettenbach and Lauren Cressey performed mass spectrometry data collection and analysis. This work is incomplete but had very interesting patterns that are informative for understanding downstream targets of BCI. Larissa L Dougherty performed study conceptualization, data curation, formal analysis, investigation, methodology, project administration, validation, visualization, writing – original draft, and writing. Prachee Avasthi performed study conceptualization, formal analysis, funding acquisition, investigation, project administration, resources, software, supervision, and visualization.

We thank the Kettenbach Lab for mass spectrometry data collection and analysis and Radu Stan for preparation of the *Chlamydomonas* histology sections. We would also like to thank Ann Lavanway at the Dartmouth Imaging Facility for helping with immunofluorescence imaging, the BioMT Core at Dartmouth (funded by NIH NIGMS grant P20-GM113132) and Genomics and Molecular Biology Shared Resources Core at Dartmouth (funded by NCI Cancer Center Support grant 5P30CA023108-37) for use of equipment. This work was funded by NIH MIRA R35GM128702(PA).

INTRODUCTION

Ciliary disassembly is an important process that is tied to cell cycle reentry following quiescence (Quarmby & Parker, 2005; Tucker, Pardee, et al., 1979; Tucker, Scher, et al., 1979). Defects in ciliary disassembly, both through inhibition and increased disassembly result in various ciliary diseases including kidney cysts, polydactyly, and brain development defects (Bielas et al., 2009; Jacoby et al., 2009). Additionally, components in this process are often manipulated to promote cancer progression through enhanced cell proliferation by preventing cell cycle exit (S. Kim & Tsiokas, 2011).

This process, involving disassembling the axoneme, can occur through various signaling pathways and ultimately leads to the activation of the master disassembly regulator, aurora kinase A (AURKA) which activates the histone deacetylase HDAC6 to induce deacetylation of ciliary tubulin and ultimately feeds forward to ciliary disassembly (Kim et al., 2015). Alongside this disassembly signaling is activation of the kinesin-13 family members which disassemble the microtubule axoneme of cilia (Reilly & Benmerah, 2019). This pathway can be regulated through stability of various components in the pathway including stability of AURKA signaling through the NEDD9 scaffold as well as through post translational modifications such as ubiquitination (Ice et al., 2013).

Ubiquitin is a conserved peptide which is added to other proteins as a post translational modification to regulate protein fate (Sharp & Li, 1987). For a protein to be ubiquitinated, an activating enzyme (E1) will ligate to the ubiquitin peptide and transfer this peptide to a conjugating enzyme (E2). The E2 enzyme along with a ligase (E3) will then transfer the ubiquitin peptide to the target substrate (Pickart, 2001). Following ubiquitination, proteins can be targeted for degradation (Hough et al., 1986) or alternatively trafficked to other areas of the cell to participate in other processes (Hicke & Dunn, 2003; W. Li & Ye, 2008).

During ciliogenesis, ubiquitination of proteins can directly regulate ciliary assembly and disassembly. For example, this process can prevent ciliary disassembly through ubiquitination of NEDD9 which inhibits signaling for disassembly and increases

its proteasomal degradation (Ice et al., 2013). It has also been found that during ciliary shortening through increased tonicity, changes to ubiquitinated ciliary proteins increases which facilitates protein exit from the cilia (Huang et al., 2009; Shinde et al., 2020). Ubiquitin is also necessary for removing proteins that can stall ciliogenesis. CRL3-KCTD17, an E3 ligase, is necessary to target trychoplein, a protein localized at the centrioles and activates AURKA (Inoko et al., 2012), to the proteasome through trychoplein ubiquitylation to allow axonemal extension (Kasahara et al., 2014). In addition, the centrosomal protein CP110 is ubiquitinated for removal from the mother centriole to also allow for ciliogenesis (Shen et al., 2022). It has also been found that during ciliary shortening through increased tonicity, changes to ubiquitinated ciliary proteins increases which facilitates protein exit from the cilia (Huang et al., 2009; Shinde et al., 2020). Ubiquitination is clearly important for regulating cilia and new ciliary proteins and signaling pathways regulated through ubiquitination are still being discovered.

In our previous work, we find that dual specificity protein phosphatases (DUSPs) which regulate the MAP kinases activated by BCI-induced phosphatase inhibition in *Chlamydomonas* induce ciliary resorption through regulating various cellular processes. In this work, we induce ciliary shortening through the DUSP6 inhibitor, BCI, and investigate changes to ciliary proteins with the most significant changes in expression. Using mass spectrometry, we find that BCI changes expression of flagellar associated proteins with previously uncharacterized roles in ciliogenesis or ERK regulation. In addition, we find that BCI treatment increases cellular vacuoles and ubiquitin patterns which have not previously been implicated in regulating ciliogenesis under ERK regulation. Together, these data provide targets for BCI-induced ciliary disassembly which can aid future work in identifying molecular mechanisms for ERK-regulated ciliogenesis.

RESULTS AND DISCUSSION:

BCI increases accumulation of ~55kDa protein in ciliary lysates

We previously established that BCI induces ciliary resorption in *Chlamydomonas* (Dougherty et al., 2023). To better understand the targets of BCI with regards to ciliary shortening, we treated cells with DMSO (control) or 20 μM BCI for 2 hours and then isolated cilia from cell bodies (**Figure 3.1A-B**) according to (Craige et al., 2013). Protein lysates were run on SDS-PAGE and probed for Sypro Ruby gel stain to assess changes in protein content. Comparing band intensities between each condition some noticeable changes in each set. The cell body had increases in band intensities between ~55kDa-110kDa in BCI treated cell lysates (**Figure 3.1A**). The ciliary lysate revealed changes in densities between 160-260 kDa as well as between 30-40 kDa (**Figure 3.1A and B**, red brackets), and there was a very clear, distinct band that showed up at ~55kDa (**Figure 3.1B, red arrows**) in BCI treated cilia only. Proteins identified from cutting out this band from the gel were identified by mass spectrometry (MS) as proteins with higher molecular weights than 55kDa which suggests protein degradation. This particular band was identified to most likely be Rib72 (fold change in BCI:DMSO was 152 compared to the next two highest proteins of 5-methyltetrahydropteroyltriglutamate--homocysteine S-methyltransferase (METE) at 75.75 and Elongation factor Tu (EIF2G) at 68.22), but more analysis needs to be done to confirm that this is indeed the protein accumulating at this spot. Rib72 has 636 amino acids which is ~70kDa. It is a component of a ribbon compartment that connects A microtubules to B microtubules and radial spokes in the cilium and disintegrates in correlation with the rate of axoneme disassembly (Ikeda et al., 2003). Of the other possible proteins, METE is 816 amino acids and EIF2G is 463 amino acids which could also further indicate other protein degradation as well as increased expression of other proteins near ~55kDa.

Upregulated Proteins in BCI-treated total ciliary lysates include FAP270, proteins involved in ubiquitination, and the vacuolar ATP synthase subunit ATPvA1

Ciliary proteomics of total ciliary lysates revealed that the most upregulated protein is the flagellar associated protein FAP270. While this protein was previously identified in a ciliary proteomics screen, it is unknown functions in ciliary regulation (Pazour et al., 2005). This protein is predicted to be involved in cell motility for cellular processing (Pérez-Pérez et al., 2017), and it has clear ankyrin repeat regions (Goodstein et al., 2012). Ankyrin repeat regions are known to assist in protein-protein interactions which has a wide array of implications in the cell including in the ubiquitylation signaling pathway (USP) (Kane & Spratt, 2021).

Several additional proteins involved in the USP were also upregulated including ubiquitin itself (UBQ1 and UBQ2), a ubiquitin fusion ribosomal protein RPL40, and the small ubiquitin-like modifier SUM1 (Goodstein et al., 2012). It would be no surprise if BCI-induced signaling induces ciliary resorption through ubiquitination of proteins. It has previously been found that ubiquitination of ciliary proteins increases in resorbing *Chlamydomonas* cilia, especially of higher kDa proteins (Huang et al., 2009). Other upregulated proteins can be found in **Table 3.1**.

Another highly upregulated protein in this set is ATPvA1, a subunit of the vacuolar synthase subunit. A vacuolar H+-ATPase has been found previously to operate in the ocular ciliary epithelium where it can directly regulate ocular pressure through ion transport. Distribution of this protein can be altered due to small molecules and drugs which can ultimately impact aqueous humor production (Wax et al., 1997). In zebrafish, SNX10 is a protein with vacuolation activity and interacts with V-ATPase to target it to the centrosome to initiate ciliogenesis by regulating trafficking rab8, a protein important for membrane extension (Chen et al., 2012). It would be interesting to understand if the *Chlamydomonas* ATPvA1 subunit can regulate ciliogenesis as well either through similar mechanisms or new mechanisms, and what the function of larger vesicles is during these cell changes.

In addition to changes in protein expression between BCI treated ciliary lysates and control cells in DMSO, there were also proteins that were only found in one condition. Protein translocation and trafficking into/out of the cilium is one way that cells can regulate cell signaling and development. For example, in hedgehog (Hh) signaling, smoothened (Smo) translocates to the cilium to signal for cell development of most mammalian organs. Lack of Smo entry abolishes Hh signal transduction and ultimately disrupts development including left/right asymmetry (Y. Wang et al., 2009; Zhang et al., 2001). In addition, localization of the flagellar autotomy protein, Fa2p, is highly dynamic throughout the cell cycle. During cell cycle reentry, Fa2p becomes localized at the basal bodies, but during cell cycle exit and ciliogenesis, Fa2p moves to cilia where it is required for deciliation (Mahjoub et al., 2004). These dynamic changes could occur to other proteins that are important for cilia and cell cycle regulation, and BCI treatment could alter this localization to either allow proteins or prevent proteins from entering the cilium.

We compared top 10 most abundant proteins in the set that were found only in BCI-treated cells. Of these 10 proteins, 6 were cytosolic small ribosomal subunit proteins (RPS), and 3 were cytosolic large ribosomal subunit proteins (RPL) with one protein uncharacterized. Interestingly 8/10 of these proteins have not previously been found in the *Chlamydomonas* ciliary proteome. Incorporation of nonspecific proteins into the cilia could indicate a defect in the ciliary gate, the transition zone (TZ), which maintains tight regulation on the proteins that enter and exit the cilium. In our previous work, we did not notice visible structural differences to the TZ, however we did note a subtle change in the localization of a TZ protein, NPHP4. It would be interesting to know if this subtle change and/or other changes to the ciliary gate could be causing this disruption in normal contents (**Table 3.4**).

Downregulated Proteins in BCI-treated total ciliary lysates include FAP173 and a notchless-like WD40 repeat-containing protein

The most downregulated protein in BCI-treated cilia is the flagellar associated protein FAP173, partially characterized previously. FAP173 was found to colocalize in the middle region of regenerating cilia separated from IFT machinery (Lechtreck et al., 2009). Though this protein is predicted to not have a role in IFT, its downregulation suggests that this likely has some other role in maintaining cilia. Whether this is a role in stability, defining the middle region, or some other compartment needs to be assessed to better understand the function of this protein.

The second most significantly downregulated protein, Cre08.g382620, is also currently uncharacterized. This protein is predicted to be a notchless-like WD40 repeat-containing protein and contains many WD40 regions (Goodstein et al., 2012). These WD40 regions are ~40 amino acids ending in Trp-Asp that form a beta-propeller structure. These motifs are known to act as protein scaffolds (i.e. G protein Beta subunit or E3 ubiquitin ligase) for other proteins or DNA which ultimately facilitates signal transduction, apoptosis, and the cell cycle (Jain & Pandey, 2018; Li & Roberts, 2001). WDR92, a conserved protein with WD-repeat regions, has been found to function in ciliated organisms specifically as a cytoplasmic chaperone which is required to fold proteins involved in ciliary axonemal extension in Planaria. Knockdown of this protein results in altered cilia structure defects without altering length (Patel-King & King, 2016). Another protein containing WD-repeat regions, WDR35/IFT121, is necessary for building functional cilia due to its important role in regulating IFT transport to cilia as well as ciliary entry (Quidwai et al., 2021). Dissecting the role of Cre08.g382620 would be very interesting to understand what role it has on regulating components involved in BCI-induced ciliary disassembly. Given that this is a predicted protein in notch signaling, and components of the notch signaling pathway have been known to regulate ciliary assembly, it is possible that this protein may provide additional molecular footholds for understanding ciliary regulation through ERK and notch crosstalk. Other proteins downregulated can be found in **Table 3.2**.

Some proteins were only found in DMSO-treated cells which can be thought of as absent in BCI-treated ciliary lysates (Table 3.3). We compared the top 10 most abundant proteins in the set. While some of these proteins were not yet characterized, several proteins that have been well characterized were present and provide some insight into how these cilia might be differentially regulated in BCI treated cells. One of the top proteins was IFT25. This protein has previously been found in both the ciliary and basal body proteome, though it is not required for ciliogenesis. It is, however required for ciliary exit mediated by the BBsome, a complex that links signaling proteins to IFT machinery for ciliary transport (Dong et al., 2021; Klink et al., 2020). This IFT B complex phosphoprotein subunit has been found to form a complex with the small rab-like GTPase IFT27 which is both essential for ciliogenesis, cell cycle progression, and cytokinesis (Qin et al., 2007; Z. Wang et al., 2009). While we do not have indication of regulation to IFT27 in BCI-treated ciliary lysates, it is possible that the lack of IFT25 could prevent proper functioning of IFT27 or induce signaling of ciliary disassembly and cell cycle progression through inability to form this complex (**Table 3.3**).

GAP2 is another protein found in the DMSO-only dataset. The lack of GAP2 in BCI-treated cells could indicate another role for disrupted membrane trafficking as a result of BCI. The GAP2 human homolog, GAPDH, is recruited by the small GTPase Rab2, and has been found to directly bind to tubulin in the presence of atypical protein kinase C to recruit dynein for participation in retrograde vesicle formation in the secretory pathway (Tisdale et al., 2009). GAP2 has previously been found in the cilia in the membrane matrix fraction (Pazour et al., 2005). It is possible that this protein has roles in providing sources of plasma membrane for ciliogenesis or coordinating the movement of cargo with dynein to regulate ciliary length (**Table 3.3**).

Atx1, another protein found only in DMSO-treated cells, has also been found in cilia in the membrane matrix fraction. This is a copper chaperone which functions in regulating copper homeostasis which is required for plant growth. Excess copper or malfunctioning copper chaperones can lead to cell toxicity through generation of reactive oxygen species (ROS) which cause DNA damage as well as protein and lipid damage (Brewer, 2010; Shin et al., 2012). It would make sense that atx1 would be present in the

cilium in addition to the rest of the cell to offer immediate protection from ROS due to changes in copper concentrations wherever those may occur. In the case of BCI-treated cilia which we assay during disassembly, it may no longer be required in the cilium due to resorption of the organelle and could provide another signaling cue for cell cycle reentry. The timing of atx1 exit from cilia would be interesting to understand. If atx1 is depleted from the cilium at the early onset of ciliary resorption, it is possible that ROS buildup in the cilium could participate in the processes leading to ciliary resorption. For example, if ROS interact with ciliary proteins to induce their misfolding, these proteins could become ubiquitinated to induce ciliary exit and facilitate ciliary shortening. If atx1 exits the cilium later during ciliary resorption, it is possible that this protein must be associate with other components that could be missing from the cilium due to earlier exit of these critical other interacting components at the onset of ciliary resorption. Additionally, atx1 ciliary recruitment could be associated with active ciliary assembly. Upon blocking this protein from the cilium, signaling cascades could be induced that perpetuate ciliary resorption. Without atx1 in the cilium, it would be interesting to see if cilia could be shed due to stress from ROS buildup and if atx1 relocalization could provide a cell cycle reentry signal in addition to its effect on ubiquitination of ciliary proteins (**Table 3.3**).

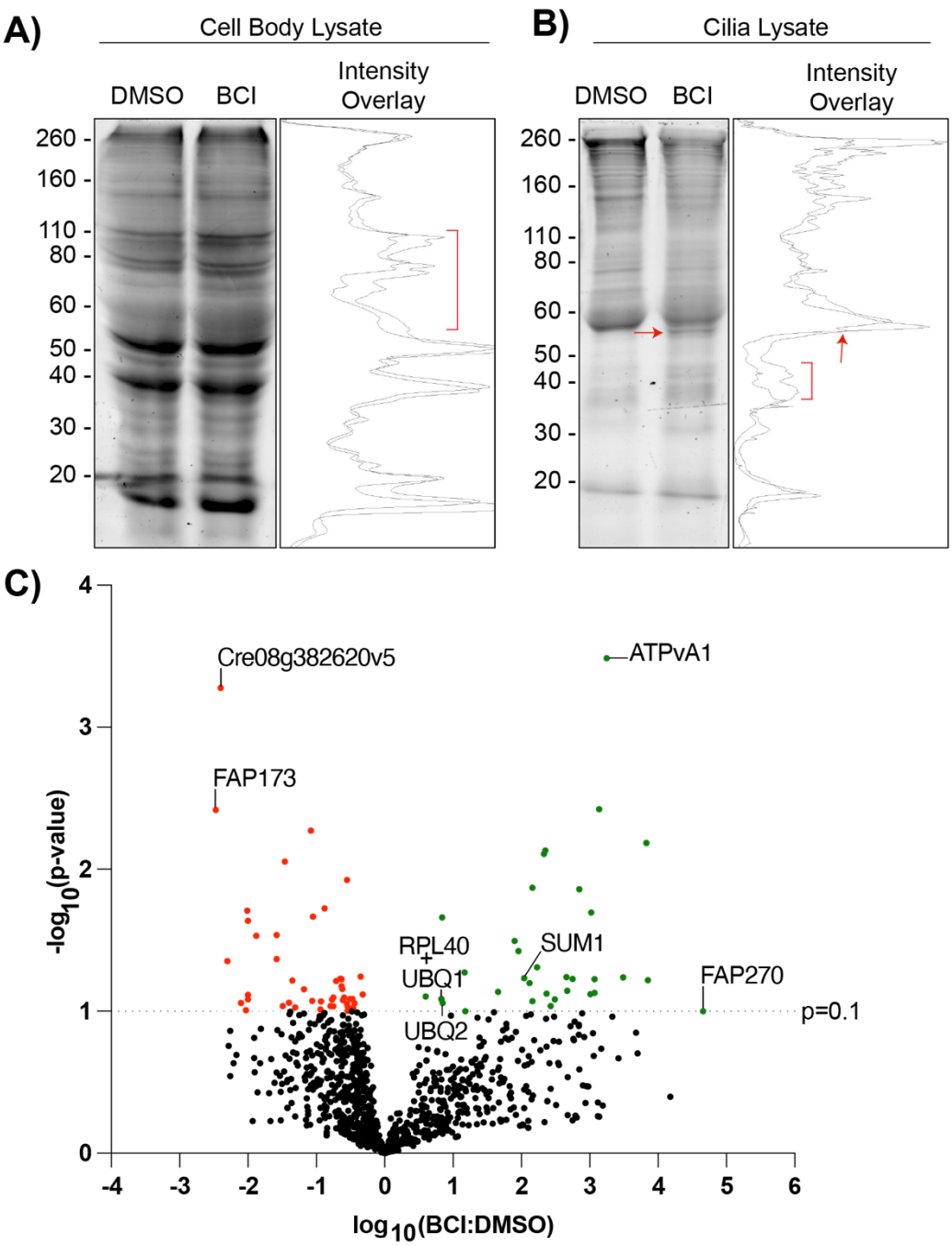

Figure 3.1. Protein expression changes to *Chlamydomonas* ciliary proteomics in BCI. **A-B)** Protein lysates from cell bodies (**A**) separated from cilia **(B)** following a 2 hour treatment in DMSO or 20 μM BCI and separated on SDS-PAGE and gels probed with Sypro Ruby total protein stain. Band intensity graphs are plotted to the right comparing band intensities between treatments. Red arrows indicate an interesting change in band intensity in the ciliary lysates. Red brackets indicate ranges of changed intensities in lysates. **C)** Expression changes to ciliary

proteomics (MS data collection and analysis performed by Arminja Kettenbach and Lauren Cressey). Proteins labeled are highest expression change (FAP270 and FAP173), highest p-value for highest expression change (ATPvA1 and Cre08g382620v5), and proteins implicated in ubiquitin signaling (RPL40, UBQ1, UBQ2, and SUM1) for p-values ≥ 0.1. Red indicates proteins significantly downregulated (left); green indicates proteins significantly upregulated (right). The dotted line at $-\log_{10}$(p-value) indicates p=0.1.

Table 3.1. Upregulated Proteins in BCI-treated cilia lysates:

UniProt Accession	Phytozome Annotation:	BCI/DMSO	p-value	M+M Fraction?	Predicted TM?
A8J7T3_CHLRE	FAP270	4.66	0.10	2	No
A0A2K3DW82_CHLRE	HEL14	3.85	0.06	4	Yes
RBL_CHLRE	rbcL	3.83	0.01	n/a	Yes
A8IUR4_CHLRE	Cre14.g631900	3.49	0.06	3	No
A8I164_CHLRE	ATPvA1	3.25	0.00	1	Yes
A8J3W1_CHLRE	DUF3700	3.14	0.00	n/a	No
A0A2K3DIA9_CHLRE	FAP356	3.07	0.07	4	No
A8JDL5_CHLRE	CYN20-3	3.07	0.06	n/a	Yes
ATPB_CHLRE	atpB	3.02	0.02	n/a	Yes
A0A2K3E787_CHLRE	Cre01.g036400	3.01	0.08	1	No
A8J3E3_CHLRE	PIN4	2.85	0.01	1	No
A8J7C8_CHLRE	TSK1	2.75	0.06	1	No
A0A2K3D937_CHLRE	SAM_1	2.67	0.07	n/a	Yes
A0A2K3CR25_CHLRE	GAL1	2.66	0.06	0	Yes
A8JEV1_CHLRE	PSBQ	2.49	0.08	1	Yes
A0A2K3D661_CHLRE	PSBP1	2.43	0.09	0	Yes
A0A2K3DMI5_CHLRE	GP2	2.37	0.08	0	Yes
A0A2K3DRJ8_CHLRE	HEL31	2.35	0.01	n/a	No

A0A2K3CV60_CHLRE	FAP277	2.33	0.01	3	Yes
A0A2K3E170_CHLRE	PAN3; PANC1	2.23	0.05	n/a	No
A8IP53_CHLRE	SUI1A	2.16	0.08	n/a	No
A8IYW5_CHLRE	Cre12.g541600	2.16	0.01	1	Yes
A0A2K3CQF9_CHLRE	Cre17.g722650	2.12	0.06	n/a	Yes
A8J3A8_CHLRE	SUM1	2.04	0.06	1	No
A8IP37_CHLRE	FAP224	1.96	0.04	5	Yes
A0A2K3DE67_CHLRE	Cre09.g391023	1.90	0.03	0	Yes
A8ITF3_CHLRE	UGP1	1.66	0.07	0	Yes
A0A2K3DDE6_CHLRE	CGLD37	1.18	0.10	3	No
A0A2K3D064_CHLRE	TBA1	1.17	0.05	n/a	Yes
A8IZZ4_CHLRE	UBQ2	0.85	0.09	5	No
A8IHF4_CHLRE	CDPK9	0.84	0.02	5	Yes
A8JCX9_CHLRE	RPL40	0.83	0.08	5	No
A0A2K3D796_CHLRE	UBQ1	0.83	0.08	5	No
A8IL29_CHLRE	FAP332/FAP333	0.60	0.08	3	No

Table 3.1. Upregulated proteins in BCI-treated cilia lysates. Listed from left to right are the UniProt accession numbers, Phytozome annotation for the gene alias referenced from UniProt, the change in protein expression in BCI treated cells compared to DMSO, the calculated p-values for expression, presence of the protein in the membrane matrix fraction ("M+M Fraction?"), and whether there is a predicted transmembrane domain ("Predicted TM?"). For the "M+M Fraction?", n/a means not found in the membrane matrix fraction. Numbers (0-27) indicate abundance of the

protein in the membrane and matrix fraction according to the *Chlamydomonas* Flagellar Proteome Database (http://chlamyfp.org/ChlamyFPv2/index.php) (Pazour et al., 2005).

Table 3.2. Downregulated Proteins in BCI-treated cilia lysates:

UniProt Accession:	Phytozome Annotation:	BCI/DMSO:	p-value	M+M Fraction?	Predicted TM?
A0A2K3CW89_CHLRE	FAP173	-2.47	0.00	1	Yes
A0A2K3DI66_CHLRE	Cre08.g382620	-2.40	0.00	0	Yes
A8IEU5_CHLRE	FAP371	-2.30	0.04	0	No
A0A2K3D3W4_CHLRE	FAP261	-2.10	0.09	0	Yes
A0A2K3CV82_CHLRE	CAM19	-2.03	0.10	0	Yes
A0A2K3DKC8_CHLRE	Cre07.g337582	-2.01	0.02	0	Yes
A0A2K3D2J5_CHLRE	Cre12.g511300	-2.00	0.02	0	Yes
A0A2K3DLJ1_CHLRE	Cre07.g354650	-2.00	0.08	0	Yes
A0A2K3DXC0_CHLRE	Cre03.g175050	-2.00	0.08	0	Yes
A0A2K3CU23_CHLRE	Cre16.g678808	-1.88	0.03	1	Yes
A0A2K3DWR3_CHLRE	PGM17	-1.58	0.03	2	No
A0A2K3D2K7_CHLRE	Cre12.g511350	-1.58	0.04	0	Yes
A8IJV3_CHLRE	FAP288	-1.49	0.09	0	Yes
A0A2K3D9Z2_CHLRE	Cre10.g432770	-1.46	0.01	0	Yes
A0A2K3E1G8_CHLRE	Cre02.g093850	-1.40	0.09	0	Yes
A0A2K3DSC5_CHLRE	DHC6	-1.35	0.06	3	Yes
A4PET3_CHLRE	DII2	-1.31	0.09	0	Yes
A0A2K3CNV7_CHLRE	Cre17.g700200	-1.18	0.07	0	Yes

Q84X70_CHLRE	Cre10.g458550	-1.08	0.01	0	No
A8IY23_CHLRE	FAP 364	-1.06	0.08	1	Yes
A0A2K3DH11_CHLRE	FAP323	-1.05	0.02	0	Yes
A8IUX7_CHLRE	FAP98	-0.94	0.10	0	No
A8JEU9_CHLRE	FAP188	-0.93	0.09	0	Yes
A0A2K3DVV8_CHLRE	FAP347	-0.88	0.02	0	No
A0A2K3DZF0_CHLRE	FAP166	-0.79	0.09	0	No
A8JF23_CHLRE	FAP222	-0.77	0.08	0	No
A8I550_CHLRE	RSP4	-0.75	0.08	0	Yes
A0A2K3DFZ1_CHLRE	FAP351	-0.75	0.09	0	Yes
A8HPK6_CHLRE	FAP68	-0.71	0.06	0	No
A0A2K3D5V4_CHLRE	DHC11	-0.65	0.06	0	No
A0A2K3E1C3_CHLRE	FAP45	-0.63	0.06	0	No
A0A2K3E0D7_CHLRE	FAP51	-0.63	0.07	0	Yes
A0A2K3DWU3_CHLRE	FAP61	-0.62	0.07	0	Yes
A0A2K3D260_CHLRE	FAP52	-0.61	0.08	0	Yes
A0A2K3E2Q0_CHLRE	DHC4	-0.59	0.08	0	Yes
A8J0X0_CHLRE	FAP112	-0.55	0.09	0	No
A0A2K3DUG8_CHLRE	FAP147	-0.55	0.01	0	Yes
A8IFZ1_CHLRE	FAP55	-0.54	0.09	0	No
A0A2K3CWI5_CHLRE	FAP391	-0.54	0.10	0	Yes
A0A2K3DQN7_CHLRE	FAP108	-0.51	0.08	0	Yes

A8I1S7_CHLRE	FAP252	-0.47	0.08	1	No
Q8LKK4_CHLRE	RIB72	-0.46	0.09	0	Yes
A0A2K3CXC4_CHLRE	DRC7	-0.46	0.10	0	Yes
A0A2K3E6T1_CHLRE	FAP187	-0.44	0.09	0	Yes
A8IY81_CHLRE	FAP363	-0.35	0.06	0	No
A0A2K3D7C7_CHLRE	FAP306	-0.32	0.08	0	No

Table 3.2. Downregulated proteins in cilia lysates. Listed from left to right are the UniProt accession numbers, Phytozome annotation for the gene alias referenced from UniProt, the change in protein expression in BCI treated cells compared to DMSO, the calculated p-values for expression, presence of the protein in the membrane matrix fraction ("M+M Fraction?"), and whether there is a predicted transmembrane domain ("Predicted TM?").

Table 3.3. DMSO only ciliary lysate proteins

Rank	UniProt Accession:	Phytozome Annotation	Relative Area:	M+M Fraction?
1	A8HS16_CHLRE	Cre13.g568000	0.708	n/a
2	Q9FYV4_CHLRE	Atx1	0.699	1
3	A0A2K3DB47_CHLRE	IFT25	0.671	3
4	A8IES9_CHLRE	Cre03.g170050	0.666	0
5	A0A2K3DAC3_CHLRE	Cre10.g438600	0.660	n/a
6	A0A2K3DGD1_CHLRE	FAP386	0.658	0
7	A8J518_CHLRE	Cre09.g416500	0.653	0
8	A0A2K3CXT5_CHLRE	CGL151	0.647	0
9	A8J5C4_CHLRE	MOT24	0.642	0
10	A8JBH7_CHLRE	GAP2	0.637	1

Table 3.3. Top 10 proteins in cilia lysates found only in DMSO-treated cells. Listed from left to right are the Rank (1 indicating highest relative area to the protein from the mass spec with the highest area), the UniProt accession numbers, the Phytozome annotation of the gene aliases for genes pulled from UniProt, the Relative Area (which the rank is based on), and presence of the protein in the membrane matrix fraction ("M+M Fraction?").

Table 3.4. BCI only ciliary lysate proteins

Rank	UniProt Accession:	Phytozome Annotation:	Relative Area:	M+M Fraction?
1	A8JGF8_CHLRE	RPS9	0.776	0
2	A8IGY1_CHLRE	RPS13	0.758	n/a
3	A8I2T0_CHLRE	RPL27a	0.756	n/a
4	A0A2K3E5F8_CHLRE	Cre01.g011450	0.754	n/a
5	A8JE07_CHLRE	RPS15a	0.751	n/a
6	A0A2K3CV04_CHLRE	RPS26	0.751	n/a
7	A8I403_CHLRE	RPS19	0.748	n/a
8	A0A2K3D2K9_CHLRE	RPS28	0.748	n/a
9	A8JHU2_CHLRE	RPL36	0.747	n/a
10	A8IZ36_CHLRE	RPS25	0.744	n/a

Table 3.4. Top 10 proteins in cilia lysates found only in BCI-treated cells. Listed from left to right are the Rank (1 indicating highest relative area to the protein from the mass spec with the highest area), the UniProt accession numbers, the Phytozome annotation of the gene aliases for genes pulled from UniProt, the Relative Area (which the rank is based on), and presence of the protein in the membrane matrix fraction ("M+M Fraction?").

FAP173 and FAP270 are not required for ciliogenesis and ciliary length maintenance

Changes to protein expression in BCI-treated lysates can help explain how ciliary shortening is induced in relation to cell cycle progression. Having identified changes to protein expression in ciliary lysates of BCI-treated cells, we wanted to utilize mutations or overexpression of these proteins to determine which BCI-induced protein expression changes result in BCI defects. We utilized mutants of the most upregulated protein, FAP270, and the most downregulated protein, FAP173 (**Figure 3.1C)** both acquired from the *Chlamydomonas* Resource Center CLiP mutant library (X. Li et al., 2019). These mutants contain an insertional cassette that disrupts gene function and serves as a knockout of the proteins. Presence of the cassette within the gene was confirmed using PCR with a primer on the coding sequence and a primer on the cassette for both FAP173 (**Figure 3.2A**) and FAP270 (**Figure 3.2B)**. We next looked at both their steady state length and their length influenced by BCI treatment. In low concentrations of DMSO (steady state lengths), cilia were the same length as wild-type; however, FAP173, and more dramatically FAP270, were shortened significantly more at the same concentrations of BCI indicating sensitivity to this drug (**Figure 3.2C).** To assess potential effects of these proteins on ciliogenesis, cells were pH shocked to induce ciliary shedding and then allowed to regrow over the course of 2 hours (Lewin et al., 1982). Both FAP173 (**Figure 3.2D)** and FAP270 (**Figure 3.3E**) were able to completely regenerate their cilia to full length within two hours indicating that these proteins are not required for ciliogenesis or maintaining steady state ciliary lengths. This could be due to redundant functions with other proteins, regulation to finer details of cilia that may not affect ciliary length and assembly but may alter cilium composition, or they may participate in cell signaling that occurs in the cilium.

It is possible that FAP270 and 173 may have extraciliary functions that are altered as a result of protein localization changes or protein expression changes which cannot be detected with changes to ciliary abundance alone. While FAP173 has not been implicated in regulating ciliogenesis, it has previously been HA-tagged and found to localize to the middle region of the cilia separately from IFT (Lechtreck et al., 2009). To investigate whether FAP270 was degraded as a result of BCI-treatment or relocalization within the

cell as well as finer ciliary dispersion, we transformed C-terminally and N-terminally 3x FLAG tagged FAP270 into FAP270 mutants, though we only successfully acquired 2 transformants for the N-terminally FLAG-tagged FAP270 (**Figure 3.2F**). In steady state cells (DMSO – top) for both transformant 3 and 4, there appeared to be strong localization of the protein in the cell body as well as in various places throughout the cilia including the center, but also at the ciliary tips. Following a 2 hour treatment with BCI, cilia did not appear to have strong signal for FAP270, and cells with cilia appeared to have unchanged cell body localization of FAP270 (**Figure 3.2F).** It is interesting that in BCI-treated cilia lysates, this protein is upregulated. It is possible that the tag could be influencing protein localization or function, or the tag could be getting cleaved in BCI-treated cells in addition to the other proteins that are degraded during this treatment. It is also possible that while this protein is upregulated in BCI-treated cells, it is also degraded or exists in fragments that are not properly removed from the cilium as a result of other alterations to gating mechanisms or protein trafficking. In DMSO-treated transformant 3 cells, FAP270 appears to have localized in various places of cilia with strong punctate signal. It would be very interesting to see if this signal colocalizes with IFT components and potentially moves throughout the cilium to aid the cell in other signals. This has been seen with at least one other flagellar associated protein, FAP89 in *Chlamydomonas.* This protein has previously been found to be regulate cell density and lipid synthesis, which are extraciliary functions, despite its localization to the cilium (Luo et al., 2018).

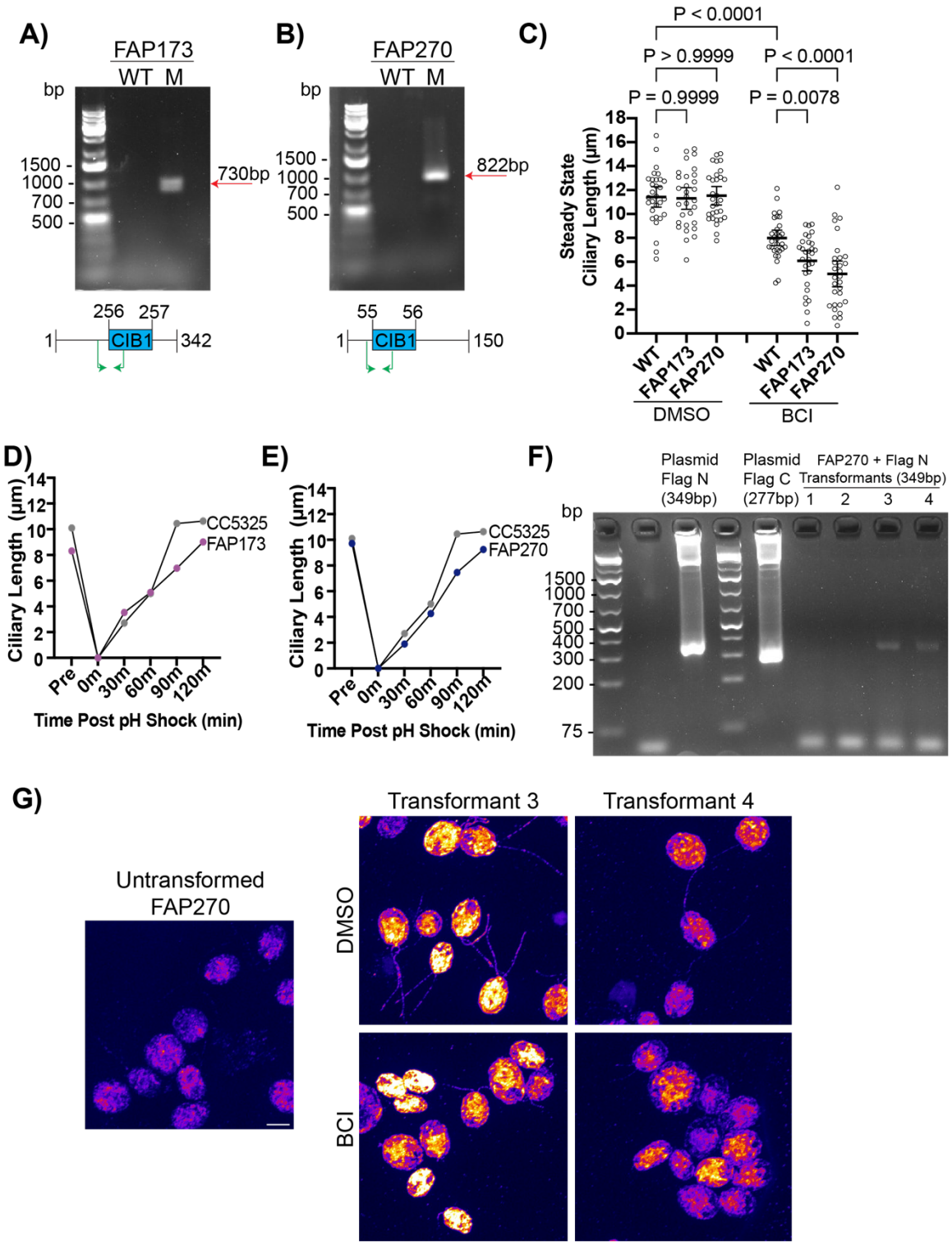

Figure 3.2. FAP173 and FAP270 exhibit normal ciliary dynamics. **A-B)** PCR gels confirming the cassette present in the gene of the mutant FAP173 and FAP270 *Chlamydomonas* strains. Mutant is "M" and Wild-type (CC-5325) is "W". Diagrams below gels indicate

positioning of the insertional cassette in the coding sequence with the corresponding base pairs. Green indicates the section amplified by the primers for the gel. **C)** Cells were treated for 2 hours with DMSO or 20 μM BCI and cilia lengths quantified. Significance was determined using a One-Way ANOVA with Šídák's multiple comparisons test (n=30). Error bars are mean with 95% confidence interval. For all statistical tests, $P<0.05$ is considered significant. **D-E)** Two hour ciliary regeneration following pH shock in wild-type (CC-5325) or mutant (FAP173 or FAP270). Averages from each timepoint are plotted (n=30**). F)** PCR gel confirming presence of the FAP270 rescue plasmid with an N-terminal 3x FLAG tag. **G)** Immunofluorescence of FLAG in untransformed FAP270 mutants or transformants 3 and 4 confirmed in **(F)** after a 2 hour treatment in DMSO or 20 μM BCI.

BCI increases vacuolar sizes

The vacuolar ATP synthase subunit A, ATPvA1 was upregulated with the highest significance score and is the 5th most upregulated protein in the ciliary lysate. Dramatic changes in this protein may affect vacuolar dynamics. We visualized these dynamics starting with contractile vacuoles which we have a labeled strain to address. Another vacuolar ATP synthase subunit, ATPvE, was venus-tagged and publicly available through the *Chlamydomonas* resource center (Mackinder et al., 2017). Using this strain which labels the contractile vacuoles in *Chlamydomonas*, we treated cells with BCI and observed the changes in the size of the labeled vacuole (**Figure 3.3A**). In the presence of BCI, vacuoles increased in size, though insignificantly (**Figure 3.3B**). Differences between treatment became even less pronounced when normalized to cell size (**Figure 3.3C**). We also compared vacuoles of the wild-type (CC-5325) to one of phosphatases previously implicated partially in ciliary regulation, mkp2 using a membrane dye to stain contractile vacuoles (**Figure 3.3D**) (Dougherty et al., 2023). Similar to ATPvE, cells in BCI were insignificantly increased at steady state which became increasingly insignificant when comparing cell sizes **(Figure 3.3 E and F).**

The subtle, though insignificant changes in contractile vacuoles made us curious if other vacuoles in the cell might be differentially affected using toluidine blue dye on fixed cells following a 2 hour treatment in DMSO or BCI. Cells with dark densities both near the pyrenoid as well as near the nucleus (large panel/red asterisks**, Figure 3.3G**) were compared for vesicle size and quantity (small panel/red arrows**, Figure 3.3G**). BCI-treated cells retained larger vacuoles (**Figure 3.3H**), though there were fewer overall per cell (**Figure 3.3I**). These results identify another structural modification because of BCI-treatment. Previously, we found that cilia shortened even quicker in the presence of Brefeldin A (BFA) with BCI which collapses Golgi in *Chlamydomonas* (Dentler, 2013; Dougherty et al., 2023). This suggested that either BCI was exacerbating Golgi collapse and membrane trafficking, or it was affecting other membrane pathways including endocytic mechanisms and recycling of membrane. Given that vesicles increase in size in

addition to cell size, it is possible that instead of membrane trafficking to cilia, it is redirected to these other structures to facilitate cell growth (**Figure 3.4**).

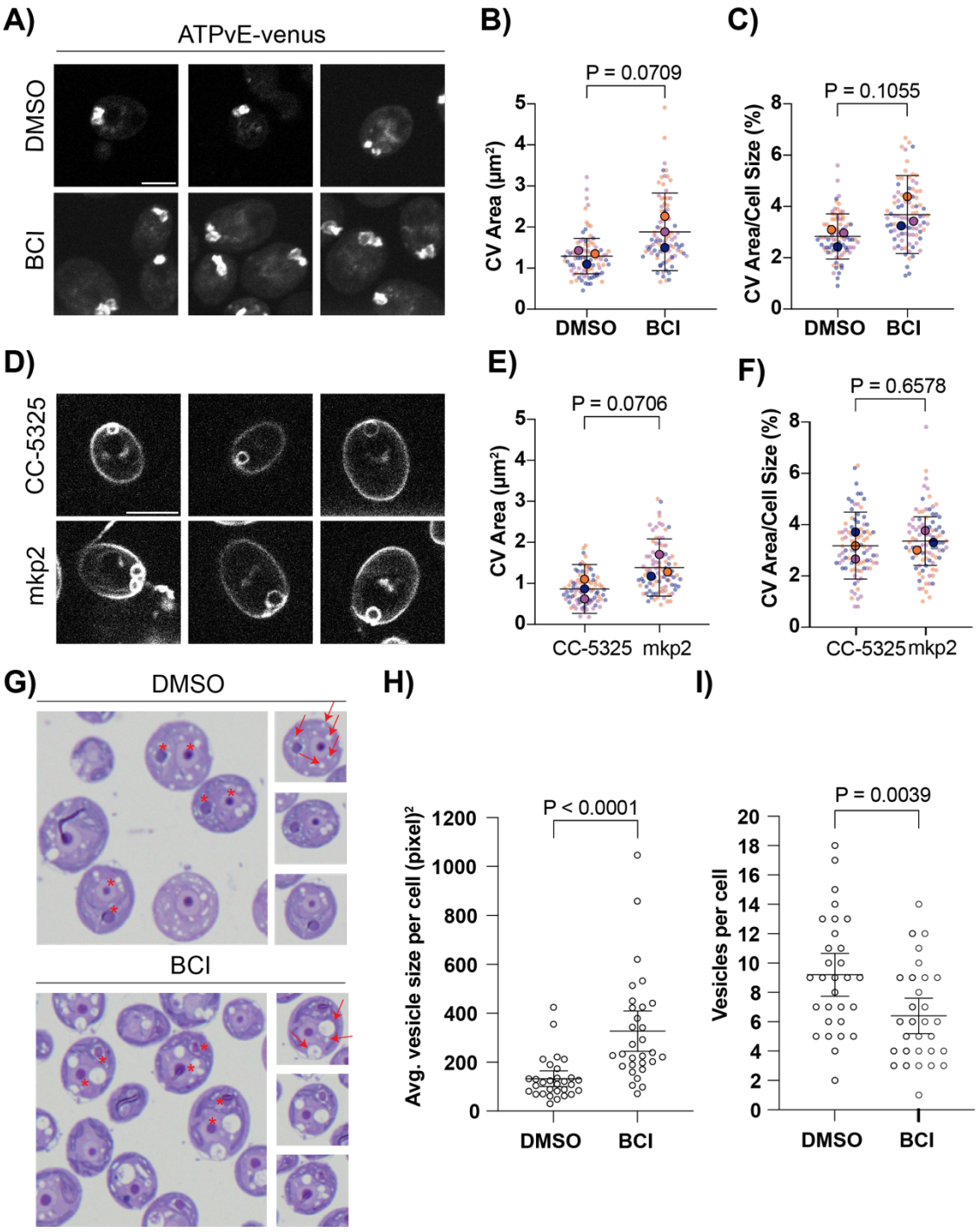

Figure 3.3. BCI induces changes to vacuole size. A and D) Representative images of cells expressing ATPvE-venus (**A**) or vacuoles labeled with the membrane dye FM1-43 (**D**) after a 2 hour treatment in DMSO or 20 µM BCI. **B and E)** Area of the ATPvE-venus fluorescence used as a proxy for contractive vacuole (CV) area. Statistics were determined using a t-test (n=30, N=3). Error bars are mean with 95% confidence interval. **C and F)** CV area normalized to cell

size. Statistics were determined using a t-test (n=30, N=3). Error bars are mean with 95% confidence interval**.** **G)** Histology sections of *Chlamydomonas* cells prepared for EM following a 2 hour DMSO or 20 μM BCI treatment. Red asterisks indicate the visible nuclear area and pyrenoid area used as a basis for comparing cells of equal slices. Red areas point to the vacuoles which are the object of measurement. **H**) Average number size of vesicles per cell. Statistics were determined using a t-test (n=30). Error bars are mean with 95% confidence interval. **I)** Total number of vesicles per cell. Statistics were determined using a t-test (n=30). Error bars are mean with 95% confidence interval.

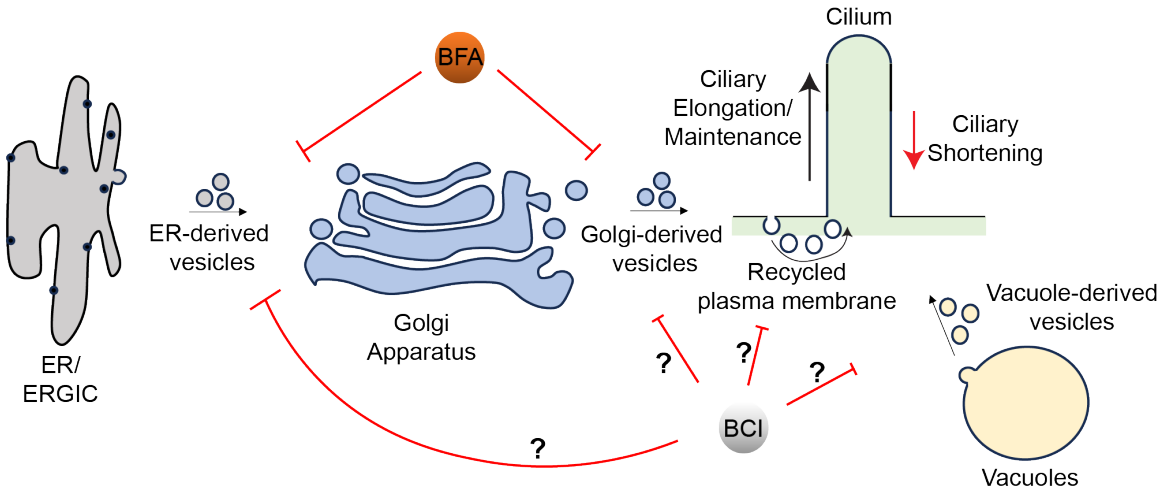

Figure 3.4. Proposed mechanisms for BCI induced ciliary resorption through membrane pathways. BFA is known to collapse the Golgi through inhibited vesicular trafficking from rough endoplasmic reticulum (ER) or ER-Golgi Intermediate Complex (ERGIC)-derived vesicles which ultimately leads to ciliary shortening. In the presence of BCI and BFA, cilia shorten faster which could potentially be due to various different mechanisms. We proposed previously that BCI may have an epistatic effect when paired with BFA which induces quicker ciliary resorption. In addition or separately, BCI could be inhibiting other sources of membrane that may be required for ciliary maintenance and elongation including inhibiting Golgi-derived vesicles, endocytically-derived plasma membrane, and/or vacuole-derived vesicles.

Whole cell protein ubiquitination is increased in BCI-treated cells

The ubiquitin-related proteins UBQ1, UBQ2, RPL40, and SUM1 were significantly upregulated in *Chlamydomonas* ciliary lysates (**Figure 3.1C, Table 3.1**). Ubiquitination has previously been known to regulate ciliary proteins such as by facilitating normal ciliary signaling dynamics (Desai et al., 2020; Lv et al., 2021), normal ciliogenesis by increasing protein stability (Chiuso et al., 2023), and increasing ciliary disassembly through tubulin labeling (Q. Wang et al., 2019). We wanted to check the change in ubiquitination in the ciliary lysate compared to other ciliary resorption agents, IBMX, and NaPPi, to compare previously studied forms of ciliary resorption to BCI specific changes (**Figure 3.5A**). We checked the change in ubiquitin in the cilia lysate (**Figure 3.5B**) compared to the cell body (**Figure 3.5C).** While the ciliary lysates did not indicate strong differences in ubiquitination across the other ciliary resorption agents IBMX and NaPPi (**Figure 3.5D**), ubiquitinated proteins in the cell body of BCI treated cells increased significantly whereas cell body proteins in IBMX and NaPPi were not altered **(Figure 3E).**

The high presence of ubiquitinated proteins in the cell body made us curious if this is a function of the ciliary length, so we tested a range of concentrations for BCI which induce varying degrees of ciliary shortening (**Figure 3.6C**). Interestingly, ubiquitination was present in cells the most when cilia were present and resorbing compared to when cilia were completely resorbed at 45 μM and 60 μM BCI (**Figure 3.5A and B**). Upon regenerating cilia in the presence or absence of BCI, we found that ubiquitination of proteins in BCI-treated whole cell lysates consistently maintained ubiquitination of higher molecular weight proteins whereas proteins in the lysate of cells able to regenerate cilia mostly maintained noticeable ubiquitination of proteins between 20 and 30 kDa (**Figure 3.6D**). These data indicate that BCI induces differential ubiquitination of proteins during inhibited ciliogenesis.

It is interesting that in both the 0 minute timepoint and pre timepoint, lower kDa proteins are ubiquitinated, though the signal is weaker in 0 minutes suggesting that these proteins could include ciliary proteins which are lost during deciliation (**Figure 3.6D**).

It's also interesting that both during ciliary resorption and inhibited ciliogenesis due to BCI treatment, higher molecular weight proteins are both increased in these whole cell lysates. It would be good to know if these proteins are the same in either case which could point to a common mechanism for both inhibited ciliogenesis and ciliary resorption.

Together, this work provides a deeper molecular dive into what proteins are changing more specifically as a result of BCI treatment. BCI induces changes to many downstream targets, but immediately downstream of BCI still remains to be determined in *Chlamydomonas rein*hardtii. In mammalian cells BCI allosterically inhibits the ERK1/2 phosphatase DUSP6/MKP3 (Molina et al., 2009); however its impacts on ubiquitination dynamics have not previously been identified. Further work needs to be done to assess potential crosstalk between MAP kinase signaling/phosphorylation cascades and ubiquitination signaling and other downstream targets. However, this work lays the groundwork for future research into the potential mechanisms of action both for this drug as well as how DUSP inhibition can be inhibiting ciliogenesis.

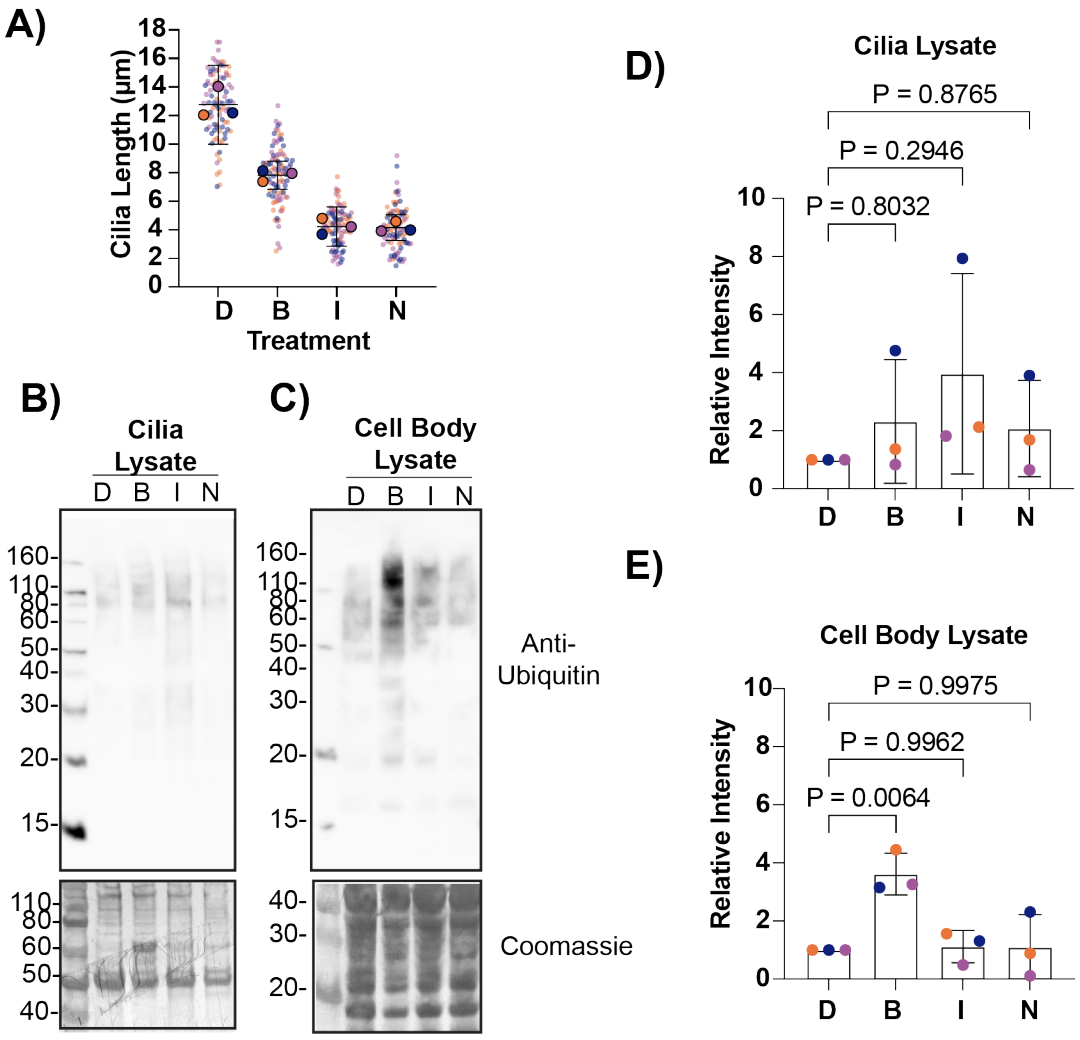

Figure 3.5. BCI induces ubiquitination in proteins differently from other ciliary resorption reagents. A) Ciliary lengths measured for 2 hour treatment in DMSO ("D") or the ciliary resorption agents BCI ("B"), IBMX ("I"), and NaPPi ("N"). Error bars are mean with 95% confidence interval (n=30, N=3). **B-C)** Following a 2 hour treatment in ciliary resorption agents, cilia were isolated **(B)** from the cell bodies **(C)**, running lysates on SDS-PAGE, transferring to PVDF and probing for ubiquitin (top) or total protein via Coomassie (bottom). **D-E)** Quantification of western blot band intensities in **(B-C).** Statistics were determined using a One-way ANOVA with Dunnett's multiple comparisons test **(D)** or Šídák's multiple comparisons test **(E)** (N=3). Error bars are mean with standard deviation.

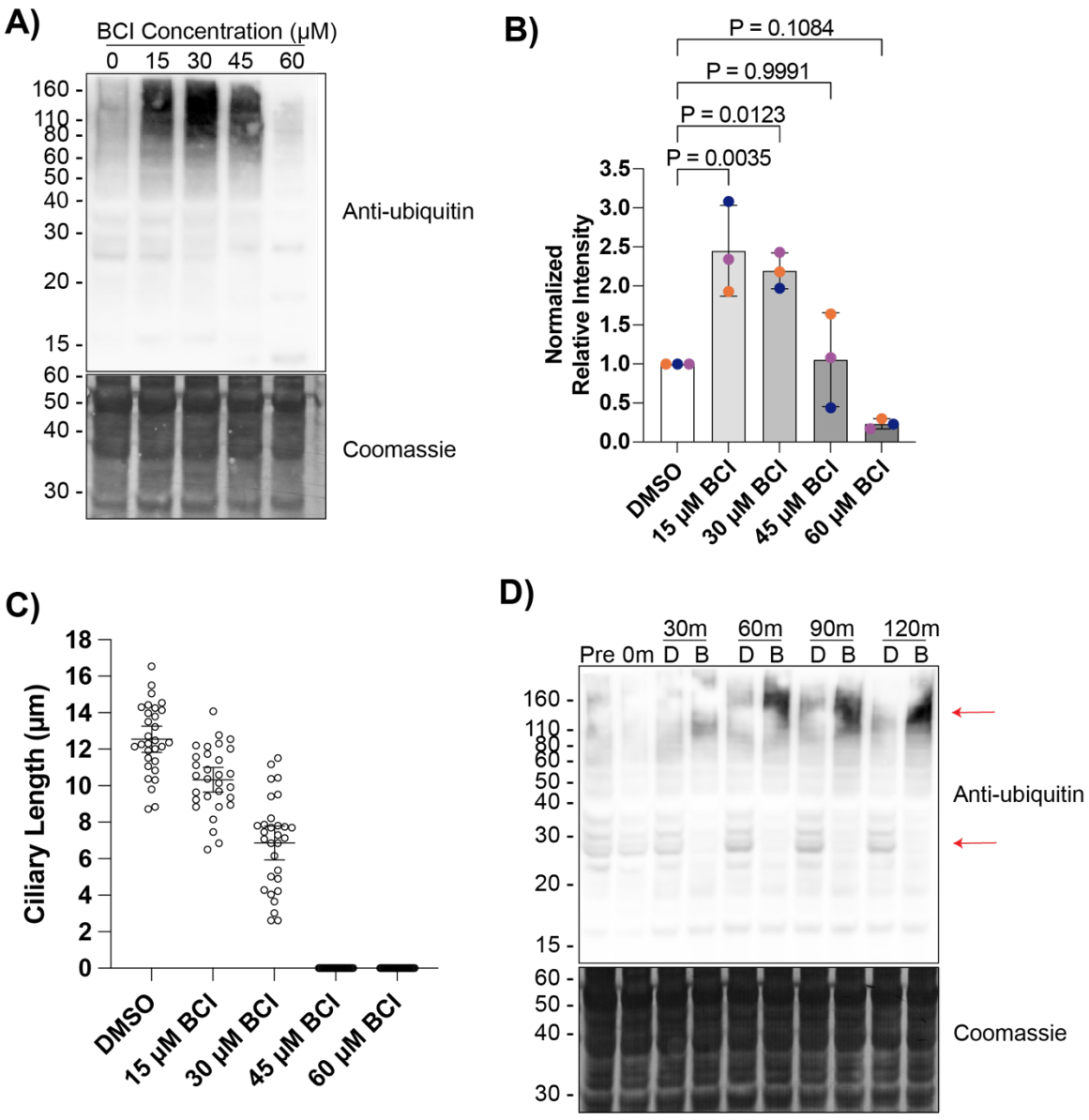

Figure 3.6. BCI induces changes to the ubiquitination pattern of whole cell lysates.

A) Steady state ubiquitin profile for whole cell lysates. Cells were treated with increasing concentrations of BCI for 2 hours and then protein was collected and separated using SDS-PAGE and blotting onto PVDF membrane. Membranes were probed with anti-ubiquitin and then stained with Coomassie for total protein**. B)** Quantification of **(A).** Statistics were determined using a One-way ANOVA with Dunnett's multiple comparisons test. Error bars are mean with standard deviation (N=3). **C)** Ciliary length measurements of cells treated in **(A)**. Error bars are mean with 95% confidence interval (n=30). **D)** Ubiquitin profile for whole cell lysates regenerating in DMSO ("D") or 20 μM BCI ("B") across 2 hours following pH shock. Western blots were

prepared and probed as described in **(A)**. Red arrows indicate interesting changes to the ubiquitination pattern in DMSO vs. BCI-treated regenerating cells.

MATERIALS AND METHODS

Strains and maintenance:

The wild-type strain (CC-5325), *mkp2* mutant (LMJ.RY0402.168348), ATPvE (CSI_FC1E07), *FAP173* mutant (LMJ.RY0402.122974) and *FAP270* mutant (LMJ.RY0402.059761) were obtained from the Chlamydomonas Resource Center. These cells were grown and maintained on 1.5% Tris-Acetate-Phosphate (TAP) agarose plates under constant illumination. For experiments, cells were inoculated into liquid TAP media with constant agitation and light overnight.

Genotyping:

Genotyping was performed as described in (Dougherty et al., 2023) with slight modifications to the PCR parameters:

- 95°C: 5 min
- **(95°C: 30s**
- **58°C: 45 sec**
- **72°C: 2 min) X 34 cycles**
- 72°C: 10 min
- 10°C: ∞

The N-terminally FLAG tagged FAP270 construct was generated by TwistBio in the pChlamy4 vector generated by Thermofisher and transformed into FAP270 mutant cells according to (L. Wang et al., 2019) with slight modifications. Cells were electroporated using a Bio Rad electroporator set to Exponential Decay, 500V, 50 μF, and 800 Ohms in a 4 cm cuvette. Cells were allowed to recover overnight in TAP+40mM sucrose and then spread on 10μg/mL Zeocin + TAP plates for selection. Positive colonies were screened using a forward and reverse primer specific to pChlamy4 and placed just outside of the gene insertion.

Primers:

FAP270 Forward Primer: 5' - CCGCCTAAGGATATCTACGA - 3'

FAP173 Forward Primer: 5' - TACTTCGACACGCTCAAGGA - 3'

Reverse Primer: 5' - CCGAGGAGAAACTGGCCTTCT – 3'

pC4 Forward Primer: 5' – GAAGCAGACCCTGAACTTCGAC – 3'

pC4 Reverse Primer: 5' – GGCAAGGCTCAGATCAACGA – 3'

Imaging and Quantification:

Ciliary length experiments:

DIC and ciliary length measurements for steady state and regenerations were performed and analyzed as described in (Dougherty et al., 2023).

FLAG immunofluorescence:

Cells fixed and stained the same way as microtubule fixation (L. Wang et al., 2013) with the same modifications described in (Dougherty et al., 2023). Flag antibody (sigma, F1804-200UG) was diluted 1:100 in 20% block (1% BSA, 0.2% fish gelatin, 1x PBS). Secondary (Alex Fluor 488 goat anti-mouse IgG, Invitrogen, A11001) was diluted 1:500 in 20% block.

ATPvE imaging and Membrane staining:

Following a 2 hour BCI treatment, ~10 µL cells were placed on coverslips in 100 µL TAP, allowed to swim down, and then incubated with 1uL FM 4-64 dye just long enough to see membrane labeling (~5 seconds) before the whole cell became saturated (which we find is also when Sytox Green, a cell viability dye indicating dead cells, also

saturates cells). For ATPvE, cells were allowed to swim down and then imaged the same way.

For quantification, z stacks were taken and max immunoprojections were generated. Area of the vacuoles was measured using the elliptical selections tool in FIJI. In addition, cell sizes were measured using these same methods.

Histology vacuole measurements:

For measuring the size of vacuoles, cells that had visible dark densities in both the nuclear area and pyrenoid area of the cell were identified and used for vacuole comparisons to indicate similar slices. After identifying these cells, a mask was applied to threshold the size of vacuoles and then the area and total vacuoles per cell was recorded using the ROI function in FIJI.

Cilia Isolations:

Cilia isolations were performed similar to (Craige et al., 2013). For CC-5325 cilia, cells were grown in TAP initially. The day before the isolation, cells were incubated in M-N to synchronize cilia for ~8 hours and then resuspended in TAP overnight. The next day, cells were incubated with DMSO, BCI, IBMX, or NaPPi. For NaPPi, media equivalent to the volume of NaPPi was removed and replaced with the volume of NaPPi solution.

SDS-PAGE and Immunoblotting:

Either following cilia isolations or following *Chlamydomonas* whole cell lysate extraction described in (Dougherty et al., 2023), lysates were boiled at 70C, run on 1.5mm 10% bis-tris gels (Thermofisher) and transferred to PVDF membrane. Western blots were blocked in 5% milk, incubated overnight in primary antibody diluted 1:500 (anti-ubiquitin, BioLegend P4G7) in 1% milk (Signature, Instant Nonfat dry Milk) with

5% Bovine Serum Albumin (BSA, VWR) in 1x PBS at 4˚C. The next day, blots were washed 3x10 minutes in PBST (1x PBS with 0.1% tween), incubated in secondary antibody (information) also diluted in 1% milk with 5% BSA in PBS for 1 hour at RT, washed 3x10 minutes in PBST, and then imaged with pico chemiluminescent substrate (Thermo) and imaged on a Bio-Rad ChemiDoc MP. Following imaging, PVDF membranes were incubated in Coomassie brilliant blue stain for ~30 minutes, destained in 40% MeOH/10% acetic acid, allowed to dry, and imaged once more on the ChemiDoc MP. Blot band intensities were determined using FIJI.

CHAPTER 4:

Determinants of cytoplasmic microtubule depolymerization during ciliogenesis in *Chlamydomonas reinhardtii*

Larissa L Dougherty[1], Prachee Avasthi[1,§,*]

[1]Biochemistry and Cell Biology Department, Geisel School of Medicine at Dartmouth College, Hanover, New Hampshire

[§]Address correspondence to prachee.avasthi@dartmouth.edu at Geisel School of Medicine at Dartmouth College

[*]Prachee Avasthi is the CSO at Arcadia Science

Abbreviations

- CytoMTs = Cytoplasmic Microtubules
- IFT = Intraflagellar Transport
- MS = Mechanical Shear
- PTX = Paclitaxel

The text and figures from chapter 4 represent a paper published on BioRxiv (**doi:** 10.1101/2023.04.07.536038). Larissa L Dougherty performed conceptualization, data curation, formal analysis, investigation, methodology, project administration, validation, visualization, writing – original draft, and writing – review and editing. Soumita Dutta performed conceptualization, data curation, investigation, methodology, and writing – review and editing. Prachee Avasthi performed conceptualization, formal analysis, funding acquisition, investigation, project administration, resources, software, supervision, visualization, and writing – review and editing.

We would like to thank the Barlowe Lab at Dartmouth College and Brae Bigge at Arcadia Science for their feedback on experimental ideas and revising the manuscript.

We would like to thank Karl Lechtreck for his close reading of the manuscript and catching an error in mutant identification. We would like to thank reviewers for their constructive suggestions to enhance the clarity of the manuscript. We would also like to thank Ann Lavanway at the Life Sciences Light Microscopy Facility at Dartmouth for help with microscopy. We would also like to thank the Biochemistry and Cell Biology Department at Dartmouth College for providing resources to complete this work. This work was funded by NIH MIRA R35GM128702(PA).

ABSTRACT

At the core of cilia are microtubules which are important for establishing length and assisting ciliary assembly and disassembly; however, another role for microtubule regulation on ciliogenesis lies outside of the cilium. The microtubule cytoskeleton is a highly dynamic structure which polymerizes and depolymerizes rapidly to assist in cellular processes. These processes have been studied across various organisms with chemical as well as genetic perturbations. However, these have generated conflicting data in terms of the role of cytoplasmic microtubules (CytoMTs) and free tubulin dynamics during ciliogenesis. Here we look at the relationship between ciliogenesis and cytoplasmic microtubule dynamics in *Chlamydomonas reinhardtii* using chemical and mechanical perturbations. We find that not only can stabilized CytoMTs allow for normal ciliary assembly, but high calcium concentrations and low pH-induced deciliation cause CytoMTs to depolymerize separately from ciliary shedding. In addition, we find that ciliary shedding through mechanical shearing, cilia regenerate earlier despite intact CytoMTs. Our data suggests that cytoplasmic microtubules are not a sink for a limiting pool of cytoplasmic tubulin in *Chlamydomonas*, depolymerization that occurs following deciliation is a consequence rather than a requirement for ciliogenesis, and intact CytoMTs in the cytoplasm and the proximal cilium support more efficient ciliary assembly.

INTRODUCTION

Ciliogenesis describes the formation of cilia which are microtubule extensions from the plasma membrane that serve as signaling and sometimes motile components of quiescent cells (Tucker et al., 1979). These largely microtubule-based structures are assembled and maintained through intraflagellar transport (IFT) where tubulin monomers among other components are taken to the tip of the cilium for ciliary assembly and maintenance (Craft et al., 2015; Kozminski et al., 1993). This process is influenced by not only the core proteins required for IFT, but also ciliary gene transcription, protein synthesis, trafficking, and complex pre-assembly occurring outside of the cilium. All of the required structures and components generate a highly regulated structure and signaling environment within cilia, and because of this, disruptions to any of these components can lead to various diseases (Reiter & Leroux, 2017). Therefore, it is important to understand how manipulation of cellular processes and components can influence ciliary assembly.

While cilia are themselves a microtubule superstructure, microtubules are also highly dynamic components elsewhere in the cell. They provide structure and polarity to the cell, serve as highways for molecular trafficking, and facilitate cell division among many other roles (de Forges et al., 2012; Parker et al., 2014). To serve these many roles, tubulin assembles and disassembles very rapidly through the process of dynamic instability which describes how tubulin can disassemble into monomers very quickly from GTP hydrolysis (Alushin et al., 2014; Mitchison & Kirschner, 1984).

Disruption of cytoplasmic microtubule (CytoMT) dynamics has previously been shown to directly impact the ability for cilia to assemble through chemical perturbations. For example, through the use of microtubule inhibitors such as colchicine or colcemid which promote CytoMT depolymerization, cilia cannot assemble at all in Chinese hamster fibroblasts (Stubblefield & Brinkley, 1966) *Chlamydomonas* (Rosenbaum et al., 1969) and *Tetrahymena* (Rosenbaum & Carlson, 1969). Conversely, use of the microtubule stabilizer, taxol, has more recently been shown to inhibit acute ciliary elongation in *Chlamydomonas reinhardtii* (Wang et al., 2013). However, while

microtubule destabilizing drugs were found to inhibit ciliary assembly, taxol was previously not found to have any effects in PtK1 cells on either assembly or disassembly of primary cilia (Jensen et al., 1987). In contrast, taxol can prevent actin stabilization and microtubule depolymerization-induced ciliary elongation through forskolin, jasplakinolide, and the PKA inhibitor CD. Consistently, the MT depolymerizing drug nocodazole was shown to increase ciliary length likely by freeing up tubulin for ciliogenesis in RPE cells whereas taxol itself shortened cilia (Sharma et al., 2011). Given these cell-type specific and chemical specific discrepancies describing the interplay between CytoMT dynamics and ciliary dynamics, it is important to continue investigating how these processes impact one another to better understand how ciliary dynamics are regulated.

CytoMT dynamics with respect to ciliary dynamics have predominantly been studied through chemical perturbations. Here we explore the requirement for microtubule dynamics in the ciliary model organism *Chlamydomonas reinhardtii* with both chemical perturbations and mechanical perturbations to better understand how microtubule dynamics can regulate ciliary assembly. We ultimately find that total CytoMT depolymerization is not required for ciliary assembly.

RESULTS

Paclitaxel-stabilized CytoMTs do not inhibit ciliary assembly to full length in 2 hours

Paclitaxel (PTX), the non-branded Taxol, is a chemical that is well-known for its ability to stabilize microtubules through binding to β-tubulin polymers (Manfredi et al., n.d.; Parness & Horwitz, 1981). Stabilizing microtubules with taxol has previously been found to shorten steady state length in *Chlamydomonas reinhardtii.* Additionally, it has been found that through common methods of deciliation in *Chlamydomonas*, cytoplasmic microtubules depolymerize. This data led to the hypothesis that tubulin utilized in axonemal assembly for ciliogenesis comes from tubulin present in the cell body (cytoplasmic microtubules, CytoMTs), and microtubule dynamics are required for axonemal microtubule assembly for ciliogenesis (Wang et al., 2013). However, in our previous work, we found that a lower paclitaxel (PTX) concentration from what has previously been utilized for ciliary studies can allow for normal ciliary elongation following pH shock in *Chlamydomonas* which raised the question of whether CytoMT dynamics are truly required for ciliary assembly (Dougherty et al., 2023).

We wanted to assess how different PTX concentrations can influence ciliogenesis. To test if taxol is indeed stabilizing CytoMTs at lower concentrations in *Chlamydomonas reinhardtii*, we isolated the soluble ("S") and insoluble ("P") β-tubulin fractions after treating cells with 0.5 M acetic acid to induce deciliation ("pH shock") (Witman et al., 1972), 2 mg/mL colchicine, 1% DMSO, 15 μM PTX, or 40 μM PTX (**Figure 4.1A**). Following PTX treatment, both 15 μM and 40 μM PTX decreased the presence of β-tubulin in the soluble fraction without completely depleting the pool, confirming that both concentrations sufficiently stabilize CytoMTs in the cells (**Figure 4.1A and 1B**). To directly compare the effect of PTX on ciliogenesis extending beyond steady-state length, cells were treated with increasing concentrations of PTX in the presence or absence of 25 mM lithium chloride (LiCl) (Nakamura et al., 1987). Regardless of PTX concentration,

cilia significantly elongated in the presence of LiCl in the CC-1690 wild-type strain in M1 liquid media (**Figure 4.1C**) previously used in (Wang et al., 2013). We also checked the ability for cilia to completely regenerate from 0 μm through pH shock in the presence of 15 μM PTX, 40 μM PTX, or 60 μM PTX compared to control cells in DMSO (**Figure 4.1D**). Similarly and consistently with our previous work (Dougherty et al., 2023), cilia regenerated normally in 15 μM PTX, though even at 60 μM PTX, ciliary length did not significantly differ from DMSO treated cells at 120 minutes (**Figure 4.1D**). To compare the ability for PTX to stabilize CytoMTs during pH shock, we pretreated cells for 10 minutes with PTX and then fixed and stained them for β-tubulin at 5 minutes post pH shock when microtubules are normally depolymerized (**Figure 4.1E**). We found that, even immediately following deciliation, CytoMTs are stabilized similarly to pre-deciliated cells as defined by cells which have visible filaments extending past half the long axis of the cell (**Figure 4.1F**). While this population correlation does not give us changes to tubulin lengths or filament numbers, it provides us with a course measure of how the CytoMT polymerization responds to perturbations. Given that 1) there is already a pool of soluble tubulin at steady state without treatment, 2) decreasing this pool by inducing CytoMT stabilization does not impact ciliogenesis, and 3) increasing this pool by depolymerizing CytoMTs through pH shock also does not impact ciliogenesis, our data suggest that tuning available soluble tubulin access through CytoMT manipulation does not critically impact ciliogenesis.

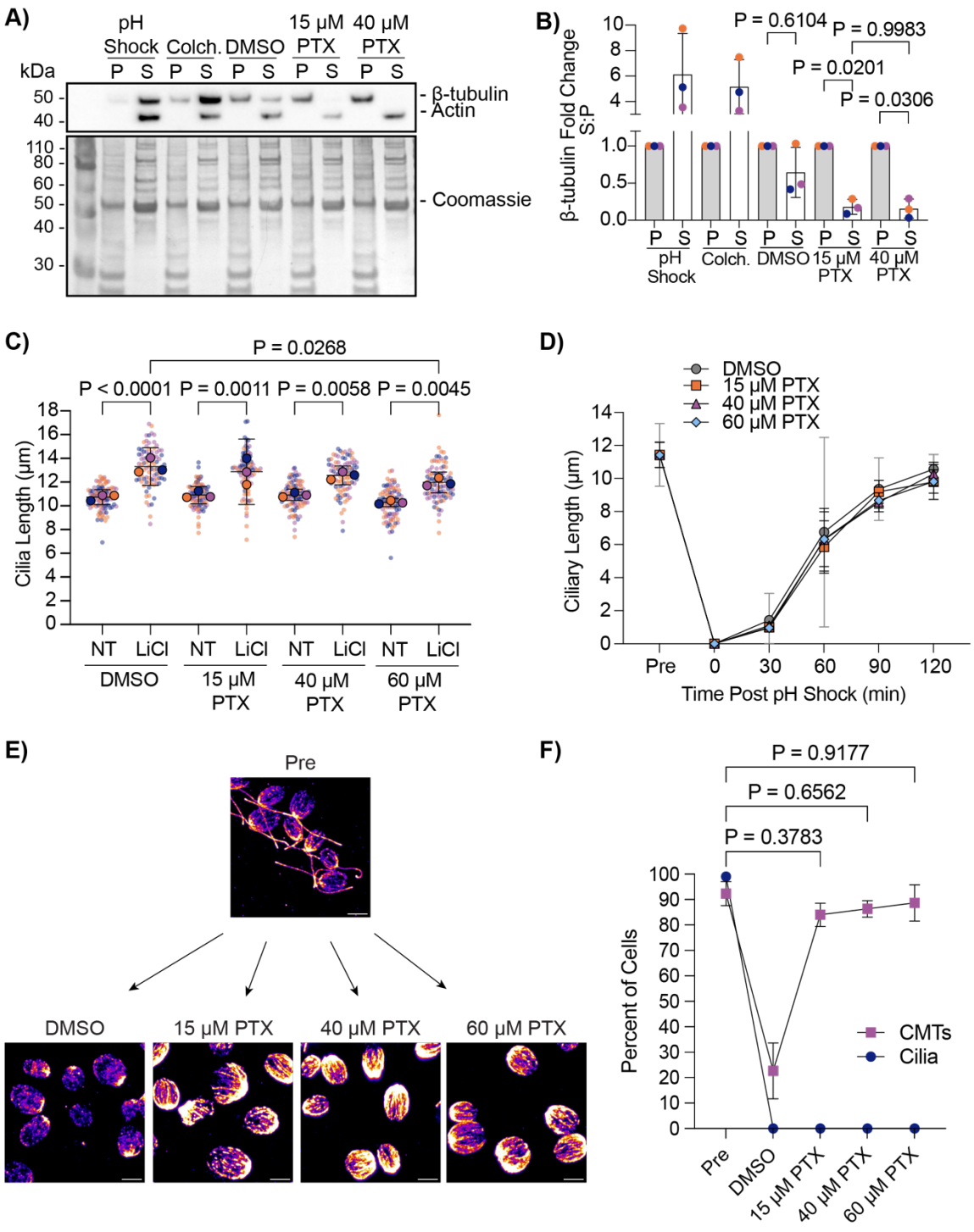

Figure 4.1. Paclitaxel-stabilized CytoMTs permit normal ciliogenesis. **A)** Wild-type cells (CC-5325) were treated with acetic acid, 2 mg/mL colchicine for 100 minutes, 1% DMSO for 10 minutes, 15 µM paclitaxel (PTX) for 10 minutes, or 40 µM PTX for 10 minutes. Protein was collected and probed for β-tubulin, actin (soluble protein control), or total protein with

Coomassie on a PVDF membrane. **B)** Quantification of western blot band intensity in **(A)**. Microtubule intensity was normalized to total protein and then the soluble tubulin (S) intensity was compared to the insoluble intensity (P). Significance was determined using a One-Way ANOVA with Šídák's multiple comparisons test (N=3). Error bars are mean with standard deviation. For all tests, $P<0.05$ is considered significantly different. **C)** Wild-type cells (CC-1690) were grown in M1 media overnight and then treated with 1% DMSO or increasing concentrations of PTX with or without 25 mM LiCl for 30 min. Significance was determined with a One-Way ANOVA and Šídák's multiple comparisons test (n=30, N=3). **D)** Wild-type cells (CC-5325) were grown in TAP media overnight, pretreated in increasing concentrations of PTX for 10 min, and then regenerated for 2 h after pH shock with acetic acid and PTX. Significance was determined with a One-Way ANOVA and Šídák's multiple comparisons test (n=30, N=2). Error bars are mean with 95% confidence interval. E) Representative images of β-tubulin-stained cells at the 5 min timepoint post pH shock in **(D)**. Scale bars are 5 μm. **F)** Quantification of the percent of cells with cilia and polymerized cytoplasmic microtubules (CytoMTs) at 5 min post pH shock in DMSO or PTX. Navy blue circles are cilia; purple squares are CytoMTs. Error bars are mean with standard deviation (n=100, N=3). Significance for CytoMTs is represented on the graph and determined using a One Way ANOVA with Šídák's multiple comparisons test. Cells considered to have polymerized microtubules have visible B-tubulin containing filaments extending past half of the cell.

While deciliation and regrowth of cilia from 0 μm is coincident with CytoMT depolymerization and stabilization of CytoMTs does not affect cilium regrowth, we wondered whether cilium growth from cilia maintained at steady state showed similar patterns of CytoMT depolymerization. Acute growth from multiple lengths may indicate whether CytoMTs depolymerization is specific to cilium growth or deciliation. Using 25 mM LiCl to induce ciliary elongation, we checked the polymerization status of CytoMTs across 30 minutes during treatment (**Figure 4.2A**). Throughout this time, cells were able to elongate ~2 μm as reported in Wang et al., 2013 (**Figure 4.2B**). However, upon checking CytoMT polymerization throughout this process, we find that these microtubule arrays remained undisturbed in both untreated- and LiCl-treated cells (**Figure 4.2C**). This data suggests that CytoMT depolymerization is not necessary for ciliary assembly,

though it is possible that finer CytoMT depolymerization could occur on a level that is not detectable with these methods.

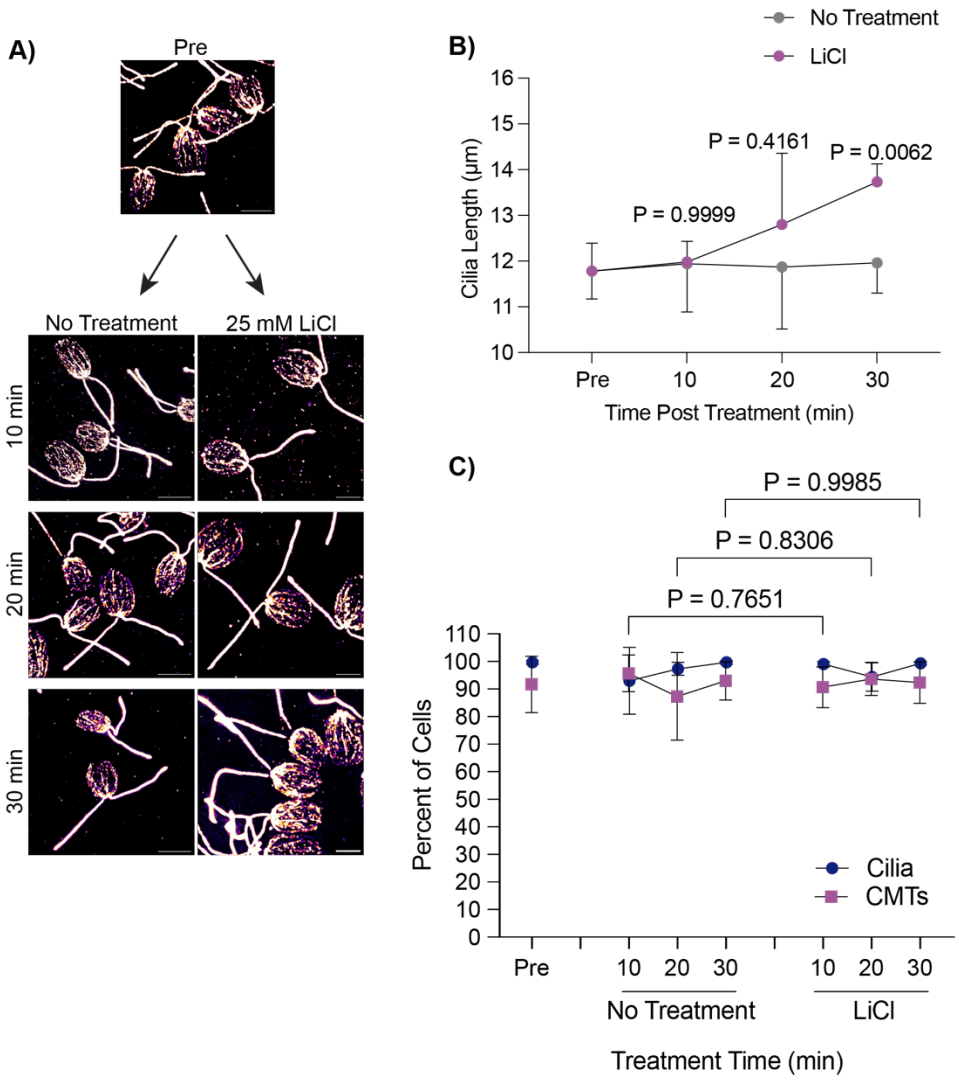

Figure 4.2. Lithium chloride-induced ciliary elongation does not require CytoMT depolymerization from steady state. A) Wild-type cells were treated with either 25 mM LiCl or no treatment for 30 minutes and then fixed and stained for β-tubulin. Scale bars are 5 µm. **B**) Quantification of cilia length for the experiment described in (**A**). Error bars are mean with 95% confidence interval (n=30, N=3). Significance compares cilia length at 30 min between treatments and was determined with a Two Way ANOVA with Šídák's multiple comparisons test. C) Quantification of percent of cells with cilia versus polymerized microtubules for the experiment described in (**A**). Error bars are mean with standard deviation (n=100, N=3). Significance for CytoMTs is represented on the graph and determined using a One-Way ANOVA with Šídák's multiple comparisons test.

Chemically induced ciliary shedding occurs separately from CytoMT depolymerization

Given that CytoMT depolymerization does not occur following ciliary elongation from steady state lengths (**Figure 4.2**) and cilia assemble to full length in two hours with an available pool of soluble tubulin despite CytoMT stabilization (**Figure 4.1**), we suggest that detectable CytoMT depolymerization through pH shock is not a requirement for ciliary assembly. To better understand if depolymerization is a result of physical loss of the cilium versus other factors coincident with cilium loss, we utilized a previously characterized *fa2-1* mutant encoding a mutant NIMA family kinase which cannot deciliate in the presence of calcium or acid (Mahjoub et al., 2002) (**Figure 4.3A**). Following pH shock, we found that while wild-type cells shed 100% of their cilia and depolymerized ~70% of their CytoMTs (**Figure 4.3B, left**), the *fa2-1* mutants maintained cilia as expected, but also depolymerized CytoMTs similar to wild-type (**Figure 4.3B, right**). This is surprising because it was previously reported that CytoMT depolymerization is required for ciliogenesis (Wang et al., 2013), but here we see that even in the absence of deciliation and during pH shock, CytoMTs still depolymerize. This suggests that CytoMT depolymerization could be an artifact or consequence of pH shock and is not strictly tied to loss of cilia.

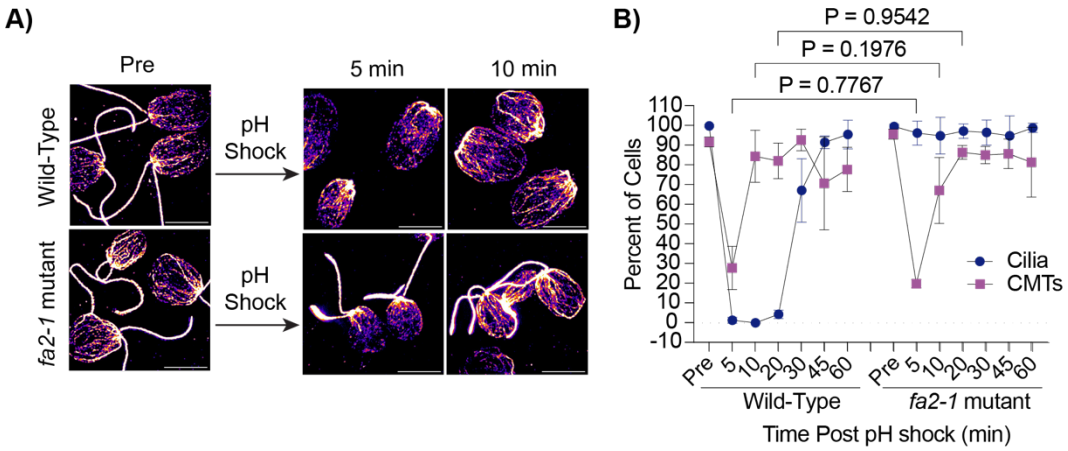

Figure 4.3. CytoMT depolymerization occurs separately from ciliary shedding following pH shock. A) Wild-type or *fa2-1* mutants were pH shocked with acetic acid for 45 sec and then regrown in fresh TAP for 60 min. Cells were fixed and stained for β-tubulin. Scale bars are 5 μm. **B)** Quantification of percent of cells with cilia or CytoMTs post pH shock. Error bars are mean with standard deviation (n=100, N=3). Significance was determined with a One-Way ANOVA and Šídák's multiple comparisons test for comparisons between CytoMTs.

To test if CytoMT depolymerization was specific to pH shock or if other agents that induce ciliary shedding can also induce CytoMT depolymerization separately. It has previously been established that pH shock induces a calcium influx into the cell (L. M. Quarmby, 1996), and introducing the cell to higher concentrations of calcium can induce ciliary shedding (L. Quarmby & Hartzell, 1994). To further test what triggers CytoMT depolymerization coincident with deciliation, we tested if calcium influx, known to occur upon pH shock, was also sufficient to induce CytoMT depolymerization. We introduced cells to 75 mM calcium chloride ("$CaCl_2$") in 5 mM HEPES ("Buffer") for 10 minutes which is long enough to induce robust ciliary shedding. Following ciliary shedding, cilia regenerated similar to cilia exposed to pH shock (**Figure 4.4A**). We then measured the effect of calcium-induced ciliary shedding on CytoMT stability. Upon ciliary shedding, we found that CytoMTs also depolymerized quickly and then reformed similar to pH shock (**Figure 4.4B**). To determine if calcium has the same effect on ciliated cells, we repeated this experiment in *fa2-1* mutants (**Figure 4.4C-E**). Similar to wild-type cells,

fa2-1 mutants also exhibited depolymerized microtubules though they did not depolymerize to the same degree as wild-type (**Figure 4.4E**). This data indicates that depolymerization is specific to calcium-mediated mechanisms rather than cilia loss.

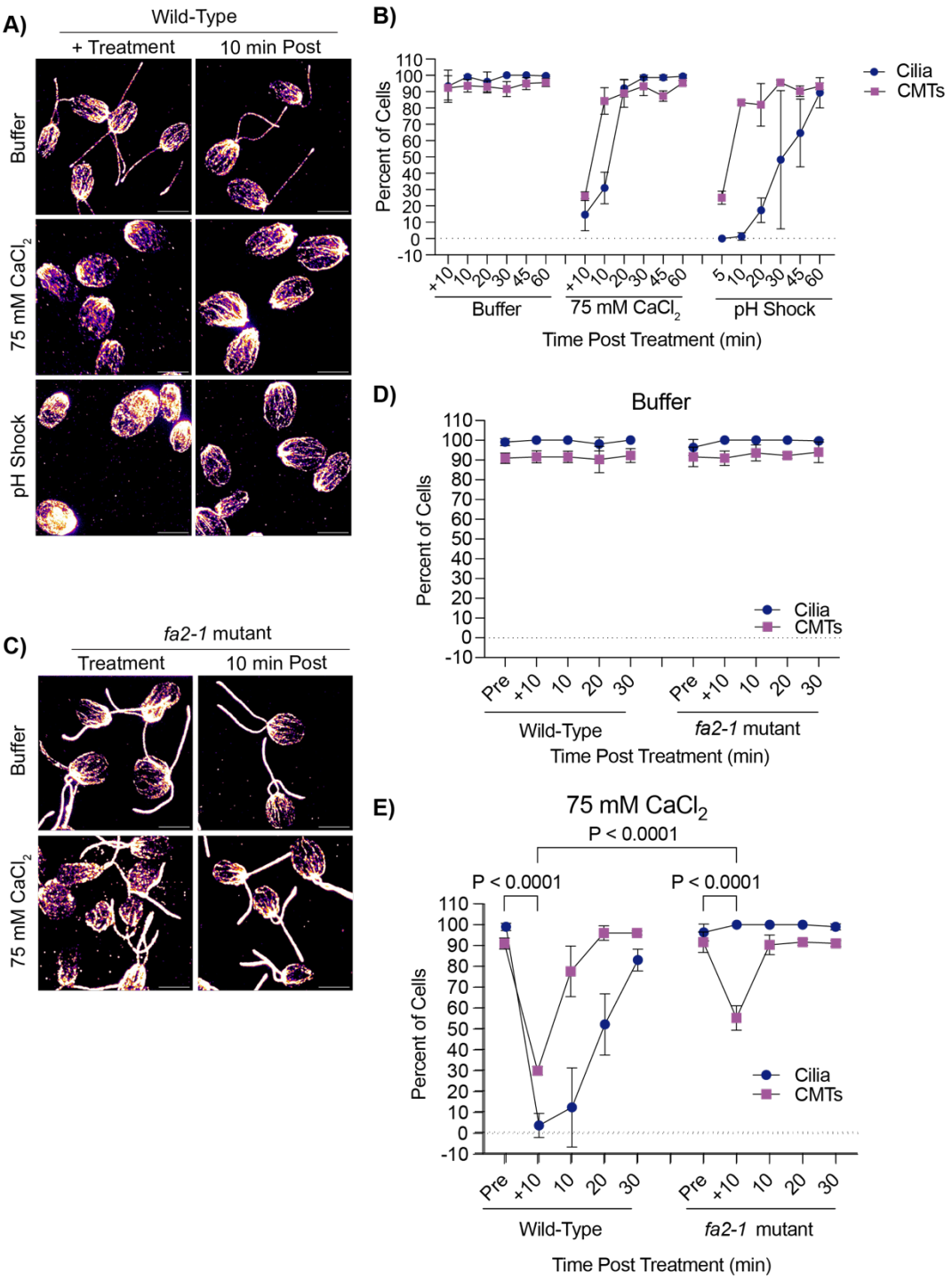

Figure 4.4. Cytoplasmic microtubule depolymerization occurs separately from ciliary shedding during high calcium. A) Wild-type cells were either pretreated for 10 minutes in 5 mM HEPES ("Buffer"), 10 minutes in 75 mM $CaCl_2$, or 45 seconds in acetic acid, and then fixed and stained for β-tubulin. Scale bars are 5 µm. **B)** Quantification of cilia and

CytoMTs from (**A**). Error bars are mean with standard deviation (n=100, N=3). **C)** Representative images of *fa2-1* mutants following treatment in buffer or 75 mM $CaCl_2$. Cells were fixed and stained for β-tubulin. Scale bars are 5 μm. **D-E)** Quantification of wild-type (CC-5325) or *fa2-1* mutants in buffer **(C)** or 75 mM $CaCl_2$ **(E)**. Error bars are mean with standard deviation (n=100, N=3) for the experiment described in **(C).** Statistics compare CytoMTs and were determined using a One-Way ANOVA and Šídák's multiple comparisons test.

Mechanically sheared cilia do not depolymerize CytoMTs and regenerate cilia faster than following chemical shearing

Next we wanted to assess changes to CytoMT polymerization through non-chemical means of ciliary loss. We introduced the cells to a cell homogenizer/bead beater for 3 minutes to excise cilia and then looked at CytoMTs as cilia regenerated (**Figure 4.5A**). Interestingly, mechanical shearing did not induce robust CytoMT depolymerization (**Figure 4.5B**). Further, mechanically sheared cilia were able to regenerate back to full length much faster (in 60 minutes) whereas cilia shed via pH shock were only able to regenerate to half-length in this time (**Figure 4.5C**). Looking more closely at regeneration in these processes, we found that mechanically sheared cilia, which maintain a ~1 μm ciliary track immediately following ciliary excision, can immediately begin steadily regenerating overtime (**Figure 4.5C**). In contrast, pH shocked cells have delayed ciliogenesis, but after this process is started, cells can more rapidly regenerate cilia (**Figure 4.5B-C**). To confirm that this was not a consequence of CytoMT reestablishment, we compared ciliogenesis to CytoMT polymerization. Though pH shocked cells repolymerized CytoMTs within 10-20 minutes, ciliogenesis did not continue until 30-45 minutes post deciliation unlike mechanically sheared cells which maintained both unperturbed CytoMTs and cilia throughout (**Figure 4.5B-C**). These data show that in the case where cilium growth happens faster, CytoMT depolymerization does not occur. Our data may suggest that polymerized CytoMTs facilitate more rapid ciliogenesis. Alternatively, the existence of cilium initial segments may promote more rapid assembly completely independent of CytoMT state that is dependent instead upon

calcium influx (**Figure 4.4**) that may not be triggered upon mechanical shearing. It could be that initiation of ciliary assembly is rate limiting.

The delay in ciliary shedding due to pH shock may differentially affect CytoMTs based on modifications that add stability. One microtubule modification, acetylation, provides stability, strength, and flexibility to microtubules (Janke & Montagnac, 2017). It's possible that during pH shock, changes to acetylation can occur that may be the cause for the delay in ciliogenesis. To test this, we also compared the presence of acetylated α-tubulin in pH shocked cells versus mechanically sheared cells. Deacetylation of α-tubulin has been found to work in concert with ciliary disassembly during mitosis, and acetylation can act as a signal for downstream events such as cell differentiation in adipocytes (Forcioli-Conti et al., 2016). Acetylation recruits further modifications to tubulin that allow for motility and ciliary length maintenance in *Chlamydomonas* as well as human cells (Tripathi et al., 2021). It is possible that pH shock could be inducing upstream pathways that inhibit CytoMT acetylation must be maintained for ciliogenesis. Comparing pH shock to mechanical shearing, we found that during pH shock, acetylated CytoMTs were significantly shorter both overall (**Figure 4.5D and E**) and when comparing the longest acetylated CytoMT per cell (**Figure 4.5D and F**). These data show that pH shock may affect both stabilized and non-stabilized CytoMTs or affect the degree of acetylation of the stabilized population.

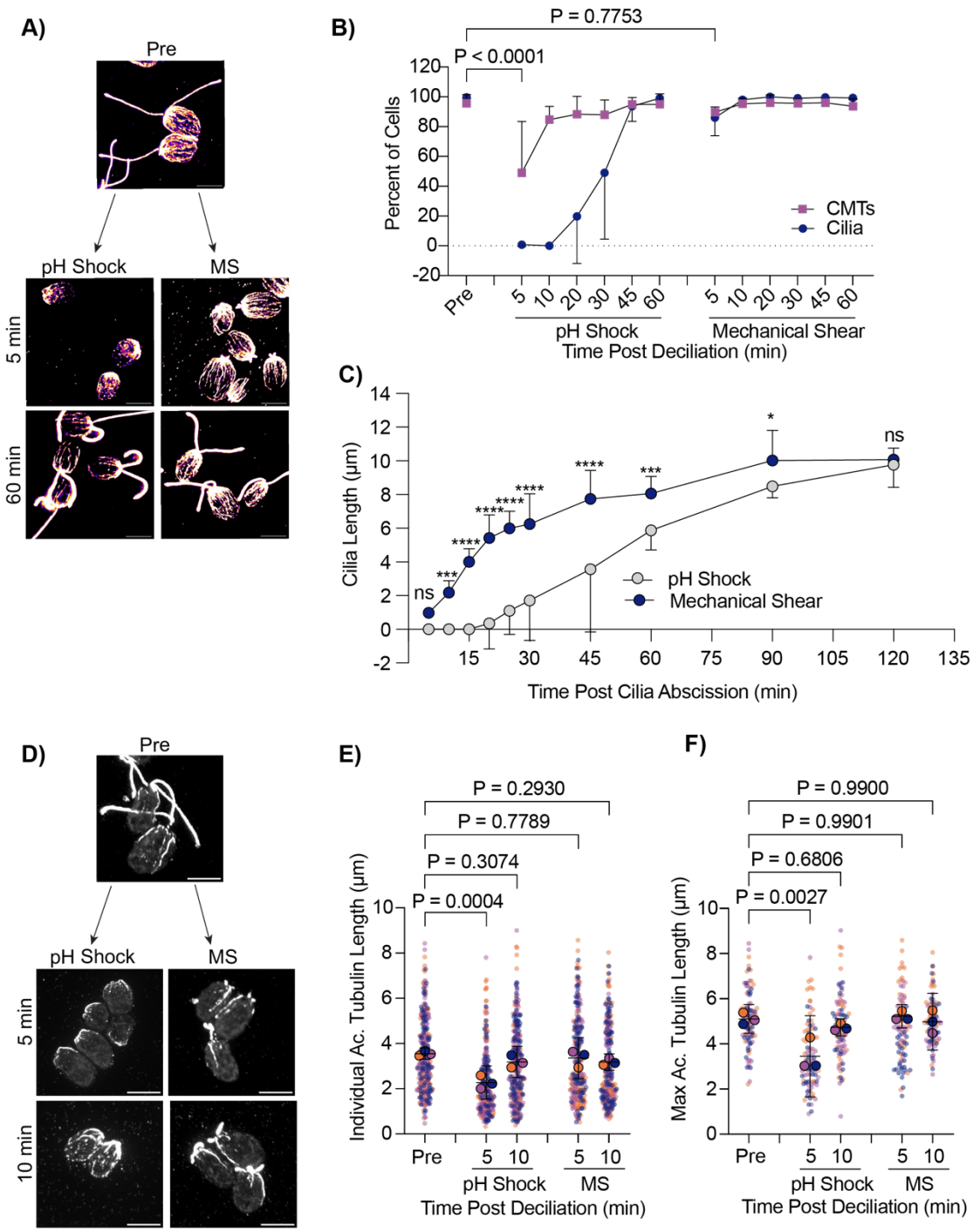

Figure 4.5. Cells maintain intact cytoplasmic microtubules during mechanical shearing and regenerate cilia more quickly. A) Wild-type cells were either pH shocked for 45 s or placed in a cell homogenizer ("Mechanical Shear", "MS") for 3 minutes. Representative images are cells fixed and stained for β-tubulin. Scale bars are 5 µm**. B)** Quantification of percent of cells with cilia (navy circles) compared to polymerized microtubules (purple squares) between

pH shock (left) and MS (right). Error bars are mean with standard deviation. Statistics compare CytoMTs. Significance was determined using a One-Way ANOVA and Šídák's multiple comparisons test (n=30, N=3). **C)** Quantification of cilia length over 2 hours. Error bars are mean with 95% confidence interval (n=30, N=3). Statistics were determined using a Two-Way ANOVA with Šídák's multiple comparisons test (n=30, N=3). (ns - P>0.05, * P≤0.05, ** P≤0.01, *** P≤0.001, **** P≤0.0001). **D)** Wild-type cells were fixed and stained for acetylated α-tubulin following pH shock or MS. Scale bars are 5 μm. **E-F)** Quantification of individual (**E**) or max (**F**) acetylated microtubule lengths. Error bars are mean with 95% confidence interval. Statistics were determined using a One-Way ANOVA and Dunnett's multiple comparisons test (n=30 cells, N=3).

Delayed ciliogenesis upon microtubule depolymerization could indicate that there is a recruitment defect for proteins necessary for ciliogenesis on the cytoplasmic tracks needed for this recruitment or local organization. Using a previously tagged mScarlet-IFT54 anterograde IFT subunit and sfGFP tagged retrograde IFT140 subunit generated and validated by (Wingfield et al., 2021), we compared fluorescence of these complexes at the ciliary base during pH shock and mechanical shear (**Figure 4.S1A and 4.S1C**). We found that during pH shock, there is a significant and more robust increase in fluorescence at the base of cilia for both anterograde (**Figure 4.S1A and 4.S1B**) and retrograde (**Figure 4.S1C and 4.S1D**) trafficking complexes during pH shock as compared to mechanical shearing which remains increased at 10 minutes when CytoMTs have reformed (**Figure 4.3B**). The mitigation of the robust increase in mechanically sheared cells may be due to the availability of a ciliary sink as the cilia are more rapidly growing in this case. In other words, these data suggest two potential factors that impact the quantity of IFT proteins at the ciliary base: 1) the availability of CytoMTs for organization or recruitment of IFT proteins and 2) the presence of a fast-growing cilium with an existing ~1 μm track that acts as a sink for IFT proteins.

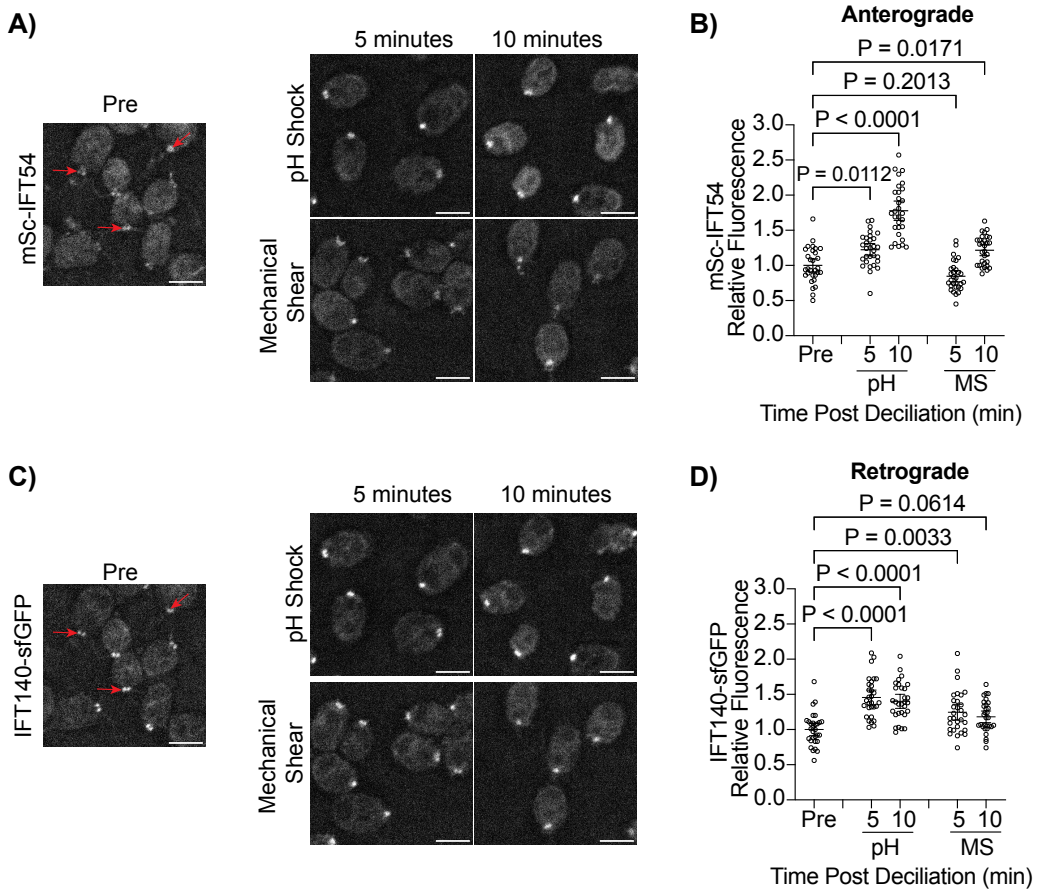

Figure 4.S1. PH shock-induced ciliary shedding increases IFT recruitment to the ciliary base. A and C) mSc-IFT54/IFT140-sfGFP were fixed and imaged. Fluorescence at the base of the cilium was quantified (red arrows). Representative images show cells pre deciliation ("Pre"), 5 min, and 10 min post treatment for both pH shock and mechanical shear for both mSc-IFT154 (**A**) and IFT140-GFP (**C**) transport. Scale bars are 5 µm. **B and D)** Quantification of mSc-IFT54 (**B**) or IFT140-sfGFP (**D**) fluorescent intensity at the ciliary base. Error bars are mean with 95% confidence interval (n=30, N=1). Statistics were determined using a One-Way ANOVA and Šídák's multiple comparisons test.

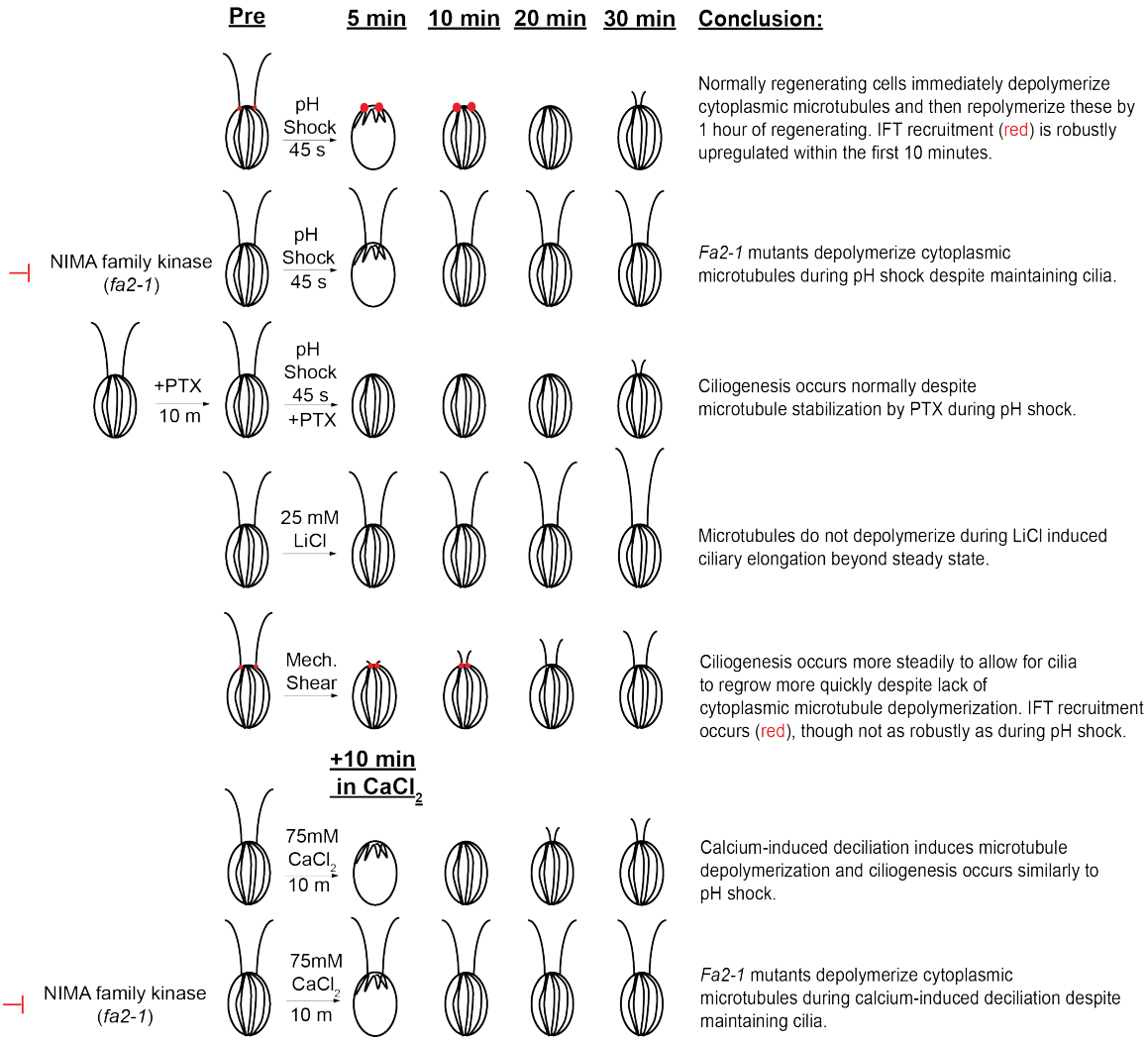

Figure 4.S2. Summary of microtubule dynamics in conjunction with ciliogenesis.

Results from each trial are summarized for each of the different conditions tested up to 30 min. Red dots represent IFT fluorescence tested for both pH shock (top) and mechanical shear (bottom). Adapted from (Dougherty et al., 2022).

DISCUSSION

Throughout this work, we identify the relationship between ciliogenesis and CytoMT polymerization which we tease apart by holding either of these processes constant while varying possible determinants. We find that while CytoMT depolymerization does occur during deciliation with some techniques commonly used to induce deciliation, these dynamics are not necessarily required for ciliary assembly and instead may inhibit ciliary assembly due to CytoMT depolymerization as we see a reestablishment in acetylated microtubule length before ciliogenesis can begin (**Figure 4.5 E-G**) and a need for IFT recruitment to the ciliary base (**Figure 4.S1**). These findings are summarized in **Figure 4.S2**. Our data are consistent with a model in which events happening during deciliation have effects on associated CytoMT processes, but these are not required for ciliogenesis. These data shed light on two important points: 1) tubulin does not necessarily need to be freed up from the cell in order to allow ciliary assembly to occur; and 2) solubilization of cytoplasmic tubulin is neither required nor does it block the mobilization of the intracellular pool of ciliary protein precursors which we see through stimulated IFT recruitment both during pH shock and mechanical shearing, though this response is less robust during mechanical shearing.

While this work addresses the requirement and assembly of tubulin in cytoplasmic microtubules for ciliary dynamics, these experiments are under conditions in which a soluble tubulin pool remains given that there is still a measurable amount of tubulin present both with 15 μM PTX and 40 μM PTX (**Figure 4.1A and B**). It is possible that this amount of tubulin is enough to supply the start of new cilia while the cell begins generating new tubulin for the assembling cilium which occurs immediately following deciliation (Albee et al., 2013). Soluble tubulin that is not incorporated into tubulin filaments during PTX treatment could be degraded or sequestered, preventing it from bind to other microtubule filaments. It is also possible that the cell homeostasis requires maintenance of some level of soluble tubulin. It has been shown that taxol can induce an increase in tubulin synthesis which makes it likely that the cell can maintain a

level of soluble tubulin which can saturate taxol in the cell and give rise to a constant pool of soluble tubulin (Stargell et al., 1992).

Effects of pH shock and calcium on live microtubule dynamics alone have previously been investigated (Liu et al., 2017), however the stability of existing microtubules has not been fully explored. Liu et al., 2017 found that, by using mNeon-Green tagged EB1, a microtubule end-binding protein found on the growing end of microtubules, microtubule growth was frozen in *Chlamydomonas* by decreasing pH and increasing calcium concentration. They also noted that the different *Chlamydomonas* tubulin isoforms have different isoelectric points (α-tubulin = 5.01, β-tubulin = 4.82, and EB1 = 5.7), so dropping the pH below these values which allows for sufficient calcium influx to induce ciliary shedding is also sufficient to separately induce CytoMT depolymerization, along with the ability for calcium alone to inhibit microtubule dynamics. However, despite the effect of pH on CytoMT stability shown in this work, there is also a considerable lag between the time that CytoMTs are reestablished and the timing of initial ciliogenesis (**Figure 4.3B and 4.5B**) which raises the possibility that other signaling pathways that influence ciliogenesis are inhibited during this process. For example, it was previously found that pH shock activates the microtubule depolymerizing kinesin CrKin13 which has also been implicated in ciliogenesis (Wang et al., 2013).

Additionally, this lag in ciliogenesis following pH shock could be due to a lack of CytoMTs altogether for recruitment or organization of proteins needed for ciliary assembly. The well-studied agglutinin protein, SAG1, is one protein which must move from the plasma membrane to the ciliary base upon induction. It has been found that this movement occurs on CytoMTs through the retrograde transport motor cytoplasmic dynein 1b, and following this movement, it can diffuse into the peri-ciliary membrane independent of IFT (Belzile et al., 2014; Cao et al., 2015; Ranjan et al., 2019). Additionally, other ciliary proteins have been found to be assembled in the cytoplasm before reaching the cilium including the cytoplasmic dynein arm 1I (Viswanadha et al., 2014) and channelrhodopsin which move on acetylated rootlet microtubules through IFT to reach the eyespot (Awasthi et al., 2016; Mittelmeier et al., 2011). During pH shock-induced CytoMT depolymerization, it is possible that without the cytoplasmic highways,

proteins cannot reach the ciliary base for transport into the cilium and this is one factor by which ciliogenesis could also be stalled in addition to the delayed build up of IFT at the ciliary base following 10 minutes (**Figure 4.S1B**) when microtubules are repolymerized (**Figure 4.4A**). Future work needs to be done to better understand how different methods of deciliation can ultimately impact cellular processes that directly regulate ciliogenesis and what molecular factors regulate the entry of proteins already at the base during pH shock-induced deciliation versus other mechanisms of deciliation.

MATERIALS AND METHODS

Strains and Maintenance

The wild-type strains (CC-5325 and CC-1690), *fa2-1* mutant (CC-3751), and IFT strain (ift140-1::IFT140-sfGFP ift54-2::mS-IFT54 mt; CC-5862) were acquired from the *Chlamydomonas* Resource Center. Cells were maintained on 1.5% Tris-Acetate-Phosphate (TAP) plates under constant light. For experiments, CC-1690 cells were inoculated into liquid M1 media, and CC-5325 cells, *fa2-1* mutant cells, and IFT cells were inoculated in TAP and grown overnight under constant light and agitation. All media recipes were used according to the *Chlamydomonas* Resource Center.

Ciliary Length Experiments

Steady State Ciliary Length Experiments: overnight cultures were resuspended in fresh TAP or M1 (CC-1690) the next morning. Cells were treated with either DMSO, paclitaxel (PTX, Invitrogen P3456), Colchicine, or LiCl, fixed in equal amounts of 2% Glutaraldehyde, and then imaged on a Zeiss Axioscope 5 DIC with 40x magnification and Zeiss Zen 3.1 software.

PH Shock-Induced Ciliary Shedding and Regeneration: overnight cultures were resuspended in fresh TAP and pretreated or not with PTX 10 minutes prior to deciliation. To induce deciliation, 0.5 M acetic acid was added to the cell suspension to bring the pH down to 4.5 for 45 sec, and then brought back up to 7.0 with 0.5 M potassium hydroxide. Cells were then spun down at 600xg for 1 minute and resuspended in new TAP with or without PTX.

Calcium Chloride-Induced Ciliary Shedding and Regeneration: overnight cultures resuspended in fresh TAP were spun down for 60 seconds at 600xg at room temperature and resuspended in either 5 mM HEPES or 75 mM calcium chloride in 5 mM HEPES for 10 minutes. Then cells were resuspended in fresh media and allowed to regenerate cilia.

Mechanical Shear-Induced Ciliary Shedding and Regeneration: overnight cultures resuspended in fresh TAP were placed in a cell homogenizer (Analog Disruptor Genie) for 3 minutes, spun down for 60 seconds at 600xg at room temperature, and then resuspended in fresh TAP to regenerate.

Immunofluorescence and Quantification

β-Tubulin: Staining was performed as described in (Wang et al., 2013). Briefly, cells were adhered to poly-lysine coated coverslips, fixed in 30 mM HEPES (pH=7.2), 3 mM EGTA, 1 mM $MgSO_4$, and 25 mM KCl with 4% paraformaldehyde ("PFA") for 5 minutes, permeabilized with 0.5% NP-40 for 5 minutes, and then fixed in ice cold methanol for 5 minutes. Coverslips were blocked in 5% BSA and 1% Fish ("Block") gelatin for 30 minutes, then in block with 10% Normal Goat Serum ("NGS", Sigma), and then incubated in β-tubulin primary antibody (CST, 2146S) diluted in 20% block in PBS overnight at 4˚C. Coverslips were washed 3x10 minutes in PBS, incubated in secondary antibody (Alexafluor 488 goat anti-rabbit IgG, A11008, 1:500) for 1 hour, washed 3x10 minutes in PBS, and allowed to dry. Coverslips were mounted in Fluoromount G (Thermo Scientific) before imaging. Cells were imaged on a Nikon Yokogawa SoRa super resolution spinning disk confocal with 100x oil objective (data collection) and 2.8x magnifier (representative images). For quantification, max immunoprojections were generated from z stacks and 100 cells per time point were counted using the Cell Counter tool in FIJI for either having cytoplasmic microtubules polymerized (spanning > half the cell) or not having microtubules polymerized (spanning < half the cell).

Acetylated α-Tubulin: Cells adhered to coverslips were fixed in 4% PFA in 10 mM HEPES for 15 minutes, placed in ice cold 80% acetone for 5 minutes, placed in ice cold 100% acetone for 5 minutes, and then allowed to dry before rehydrating for 5 minutes in PBS. Then cells were blocked in 100% Block for 30 minutes, 10% NGS, and stained for acetylated tubulin (1:1000) overnight at 4˚C. Coverslips were washed 3x10 minutes in PBS incubated with secondary (Alexa Fluor 499 goat anti-mouse IgG, Invitrogen A11001) for 1h at RT, covered, and then washed 3x10 minutes in PBS, covered before allowing to dry completely and mount with Fluoromount G. For

quantification, max IPs were generated and acetylated microtubules were measured using FIJI's segmented line tool starting at the apex of the cell where acetylated microtubules originate and following along the length of the continuous acetylation signal for 30 cells per timepoint.

IFT140/54: Cells adhered to coverslips were placed in ice cold 100% methanol 2x5 minutes, 50% methanol in PBS for 5 minutes, then PBS for 5 minutes before allowing to dry, mount, and image. For quantification, z stacks were summed together, background subtracted with rolling ball radius = 50, and then equal sized circles drawn over the signal at the base of the cilium. Fluorescent intensity was calculated using the calculation for CTCF as previously described (Dougherty et al., 2023)

SDS-PAGE and Immunoblotting

Soluble (S) and insoluble (P) fractions were collected similarly to (Wang et al., 2013). Briefly, 1 mL of treated cells were collected by centrifugation at 600xg for 1 minute at room temperature (RT) and resuspended in 50 µL TMMET Buffer (20 mM Tris-HCl [pH 6.8], 0.14 M NaCl, 1 mM MgCl2, 2 mM EGTA, 4 µg/mL Taxol, and 0.5% Nonidet P-40 Substitute) with 2x30 seconds of vigorous pipetting and 2x30 seconds of gentle vortexing (half-max vortex speed). Cells sat for 10 minutes with 1 gentle round of vortexing at 5 minutes and at 10 minutes before spinning down at 21000xg for 10 minutes at room temperature (RT). The supernatant was collected ("S" fraction) and then the pellet was washed with TMMET buffer. Finally, the remaining pellet was resuspended in 100 µL TMMET buffer ("P" fraction). For loading protein samples into the gel, the S fractions were diluted 1:14 in TMMET buffer and P fractions were diluted 1:56 in TMMET buffer (determined according to detectable signal within the linear range of the antibodies following blot imaging). Protein from S and P fractions were mixed with 2 µL 0.5 M DTT and 4x LDS (Invitrogen), incubated at 70˚C for 10 minutes and run on NuPAGE 10% Bis-Tris gels in MES/SDS-PAGE running buffer (1M MES, 1M Tris base, 69.3 mM SDS, 20.5 mM EDTA free acid). Protein was transferred onto PVDF membrane, blocked in 5% milk (w/v, Signature Select Instant Nonfat Dry Milk) in PBST (1x PBS, 0.1% Tween20), incubated in β-tubulin (1:1000, CST 2146S) or actin C4

(1:1000, Sigma MAB1501) diluted in 1% milk with 1% BSA in PBST overnight at 4˚C. Blots were washed 3x10 minutes in PBST, incubated in secondary antibody diluted in 1% milk with 1% BSA (1:5000, Invitrogen G21234; 1:5000, Invitrogen, 31430) for 1 hour at RT. Blots were washed 3x10 minutes in PBST and then incubated with Pico Chemiluminescent substrate (Invitrogen) and imaged on the Syngene GBOX CHEMI XR 5 using GeneSys software.

Statistical Analysis

Data was collected and organized in Excel, and then graphed and analyzed with GraphPad Prism Version 9.5.1 (528). SuperPlots were made and analyzed according to (Lord et al., 2020) where statistics were performed on the averages of 3 trials and individual trials are represented by corresponding symbol colors. For experiments, “n” is the number of cells quantified and “N” is the number of experiments.

CHAPTER 5:

CONCLUSIONS AND DISCUSSION

Summary

Together, this work brings together several common mechanisms under a ERK pathway components which have not previously been implicated in ciliary regulation. It also describes structural changes to the cell that must cooperate to facilitate ciliary disassembly or prevent elongation.

With regards to ERK-induced ciliary disassembly, we find that cells expressing a GFP-tagged ciliary kinesin motor subunit, KAP-GFP, inhibit motor subunit synthesis and increasingly inhibit its ciliary entry which could be due to slight localization changes of transition zone components including NPHP4. To continue facilitating ciliary shortening, we find that during ERK activation, the cell restricts access to plasma membrane sources for this membrane covered organelle. The cell does this by inhibiting Golgi-derived membrane trafficking to cilia and likely other sources of membrane such as plasma membrane recycling through endosomes. After checking reorganization of actin filaments, we find increased puncta at the apex of the cell which could suggest that membrane recycling and other endocytic events are stalled. Looking at the other cytoskeletal component, microtubules, we find that cytoplasmic microtubules remain depolymerized post deciliation in the presence of BCI.

Next we find that BCI induces changes to the ciliary proteome. Via mass spectrometry, we find changes to proteins involved in ubiquitination which as previously been known to regulate protein trafficking across the transition zone. We find that while proteins in the ciliary lysate are not statistically differentially ubiquitinated in BCI despite finding ubiquitin and ubiquitin-like proteins, we find that the whole cell lysate is significantly differentially ubiquitinated and this pattern of ubiquitination changes in cells regenerating in BCI compared to DMSO. We expand on some of the interesting proteins that are also identified in this data set that provide new avenues to explore for ERK regulation in ciliary dynamics and cell cycle regulation. Among these proteins, we find that vacuole sizes are changed in the presence of BCI indicating new potential mechanisms for ERK-mediated ciliary regulation through membrane sourcing.

Finally, we explore the role for tubulin dynamics in regenerating cilia. We find that pH shock induces cytoplasmic microtubule depolymerization separate from inducing ciliary

shedding. We find mutants which are defective in ciliary shedding through pH shock also depolymerize cytoplasmic microtubules which indicates aberrant processes occurring as a result of pH change. Through mechanically shearing cilia, we also find that not only do cytoplasmic microtubules not depolymerize as a result of an acute need for cilia, but cilia can also immediately begin assembly within 5 minutes of shearing whereas pH shock induces stalling. This work revisits common methods of ciliary shedding and provides a new interpretation for what is required for ciliogenesis.

Implications for ERK signaling in regulating ciliogenesis

It has previously been found that ERK can regulate cellular functions outside of gene transcription. For example, in MCF10A breast epithelial cells and 10T1/2 fibroblasts, ERK is found physically associated with microtubules and mitotic spindles which increases with ERK activation through mutant active H-ras. This, in turn, causes decreased microtubule stability (Harrison & Turley, 2001). During inactivation, ERK1/2 is also known to be retained in the cytosol through binding to MEK (Fukuda, 1997), microtubules (Reszka et al., 1995), and phosphatases such as DUSP6/MKP3 (Karlsson et al., 2004; Mebratu & Tesfaigzi, 2009). While we see microtubule reorganization defects with BCI, we do not see this in the DUSP6 ortholog mutants. This could indicate an off-target effect for BCI, but it could also point to a regulatory role for pERK compared to ERK. In the DUSP6 ortholog double mutants, ERK cannot be phosphorylated/activated with BCI whereas in wild-type cells, ERK is phosphorylated/activated. There is a possibility that pERK specifically can directly regulate microtubule dynamics.

There is also a connection between calcium signaling, known to be stimulated through pH shock induced deciliation (Wheeler et al., 2007), and ERK signaling where signaling of each can regulate the downstream individual outcomes of the other. Calcium can regulate ERK protein interactions which alters its subcellular localization which ultimately regulates ERK's ability to phosphorylate targets in the nucleus or in the cytoplasm. These changes in phosphorylation can regulate gene expression, protein expression, and stability of downstream targets (Chuderland & Seger, 2008). When ERK is phosphorylated, it can move from the cytoplasm into the nucleus to affect gene

transcription. However, increasing calcium can inhibit this nuclear translocation to regulate ERK interactions (Chuderland et al., 2020).

In the case where deciliation occurs in the presence of BCI (**Figure 2.1E**), it is possible that the calcium signaling induced through pH shock can prevent activated ERK from moving to the nucleus for gene transcription; however, it is interesting that without inducing deciliation, cilia still shorten and protein translation, at least in the case of KAP-GFP, is inhibited. It would be interesting to know if BCI causes cell cycle entry and then also cell cycle arrest. While ERK activation causes downregulated of antiproliferative genes from G1 to S phase, persistent ERK activation can inhibit cell cycle progression It is known that stress responses can impact protein translation, and protein translation varies throughout the cell cycle where it is generally reduced during mitosis (Anda & Grallert, 2019).

In addition, we find that BCI induces ubiquitination in the whole cell lysate of *Chlamydomonas* cells separate from the cilia. BCI has previously been found to arrest cells at the S phase and induce intrinsic apoptotic pathways in cancer cells in a dose dependent manner (Shin et al., 2018). It would be very interesting to know if this ubiquitination is happening as a result of ERK signaling or occurs alongside ERK signaling. We find that ubiquitination increases in whole cell lysates with concentrations of BCI that induce ciliary shortening but not full resorption by 2 hours (**Figure 3.5A**), and we see a progressive buildup of ubiquitinated proteins in the whole cell lysate during regeneration in BCI, especially between 30- and 60-minutes post deciliation (**Figure 3.5D**). These data suggest that ubiquitination events are occurring downstream of the direct ERK activation that occurs within 15 minutes of BCI treatment, or secondary effects on cell cycle arrest or other pathways are occurring simultaneously.

Implications for plasma membrane sources for ciliogenesis

ERK signaling is known to regulate clathrin-independent endosomal trafficking through Arf6. U0126 inactivation of ERK perturbs endocytic recycling (u0126 inhibits MEK1/2 and reduces surface expression of the class I major histocompatibility complex

molecule (MHC1) suggesting that steady state ERK activation facilitates endocytosis in mammalian cells (Robertson et al., 2006). This could be occurring in *Chlamydomonas* additionally as we see with the BFA data that there is a possibility for both Golgi trafficking and other sources of membrane to be impacted which could certainly include plasma membrane sources (**Figure 2.5A**). However, it is interesting that with the ERK activation, we see a more severe phenotype for cilia length in conjunction with BFA. In addition, we find that there is a change in the overall vacuole size in Chlamydomonas which could indicate either a redirected source for this membrane, or inhibited membrane trafficking from vacuoles to reduce these vacuole sizes (**Figure 3.3**). While vacuolar ATP synthases have previously been implicated in regulating ciliogenesis through trafficking proteins required for ciliogenesis (Chen et al., 2012), the impact of vacuole size on ciliogenesis potentially through withholding membrane has not been explored and requires more investigation.

Implications for the role of microtubule dynamics on ciliary regulation during pH shock-induced deciliation

The inhibited processes we describe through DUSP6 inhibition/ERK activation could be partially due to inhibited reorganization of cytoplasmic tubulin in response to BCI-induced DUSP6 inhibition. It is unclear if BCI directly binds tubulin to destabilize tubulin filaments and/or if BCI and ERK signaling is ultimately acting through microtubule binding proteins to induce these changes, but it is very likely possible that due to this inhibited reorganization, tubulin cannot be incorporated into cilia or into cytoplasmic microtubule filaments for elongation or maintenance.

However, a need for large scale microtubule rearrangement is not observed in this data for regulating ciliogenesis. While it is reasonable for the cell to require incorporation of monomers into tubulin filaments for maintenance and/or elongation, acute needs for vast amounts of tubulin, such as in assembling a complete cilium in 2 hours, does not require whole-cell tubulin reorganization to free up tubulin monomers as previously thought (Sharma et al., 2011; Wang et al., 2013). It is possible that the cell may regulate tubulin dynamics to prepare for mitosis which requires tubulin reorganization into

spindles (Rasmussen et al., 2013) in addition to the microtubule organizing centers (MTOCs), the basal bodies, to function once again as centrioles alongside newly duplicated daughter centrioles (Kobayashi & Dynlacht, 2011). In steady state cells where there is no induction of cell cycle reentry, this need for rearrangement is not indicated in the data and could explain the ability for immediate ciliogenesis if cytoplasmic microtubules remain intact. It would make sense that maintaining these molecular highways prior to ciliogenesis would allow for quicker cargo and IFT recruitment to the basal bodies for ciliary entry, though we do not observe length differences after a 2 hour growth which suggests lack of changing ciliogenesis speed with taxol stabilized microtubules prior to deciliation with pH shock (**Figure 4.1D**). This could be due to taxol strongly stabilizing microtubules independently of signaling induced regulation and is more competitively binding tubulin compared to the proteins that could mediate this interaction.

This also suggests that cell stresses induce other defects responsible for ciliogenesis. Following pH shock-induced deciliation, cells regenerate cilia more rapidly than at later stages when cilia approach steady state. This could be due to reorganization of the transition zone which could allow for rapid induction of fully assembled trains, rapidly increased protein synthesis or gene transcription (Albee et al., 2013), and/or rapid recruitment of protein and cargo which we see is the case for IFTA/B at the ciliary base (**Figure 4.S1**) (Ludington et al., 2013; Van Den Hoek et al., 2022). This indicates regulation of other components that may be implicated in this type of regulation. It would be interesting to know if AURKA is activated for a short time but then this signal degrades because cells are in quiescence, or the calcium signal is stopped because of removal of the stressor inducing calcium signaling. We know that CrKin13 proteins are stimulated by pH shock (Wang et al., 2013), and pH shock in addition to high concentrations of extracellular calcium can induce calcium-mediated ciliary autotomy (Quarmby, 1996). This calcium signaling could also be signaling to other pathways via Calmodulin which is activated in proportion to the concentration of calcium in the cell and ultimately acts on AURKA to promote ciliary disassembly and prevent assembly (Plotnikova et al., 2012). Upon restoration of calcium stores within the cell, the cell may return to normal quiescent signaling to allow for ciliogenesis.

Conclusions and Future Directions

Overall, our work brings together cell mechanisms of structural changes in the cell that can regulate ciliogenesis. We find that the DUSP6 inhibitor, BCI, can induce changes to cilia in both *Chlamydomonas* cells and in human cells. Ciliary shortening has been extensively studied recently for molecular mechanisms, but this work really ties in the larger aspects of how the cell must coordinate cellular processes to either facilitate ciliary shortening or prevent early ciliogenesis altogether. Beyond the identification of structural changes to cilia, we have also discovered a link between dual specificity phosphatases and ciliary regulation which has not previously been discovered. Through this research, we further implicate the ERK1/2 pathway in ciliary regulation beyond what has previously been known with MEK1/2 regulation, and we find a presence for this pathway signaling in *Chlamydomonas* which does not have a characterized ERK pathway mechanism.

This work has opened up many avenues for future research. ERK activation highlights conserved functions in ERK activation in *Chlamydomonas*, zebrafish, and hERT-RPE1 cells, as well as conserved functions in ciliary shortening in both *Chlamydomonas* and zebrafish. This work ties together various avenues of research describing how the cell can tune various processes to induce ciliary shortening. ERK has hundreds of cellular targets in the nucleus and the cytoplasm which creates signaling mechanism complexity which can be teased apart with known mechanisms regulating ciliary assembly to determine the proximate drivers of cell-cycle and ciliogenesis crosstalk. BCI induces pMAPK activation which we find is inhibited in BCI-treated DUSP double mutants for *Chlamydomonas,* also indicating similar targeting for this drug and finding new proteins in the uncharacterized ERK pathway in *Chlamydomonas* that can control ciliary length with the cell cycle. Further work is needed to determine exactly how DUSP6 in mammalian cells or MKP2/3/5 can work together either with downstream proteins or in conjunction with other pathways to induce changes to cell programming that create dramatic changes to cell dynamics both during early ciliogenesis and during ciliary resorption. Following this work, it would also be very interesting to know if ERK induces signaling for ciliary shortening through AURKA, through separate mechanisms,

or through a combination of mechanisms. It would also be interesting to see if ERK signaling has separate mechanisms for cell tuning from AURKA activation through other pathways that provide specificity for this pathway in regulating ciliogenesis alongside other pathways that are activated at the same time for cell cycle reentry.

REFERENCES

Adams, G. M. W., Huang, B., & Luck, D. J. L. (1982). Temperature-sensitive, assembly-defective flagella mutants of Chlamydomonas Reinhardtii. *Genetics*, *100*(4), 579–586. https://doi.org/10.1093/genetics/100.4.579

Albee, A. J., Kwan, A. L., Lin, H., Granas, D., Stormo, G. D., & Dutcher, S. K. (2013). Identification of cilia genes that affect cell-cycle progression using whole-genome transcriptome analysis in chlamydomonas reinhardtti. *G3: Genes, Genomes, Genetics*, *3*(6), 979–991. https://doi.org/10.1534/g3.113.006338

Alsolami, M., Kuhns, S., Alsulami, M., & Blacque, O. E. (2019). ERICH3 in Primary Cilia Regulates Cilium Formation and the Localisations of Ciliary Transport and Sonic Hedgehog Signaling Proteins. *Scientific Reports*, *9*(1), 1–13. https://doi.org/10.1038/s41598-019-52830-1

Alushin, G. M., Lander, G. C., Kellogg, E. H., Zhang, R., Baker, D., & Nogales, E. (2014). High-Resolution Microtubule Structures Reveal the Structural Transitions in αβ-Tubulin upon GTP Hydrolysis. *Cell*, *157*(5), 1117–1129. https://doi.org/10.1016/j.cell.2014.03.053

Anda, S., & Grallert, B. (2019). Cell-Cycle-Dependent Regulation of Translation: New Interpretations of Old Observations in Light of New Approaches. *BioEssays*, *41*(8), 1900022. https://doi.org/10.1002/bies.201900022

Anvarian, Z., Mykytyn, K., Mukhopadhyay, S., Pedersen, L. B., & Christensen, S. T. (2019). Cellular signalling by primary cilia in development, organ function and disease. *Nature Reviews Nephrology*, *15*(4), 199–219. https://doi.org/10.1038/s41581-019-0116-9

Auclair, W., & Siegel, B. W. (1966). Cilia Regeneration in the Sea Urchin Embryo: Evidence for a Pool of Ciliary Proteins. *Science*, *154*(3751), 913–915. https://doi.org/10.1126/science.154.3751.913

Avasthi, P., Marley, A., Lin, H., Gregori-Puigjane, E., Shoichet, B. K., von Zastrow, M., & Marshall, W. F. (2012). A Chemical Screen Identifies Class A G-Protein Coupled

Receptors As Regulators of Cilia. *ACS Chemical Biology*, *7*(5), 911–919. https://doi.org/10.1021/cb200349v

Avasthi, P., & Marshall, W. F. (2012). Stages of ciliogenesis and regulation of ciliary length. *Differentiation*, *83*(2), S30–S42. https://doi.org/10.1016/j.diff.2011.11.015

Avidor-Reiss, T., & Leroux, M. R. (2015). Shared and Distinct Mechanisms of Compartmentalized and Cytosolic Ciliogenesis. *Current Biology*, *25*(23), R1143–R1150. https://doi.org/10.1016/j.cub.2015.11.001

Awasthi, M., Ranjan, P., Sharma, K., Veetil, S. K., & Kateriya, S. (2016). The trafficking of bacterial type rhodopsins into the Chlamydomonas eyespot and flagella is IFT mediated. *Scientific Reports*, *6*(1), 34646. https://doi.org/10.1038/srep34646

Awata, J., Takada, S., Standley, C., Lechtreck, K. F., Bellvé, K. D., Pazour, G. J., Fogarty, K. E., & Witman, G. B. (2014). NPHP4 controls ciliary trafficking of membrane proteins and large soluble proteins at the transition zone. *Journal of Cell Science*, *127*(21), 4714–4727. https://doi.org/10.1242/jcs.155275

Azimzadeh, J., & Marshall, W. F. (2010). Building the Centriole. *Current Biology*, *20*(18), R816–R825. https://doi.org/10.1016/j.cub.2010.08.010

Belzile, O., Hernandez-Lara, C., Wang, Q., & Snell, W. J. (2014). Regulated membrane protein entry into flagella is facilitated by cytoplasmic microtubules and does not require IFT. *Bone*, *23*(1), 1–7. https://doi.org/10.1016/j.cub.2013.06.025.Regulated

Bengs, F., Scholz, A., Kuhn, D., & Wiese, M. (2005). LmxMPK9, a mitogen-activated protein kinase homologue affects flagellar length in Leishmania mexicana. *Molecular Microbiology*, *55*(5), 1606–1615. https://doi.org/10.1111/j.1365-2958.2005.04498.x

Berman, S. A., Wilson, N. F., Haas, N. A., & Lefebvre, P. A. (2003). A Novel MAP Kinase Regulates Flagellar Length in Chlamydomonas. *Current Biology*, *13*, 1145–1149. https://doi.org/10.1016/S

Bielas, S. L., Silhavy, J. L., Brancati, F., Kisseleva, M. V., Al-Gazali, L., Sztriha, L., Bayoumi, R. A., Zaki, M. S., Abdel-Aleem, A., Rosti, R. O., Kayserili, H., Swistun, D., Scott, L. C., Bertini, E., Boltshauser, E., Fazzi, E., Travaglini, L., Field, S. J., Gayral, S.,

… Gleeson, J. G. (2009). Mutations in INPP5E, encoding inositol polyphosphate-5-phosphatase E, link phosphatidyl inositol signaling to the ciliopathies. *Nature Genetics*, *41*(9), 1032–1036. https://doi.org/10.1038/ng.423

Bigge, B. M., Rosenthal, N. E., & Avasthi, P. (2023). Initial ciliary assembly in *Chlamydomonas* requires Arp2/3 complex-dependent endocytosis. *Molecular Biology of the Cell*, mbc.E22-09-0443. https://doi.org/10.1091/mbc.E22-09-0443

Bradley, B. A., & Quarmby, L. M. (2005). A NIMA-related kinase, Cnk2p, regulates both flagellar length and cell size in *Chlamydomonas*. *Journal of Cell Science*, *118*(15), 3317–3326. https://doi.org/10.1242/jcs.02455

Brewer, G. J. (2010). Copper toxicity in the general population. *Clinical Neurophysiology*, *121*(4), 459–460. https://doi.org/10.1016/j.clinph.2009.12.015

Brown, J. M., Marsala, C., Kosoy, R., & Gaertig, J. (1999). Kinesin-II is preferentially targeted to assembling cilia and is required for ciliogenesis and normal cytokinesis in Tetrahymena. *Molecular Biology of the Cell*, *10*(10), 3081–3096. https://doi.org/10.1091/mbc.10.10.3081

Cao, M., Ning, J., Hernandez-Lara, C. I., Belzile, O., Wang, Q., Dutcher, S. K., Liu, Y., & Snell, W. J. (2015). Uni-directional ciliary membrane protein trafficking by a cytoplasmic retrograde IFT motor and ciliary ectosome shedding. *ELife*, *4*, e05242. https://doi.org/10.7554/eLife.05242

Chan, L. N., Murakami, M. A., Robinson, M. E., Caeser, R., Sadras, T., Lee, J., Cosgun, K. N., Kume, K., Khairnar, V., Xiao, G., Ahmed, M. A., Aghania, E., Deb, G., Hurtz, C., Shojaee, S., Hong, C., Pölönen, P., Nix, M. A., Chen, Z., … Müschen, M. (2020). Signalling input from divergent pathways subverts B cell transformation. *Nature*, *583*(7818), 845–851. https://doi.org/10.1038/s41586-020-2513-4

Chen, Y., Wu, B., Xu, L., Li, H., Xia, J., Yin, W., Li, Z., Shi, D., Li, S., Lin, S., Shu, X., & Pei, D. (2012). A SNX10/V-ATPase pathway regulates ciliogenesis in vitro and in vivo. *Cell Research*, *22*(2), 333–345. https://doi.org/10.1038/cr.2011.134

Chiuso, F., Delle Donne, R., Giamundo, G., Rinaldi, L., Borzacchiello, D., Moraca, F., Intartaglia, D., Iannucci, R., Senatore, E., Lignitto, L., Garbi, C., Conflitti, P., Catalanotti, B., Conte, I., & Feliciello, A. (2023). Ubiquitylation of BBSome is required for ciliary assembly and signaling. *EMBO Reports*, *24*(4), e55571. https://doi.org/10.15252/embr.202255571

Chuderland, D., Marmor, G., Shainskaya, A., & Seger, R. (2020). *Calcium-Mediated Interactions Regulate the Subcellular Localization of Extracellular Signal-Regulated Kinases (ERKs)*.

Chuderland, D., & Seger, R. (2008). Calcium regulates ERK signaling by modulating its protein-protein interactions. *Communicative & Integrative Biology*, *1*(1), 4–5. https://doi.org/10.4161/cib.1.1.6107

Clement, D. L., Mally, S., Stock, C., Lethan, M., Satir, P., Schwab, A., Pedersen, S. F., & Christensen, S. T. (2012). PDGFRα signaling in the primary cilium regulates NHE1-dependent fibroblast migration via coordinated differential activity of MEK1/2-ERK1/2-p90RSK and AKT signaling pathways. *Journal of Cell Science*, jcs.116426. https://doi.org/10.1242/jcs.116426

Craft, J. M., Harris, J. A., Hyman, S., Kner, P., & Lechtreck, K. F. (2015). Tubulin transport by IFT is upregulated during ciliary growth by a cilium-autonomous mechanism. *Journal of Cell Biology*, *208*(2), 223–237. https://doi.org/10.1083/jcb.201409036

Craig, E., & Avasthi, P. (2019). Visualizing Filamentous Actin in Chlamydomonas reinhardtii. *BIO-PROTOCOL*, *9*(12). https://doi.org/10.21769/BioProtoc.3274

Craige, B., Brown, J. M., & Witman, G. B. (2013). Isolation of Chlamydomonas Flagella. *Current Protocols in Cell Biology*, *59*(1). https://doi.org/10.1002/0471143030.cb0341s59

de Forges, H., Bouissou, A., & Perez, F. (2012). Interplay between microtubule dynamics and intracellular organization. *The International Journal of Biochemistry & Cell Biology*, *44*(2), 266–274. https://doi.org/10.1016/j.biocel.2011.11.009

Dentler, W. (2013). A Role for the Membrane in Regulating Chlamydomonas Flagellar Length. *PLoS ONE*, *8*(1). https://doi.org/10.1371/journal.pone.0053366

Dentler, W., & Adams, C. (1992). Flagellar microtubule dynamics in Chlamydomonas: Cytochalasin D induces periods of microtubule shortening and elongation; and colchicine induces disassembly of the distal, but not proximal, half of the flagellum. *Journal of Cell Biology*, *117*(6), 1289–1298. https://doi.org/10.1083/jcb.117.6.1289

Desai, P. B., Stuck, M. W., Lv, B., & Pazour, G. J. (2020). Ubiquitin links smoothened to intraflagellar transport to regulate Hedgehog signaling. *Journal of Cell Biology*, *219*(7), e201912104. https://doi.org/10.1083/jcb.201912104

Diener, D. R., Lupetti, P., & Rosenbaum, J. L. (2015). Proteomic analysis of isolated ciliary transition zones reveals the presence of ESCRT proteins. *Current Biology*, *25*(3), 379–384. https://doi.org/10.1016/j.cub.2014.11.066

Dong, Z., Xu, J., & Pan, J. (2021). Identification of Regulators for Ciliary Disassembly by a Chemical Screen. *ACS Chemical Biology*, *16*(11), 2665–2672. https://doi.org/10.1021/acschembio.1c00823

Doornbos, C., & Roepman, R. (2021). Moonlighting of mitotic regulators in cilium disassembly. *Cellular and Molecular Life Sciences*, *78*(11), 4955–4972. https://doi.org/10.1007/s00018-021-03827-5

Dougherty, L. L., Dutta, S., & Avasthi, P. (2023). The ERK activator, BCI, inhibits ciliogenesis and causes defects in motor behavior, ciliary gating, and cytoskeletal rearrangement. *Life Science Alliance*, *6*(6), e202301899. https://doi.org/10.26508/lsa.202301899

Forcioli-Conti, N., Estève, D., Bouloumié, A., Dani, C., & Peraldi, P. (2016). The size of the primary cilium and acetylated tubulin are modulated during adipocyte differentiation: Analysis of HDAC6 functions in these processes. *Biochimie*, *124*, 112–123. https://doi.org/10.1016/j.biochi.2015.09.011

Fritsche-Guenther, R., Witzel, F., Sieber, A., Herr, R., Schmidt, N., Braun, S., Brummer, T., Sers, C., & Blüthgen, N. (2011). Strong negative feedback from Erk to Raf confers

robustness to MAPK signalling. *Molecular Systems Biology*, *7*(1), 489. https://doi.org/10.1038/msb.2011.27

Fukuda, M. (1997). Interaction of MAP kinase with MAP kinase kinase: Its possible role in the control of nucleocytoplasmic transport of MAP kinase. *The EMBO Journal*, *16*(8), 1901–1908. https://doi.org/10.1093/emboj/16.8.1901

Gadadhar, S., Dadi, H., Bodakuntla, S., Schnitzler, A., Bièche, I., Rusconi, F., & Janke, C. (2017). Tubulin glycylation controls primary cilia length. *Journal of Cell Biology*, *216*(9), 2701–2713. https://doi.org/10.1083/jcb.201612050

Gänger, S., & Schindowski, K. (2018). Tailoring Formulations for Intranasal Nose-to-Brain Delivery: A Review on Architecture, Physico-Chemical Characteristics and Mucociliary Clearance of the Nasal Olfactory Mucosa. *Pharmaceutics*, *10*(3), 116. https://doi.org/10.3390/pharmaceutics10030116

Garcia-Gonzalo, F. R., & Reiter, J. F. (2017). Open Sesame: How transition fibers and the transition zone control ciliary composition. *Cold Spring Harbor Perspectives in Biology*, *9*(2). https://doi.org/10.1101/cshperspect.a028134

Giannakakou, P., Robey, R., Fojo, T., & Blagosklonny, M. V. (2001). Low concentrations of paclitaxel induce cell type-dependent p53, p21 and G1/G2 arrest instead of mitotic arrest: Molecular determinants of paclitaxel-induced cytotoxicity. *Oncogene*, *20*(29), 3806–3813. https://doi.org/10.1038/sj.onc.1204487

Goetz, S. C., & Anderson, K. V. (2010). The primary cilium: A signalling centre during vertebrate development. *Nature Reviews Genetics*, *11*(5), 331–344. https://doi.org/10.1038/nrg2774

Gogendeau, D., Lemullois, M., Le Borgne, P., Castelli, M., Aubusson-Fleury, A., Arnaiz, O., Cohen, J., Vesque, C., Schneider-Maunoury, S., Bouhouche, K., Koll, F., & Tassin, A. M. (2020). MKS-NPHP module proteins control ciliary shedding at the transition zone. *PLoS Biology*, *18*(3), 1–28. https://doi.org/10.1371/journal.pbio.3000640

Gonçalves, J., & Pelletier, L. (2017). The Ciliary Transition Zone: Finding the Pieces and Assembling the Gate. *Molecules and Cells*, *40*(4), 243–253. https://doi.org/10.14348/molcells.2017.0054

Goodstein, D. M., Shu, S., Howson, R., Neupane, R., Hayes, R. D., Fazo, J., Mitros, T., Dirks, W., Hellsten, U., Putnam, N., & Rokhsar, D. S. (2012). Phytozome: A comparative platform for green plant genomics. *Nucleic Acids Research*, *40*(D1), D1178–D1186. https://doi.org/10.1093/nar/gkr944

Halder, P., Khatun, S., & Majumder, S. (2020). Freeing the brake: Proliferation needs primary cilium to disassemble. *Journal of Biosciences*, *45*(1), 117. https://doi.org/10.1007/s12038-020-00090-x

Harrison, R. E., & Turley, E. A. (2001). *Active Erk Regulates Microtubule Stability in H-ras–Transformed Cells*. *3*(5).

Hartzell, L. B., Hartzell, H. C., & Quarmby, L. M. (1993). Mechanisms of Flagellar Excision. *Experimental Cell Research*, *208*(1), 148–153. https://doi.org/10.1006/excr.1993.1232

Hicke, L., & Dunn, R. (2003). Regulation of Membrane Protein Transport by Ubiquitin and Ubiquitin-Binding Proteins. *Annual Review of Cell and Developmental Biology*, *19*(1), 141–172. https://doi.org/10.1146/annurev.cellbio.19.110701.154617

Hough, R., Pratt, G., & Rechsteiner, M. (1986). Ubiquitin-lysozyme conjugates. Identification and characterization of an ATP-dependent protease from rabbit reticulocyte lysates. *Journal of Biological Chemistry*, *261*(5), 2400–2408. https://doi.org/10.1016/S0021-9258(17)35950-1

Huang, K., Diener, D. R., & Rosenbaum, J. L. (2009). The ubiquitin conjugation system is involved in the disassembly of cilia and flagella. *Journal of Cell Biology*, *186*(4), 601–613. https://doi.org/10.1083/jcb.200903066

Ice, R. J., McLaughlin, S. L., Livengood, R. H., Culp, M. V., Eddy, E. R., Ivanov, A. V., & Pugacheva, E. N. (2013). NEDD9 Depletion Destabilizes Aurora A Kinase and Heightens the Efficacy of Aurora A Inhibitors: Implications for Treatment of Metastatic

Solid Tumors. *Cancer Research*, *73*(10), 3168–3180. https://doi.org/10.1158/0008-5472.CAN-12-4008

Ikeda, K., Brown, J. A., Yagi, T., Norrander, J. M., Hirono, M., Eccleston, E., Kamiya, R., & Linck, R. W. (2003). Rib72, a conserved protein associated with the ribbon compartment of flagellar A-microtubules and potentially involved in the linkage between outer doublet microtubules. *Journal of Biological Chemistry*, *278*(9), 7725–7734. https://doi.org/10.1074/jbc.M210751200

Inaba, K., & Mizuno, K. (2016). Sperm dysfunction and ciliopathy. *Reproductive Medicine and Biology*, *15*(2), 77–94. https://doi.org/10.1007/s12522-015-0225-5

Inoko, A., Matsuyama, M., Goto, H., Ohmuro-Matsuyama, Y., Hayashi, Y., Enomoto, M., Ibi, M., Urano, T., Yonemura, S., Kiyono, T., Izawa, I., & Inagaki, M. (2012). Trichoplein and Aurora A block aberrant primary cilia assembly in proliferating cells. *Journal of Cell Biology*, *197*(3), 391–405. https://doi.org/10.1083/jcb.201106101

Ishikawa, H., & Marshall, W. F. (2017). Intraflagellar Transport and Ciliary Dynamics. *Cold Spring Harbor Perspectives in Biology*, *9*(3), a021998. https://doi.org/10.1101/cshperspect.a021998

Izawa, I., Goto, H., Kasahara, K., & Inagaki, M. (2015). Current topics of functional links between primary cilia and cell cycle. *Cilia*, *4*(1), 1–13. https://doi.org/10.1186/s13630-015-0021-1

Jacoby, M., Cox, J. J., Gayral, S., Hampshire, D. J., Ayub, M., Blockmans, M., Pernot, E., Kisseleva, M. V., Compère, P., Schiffmann, S. N., Gergely, F., Riley, J. H., Pérez-Morga, D., Woods, C. G., & Schurmans, S. (2009). INPP5E mutations cause primary cilium signaling defects, ciliary instability and ciliopathies in human and mouse. *Nature Genetics*, *41*(9), 1027–1031. https://doi.org/10.1038/ng.427

Jain, B. P., & Pandey, S. (2018). WD40 Repeat Proteins: Signalling Scaffold with Diverse Functions. *The Protein Journal*, *37*(5), 391–406. https://doi.org/10.1007/s10930-018-9785-7

James, N. E., Beffa, L., Oliver, M. T., Borgstadt, A. D., Emerson, J. B., Chichester, C. O., Yano, N., Freiman, R. N., DiSilvestro, P. A., & Ribeiro, J. R. (2019). Inhibition of DUSP6 sensitizes ovarian cancer cells to chemotherapeutic agents via regulation of ERK signaling response genes. *Oncotarget*, *10*(36), 3315–3327. https://doi.org/10.18632/oncotarget.26915

Janke, C., & Montagnac, G. (2017). Causes and Consequences of Microtubule Acetylation. *Current Biology*, *27*(23), R1287–R1292. https://doi.org/10.1016/j.cub.2017.10.044

Jensen, C. G., Davison, E. A., Bowser, S. S., & Rieder, C. L. (1987). Primary cilia cycle in PtK1 cells: Effects of colcemid and taxol on cilia formation and resorption. *Cell Motility and the Cytoskeleton*, *7*(3), 187–197. https://doi.org/10.1002/cm.970070302

Ji, W., Tang, Z., Chen, Y., Wang, C., Tan, C., Liao, J., Tong, L., & Xiao, G. (2022). Ependymal Cilia: Physiology and Role in Hydrocephalus. *Frontiers in Molecular Neuroscience*, *15*, 927479. https://doi.org/10.3389/fnmol.2022.927479

Jiang, H., Liu, S., Cheung, M.-H., Amin, A., & Liang, C. (2020). FOP Negatively Regulates Ciliogenesis and Promotes Cell Cycle Re-entry by Facilitating Primary Cilia Disassembly. *Frontiers in Cell and Developmental Biology*, *8*, 590449. https://doi.org/10.3389/fcell.2020.590449

Joshua Mueller, †, & Catherine A. Perrone, *† Raqual Bower, * Douglas G. Cole, ‡ and Mary E. Porter. (2004). The FLA3 KAP Subunit Is Required for Localization of Kinesin-2 to the Site of Flagellar Assembly and Processive Anterograde Intraflagellar Transport. *Mol Biol Cell*, *16*(December), 1341–1354. https://doi.org/10.1091/mbc.E04

Kasahara, K., & Inagaki, M. (2021). Primary ciliary signaling: Links with the cell cycle. *Trends in Cell Biology*, *31*(12), 954–964. https://doi.org/10.1016/j.tcb.2021.07.009

Kane, E. I., & Spratt, D. E. (2021). Structural Insights into Ankyrin Repeat-Containing Proteins and Their Influence in Ubiquitylation. *International Journal of Molecular Sciences*, *22*(2), 609. https://doi.org/10.3390/ijms22020609

Karlsson, M., Mathers, J., Dickinson, R. J., Mandl, M., & Keyse, S. M. (2004). Both Nuclear-Cytoplasmic Shuttling of the Dual Specificity Phosphatase MKP-3 and Its Ability to Anchor MAP Kinase in the Cytoplasm Are Mediated by a Conserved Nuclear Export Signal. *Journal of Biological Chemistry*, *279*(40), 41882–41891. https://doi.org/10.1074/jbc.M406720200

Kasahara, K., Kawakami, Y., Kiyono, T., Yonemura, S., Kawamura, Y., Era, S., Matsuzaki, F., Goshima, N., & Inagaki, M. (2014). Ubiquitin-proteasome system controls ciliogenesis at the initial step of axoneme extension. *Nature Communications*, *5*(1), 5081. https://doi.org/10.1038/ncomms6081

Khanna, H. (2015). Photoreceptor Sensory Cilium: Traversing the Ciliary Gate. *Cells*, *4*(4), 674–686. https://doi.org/10.3390/cells4040674

Kim, J., Jo, H., Hong, H., Kim, M. H., Kim, J. M., Lee, J.-K., Heo, W. D., & Kim, J. (2015). Actin remodelling factors control ciliogenesis by regulating YAP/TAZ activity and vesicle trafficking. *Nature Communications*, *6*(1), 6781. https://doi.org/10.1038/ncomms7781

Kim, J., Lee, J. E., Heynen-Genel, S., Suyama, E., Ono, K., Lee, K., Ideker, T., Aza-Blanc, P., & Gleeson, J. G. (2010). Functional genomic screen for modulators of ciliogenesis and cilium length. *Nature*, *464*(7291), 1048–1051. https://doi.org/10.1038/nature08895

Kim, S., Lee, K., Choi, J.-H., Ringstad, N., & Dynlacht, B. D. (2015). Nek2 activation of Kif24 ensures cilium disassembly during the cell cycle. *Nature Communications*, *6*(1), 8087. https://doi.org/10.1038/ncomms9087

Kim, S., & Tsiokas, L. (2011). Cilia and cell cycle re-entry: More than a coincidence. *Cell Cycle*, *10*(16), 2683–2690. https://doi.org/10.4161/cc.10.16.17009

Kim, S., Zaghloul, N. A., Bubenshchikova, E., Oh, E. C., Rankin, S., Katsanis, N., Obara, T., & Tsiokas, L. (2011). Nde1-mediated inhibition of ciliogenesis affects cell cycle re-entry. *Nature Cell Biology*, *13*(4), 351–360. https://doi.org/10.1038/ncb2183

Klink, B. U., Gatsogiannis, C., Hofnagel, O., Wittinghofer, A., & Raunser, S. (2020). Structure of the human BBSome core complex. *ELife*, *9*, e53910. https://doi.org/10.7554/eLife.53910

Kobayashi, T., & Dynlacht, B. D. (2011). Regulating the transition from centriole to basal body. *Journal of Cell Biology*, *193*(3), 435–444. https://doi.org/10.1083/jcb.201101005

Kobayashi, T., Ishida, Y., Hirano, T., Katoh, Y., & Nakayama, K. (2021). Cooperation of the IFT-A complex with the IFT-B complex is required for ciliary retrograde protein trafficking and GPCR import. *Molecular Biology of the Cell*, *32*(1), 45–56. https://doi.org/10.1091/mbc.E20-08-0556

Kong, M. J., Bak, S. H., Han, K.-H., Kim, J. I., Park, J.-W., & Park, K. M. (2019). Fragmentation of kidney epithelial cell primary cilia occurs by cisplatin and these cilia fragments are excreted into the urine. *Redox Biology*, *20*, 38–45. https://doi.org/10.1016/j.redox.2018.09.017

Korobeynikov, V., Deneka, A. Y., & Golemis, E. A. (2017). Mechanisms for nonmitotic activation of Aurora-A at cilia. *Biochemical Society Transactions*, *45*(1), 37–49. https://doi.org/10.1042/BST20160142

Kozminski, K. G., Beech, P. L., & Rosenbaum, J. L. (1995). The Chlamydomonas kinesin-like protein FLA10 is involved in motility associated with the flagellar membrane. *Journal of Cell Biology*, *131*(6), 1517–1527. https://doi.org/10.1083/jcb.131.6.1517

Kuhns, S., Schmidt, K. N., Reymann, J., Gilbert, D. F., Neuner, A., Hub, B., Carvalho, R., Wiedemann, P., Zentgraf, H., Erfle, H., Klingmüller, U., Boutros, M., & Pereira, G. (2013). The microtubule affinity regulating kinase MARK4 promotes axoneme extension during early ciliogenesis. *Journal of Cell Biology*, *200*(4), 505–522. https://doi.org/10.1083/jcb.201206013

Kulaga, H. M., Leitch, C. C., Eichers, E. R., Badano, J. L., Lesemann, A., Hoskins, B. E., Lupski, J. R., Beales, P. L., Reed, R. R., & Katsanis, N. (2004). Loss of BBS proteins

causes anosmia in humans and defects in olfactory cilia structure and function in the mouse. *Nature Genetics*, *36*(9), 994–998. https://doi.org/10.1038/ng1418

Lacey, S. E., Foster, H. E., & Pigino, G. (2023). The molecular structure of IFT-A and IFT-B in anterograde intraflagellar transport trains. *Nature Structural & Molecular Biology*. https://doi.org/10.1038/s41594-022-00905-5

Lake, D., Corrêa, S. A. L., & Müller, J. (2016). Negative feedback regulation of the ERK1/2 MAPK pathway. *Cellular and Molecular Life Sciences*, *73*(23), 4397–4413. https://doi.org/10.1007/s00018-016-2297-8

Lane, N. (2015). The unseen world: Reflections on Leeuwenhoek (1677) 'Concerning little animals.' *Philosophical Transactions of the Royal Society B: Biological Sciences*, *370*(1666), 20140344. https://doi.org/10.1098/rstb.2014.0344

Lattao, R., Kovács, L., & Glover, D. M. (2017). The Centrioles,Centrosomes, Basal Bodies, and Cilia of *Drosophila melanogaster*. *Genetics*, *206*(1), 33–53. https://doi.org/10.1534/genetics.116.198168

Lechtreck, K.-F., Luro, S., Awata, J., & Witman, G. B. (2009). HA-tagging of putative flagellar proteins in *Chlamydomonas reinhardtii* identifies a novel protein of intraflagellar transport complex B. *Cell Motility and the Cytoskeleton*, *66*(8), 469–482. https://doi.org/10.1002/cm.20369

Lechtreck, K. F., Van De Weghe, J. C., Harris, J. A., & Liu, P. (2017). Protein transport in growing and steady-state cilia. *Traffic*, *18*(5), 277–286. https://doi.org/10.1111/tra.12474

Lefebvre, P. A. (1995). Chapter 1 Flagellar Amputation and Regeneration in Chlamydomonas. In W. Dentler & G. Witman (Eds.), *Methods in Cell Biology* (Vol. 47, pp. 3–7). Academic Press. https://doi.org/10.1016/S0091-679X(08)60782-7

Lewin, R. A., Lee, T. H., & Fang, L. S. (1982). Effects of various agents on flagellar activity, flagellar autotomy and cell viability in four species of Chlamydomonas (chlorophyta: Volvocales). *Symposia of the Society for Experimental Biology*, *35*, 421–437.

Li, A., Saito, M., Chuang, J. Z., Tseng, Y. Y., Dedesma, C., Tomizawa, K., Kaitsuka, T., & Sung, C. H. (2011). Ciliary transition zone activation of phosphorylated Tctex-1 controls ciliary resorption, S-phase entry and fate of neural progenitors. *Nature Cell Biology*, *13*(4), 402–411. https://doi.org/10.1038/ncb2218

Li, D., & Roberts, R. (2001). *Human Genome and Diseases: Review*. *58*.

Li, W., & Ye, Y. (2008). Polyubiquitin chains: Functions, structures, and mechanisms. *Cellular and Molecular Life Sciences*, *65*(15), 2397–2406. https://doi.org/10.1007/s00018-008-8090-6

Li, X., Patena, W., Fauser, F., Jinkerson, R. E., Saroussi, S., Meyer, M. T., Ivanova, N., Robertson, J. M., Yue, R., Zhang, R., Vilarrasa-Blasi, J., Wittkopp, T. M., Ramundo, S., Blum, S. R., Goh, A., Laudon, M., Srikumar, T., Lefebvre, P. A., Grossman, A. R., & Jonikas, M. C. (2019). A genome-wide algal mutant library and functional screen identifies genes required for eukaryotic photosynthesis. *Nature Genetics*, *51*(4), 627–635. https://doi.org/10.1038/s41588-019-0370-6

Lin, Y. K., Wu, W., Ponce, R. K., Kim, J. W., & Okimoto, R. A. (2020). Negative MAPK-ERK regulation sustains CIC-DUX4 oncoprotein expression in undifferentiated sarcoma. *Proceedings of the National Academy of Sciences*, *117*(34), 20776–20784. https://doi.org/10.1073/pnas.2009137117

Liu, H., Kiseleva, A. A., & Golemis, E. A. (2018). Ciliary signalling in cancer. *Nature Reviews Cancer*, *18*(8), 511–524. https://doi.org/10.1038/s41568-018-0023-6

Liu, Y., Visetsouk, M., Mynlieff, M., Qin, H., Lechtreck, K. F., & Yang, P. (2017). H+- and Na+- elicited rapid changes of the microtubule cytoskeleton in the biflagellated green alga Chlamydomonas. *ELife*, *6*, e26002. https://doi.org/10.7554/eLife.26002

Lohret, T. A., McNally, F. J., & Quarmby, L. M. (1998). A Role for Katanin-mediated Axonemal Severing during *Chlamydomonas* Deflagellation. *Molecular Biology of the Cell*, *9*(5), 1195–1207. https://doi.org/10.1091/mbc.9.5.1195

Lord, S. J., Velle, K. B., Dyche Mullins, R., & Fritz-Laylin, L. K. (2020). SuperPlots: Communicating reproducibility and variability in cell biology. *Journal of Cell Biology*, *219*(6). https://doi.org/10.1083/JCB.202001064

Ludington, W. B., Wemmer, K. A., Lechtreck, K. F., Witman, G. B., & Marshall, W. F. (2013). Avalanche-like behavior in ciliary import. *Proceedings of the National Academy of Sciences*, *110*(10), 3925–3930. https://doi.org/10.1073/pnas.1217354110

Luo, Q., Song, W., Li, Y., Wang, C., & Hu, Z. (2018). Flagella-Associated WDR-Containing Protein CrFAP89 Regulates Growth and Lipid Accumulation in Chlamydomonas reinhardtii. *Frontiers in Plant Science*, *9*, 691. https://doi.org/10.3389/fpls.2018.00691

Lv, B., Stuck, M. W., Desai, P. B., Cabrera, O. A., & Pazour, G. J. (2021). E3 ubiquitin ligase wwp1 regulates ciliary dynamics of the hedgehog receptor smoothened. *Journal of Cell Biology*, *220*(9). https://doi.org/10.1083/jcb.202010177

Mackinder, L. C. M., Chen, C., Leib, R. D., Patena, W., Blum, S. R., Rodman, M., Ramundo, S., Adams, C. M., & Jonikas, M. C. (2017). A Spatial Interactome Reveals the Protein Organization of the Algal CO2-Concentrating Mechanism. *Cell*, *171*(1), 133-147.e14. https://doi.org/10.1016/j.cell.2017.08.044

Mahjoub, M. R., Montpetit, B., Zhao, L., Finst, R. J., Goh, B., Kim, A. C., & Quarmby, L. M. (2002). The *FA2* gene of *Chlamydomonas* encodes a NIMA family kinase with roles in cell cycle progression and microtubule severing during deflagellation. *Journal of Cell Science*, *115*(8), 1759–1768. https://doi.org/10.1242/jcs.115.8.1759

Mahjoub, M. R., Qasim Rasi, M., & Quarmby, L. M. (2004). A NIMA-related Kinase, Fa2p, Localizes to a Novel Site in the Proximal Cilia of *Chlamydomonas* and Mouse Kidney Cells. *Molecular Biology of the Cell*, *15*(11), 5172–5186. https://doi.org/10.1091/mbc.e04-07-0571

Majumdar, N., Paez, G. L., Inamdar, S. M., D'Rozario, M., & Marenda, D. R. (2010). MAP kinase phosphorylation is dispensable for cell division, but required for cell growth in Drosophila. *Fly*, *4*(3), 204–212. https://doi.org/10.4161/fly.4.3.12001

Manfredi, J. J., Parness, J., & Horwitz, S. B. (n.d.). *Taxoi Binds to Cellular Microtubules*.

Marshall, W. F., Qin, H., Nica, M., Brenni, R., & Rosenbaum, J. L. (2005). Flagellar Length Control System: Testing a Simple Model Based on Intraflagellar Transport and Turnover. *Molecular Biology of the Cell*, *16*, 270–278. https://doi.org/10.1091/mbc.E04

Mebratu, Y., & Tesfaigzi, Y. (2009). How ERK1/2 activation controls cell proliferation and cell death: Is subcellular localization the answer? *Cell Cycle*, *8*(8), 1168–1175. https://doi.org/10.4161/cc.8.8.8147

Merchant, S. S., Prochnik, S. E., Vallon, O., Harris, E. H., Karpowicz, S. J., Witman, G. B., Terry, A., Salamov, A., Fritz-Laylin, L. K., Maréchal-Drouard, L., Marshall, W. F., Qu, L.-H., Nelson, D. R., Sanderfoot, A. A., Spalding, M. H., Kapitonov, V. V., Ren, Q., Ferris, P., Lindquist, E., … Grossman, A. R. (2007). The *Chlamydomonas* Genome Reveals the Evolution of Key Animal and Plant Functions. *Science*, *318*(5848), 245–250. https://doi.org/10.1126/science.1143609

Mirvis, M., Siemers, K. A., Nelson, W. J., & Stearns, T. P. (2019). Primary cilium loss in mammalian cells occurs predominantly by whole-cilium shedding. *PLOS Biology*, *17*(7), e3000381. https://doi.org/10.1371/journal.pbio.3000381

Mirvis, M., Stearns, T., & James Nelson, W. (2018). Cilium structure, assembly, and disassembly regulated by the cytoskeleton. *Biochemical Journal*, *475*(14), 2329–2353. https://doi.org/10.1042/BCJ20170453

Mitchison, H. M., & Valente, E. M. (2017). Motile and non-motile cilia in human pathology: From function to phenotypes: Motile and non-motile ciliopathies. *The Journal of Pathology*, *241*(2), 294–309. https://doi.org/10.1002/path.4843

Mitchison, T., & Kirschner, M. (1984). Dynamic instability of microtubule growth. *Nature*, *312*(5991), 237–242. https://doi.org/10.1038/312237a0

Mittelmeier, T. M., Boyd, J. S., Lamb, M. R., & Dieckmann, C. L. (2011). Asymmetric properties of the Chlamydomonas reinhardtii cytoskeleton direct rhodopsin photoreceptor localization. *Journal of Cell Biology*, *193*(4), 741–753. https://doi.org/10.1083/jcb.201009131

Miyamoto, T., Hosoba, K., Ochiai, H., Royba, E., Izumi, H., Sakuma, T., Yamamoto, T., Dynlacht, B. D., & Matsuura, S. (2015). The Microtubule-Depolymerizing Activity of a Mitotic Kinesin Protein KIF2A Drives Primary Cilia Disassembly Coupled with Cell Proliferation. *Cell Reports*, *10*(5), 664–673. https://doi.org/10.1016/j.celrep.2015.01.003

Miyamoto, T., Porazinski, S., Wang, H., Borovina, A., Ciruna, B., Shimizu, A., Kajii, T., Kikuchi, A., Furutani-Seiki, M., & Matsuura, S. (2011). Insufficiency of BUBR1, a mitotic spindle checkpoint regulator, causes impaired ciliogenesis in vertebrates. *Human Molecular Genetics*, *20*(10), 2058–2070. https://doi.org/10.1093/hmg/ddr090

Miyatake, K., Kusakabe, M., Takahashi, C., & Nishida, E. (2015). ERK7 regulates ciliogenesis by phosphorylating the actin regulator CapZIP in cooperation with Dishevelled. *Nature Communications*, *6*. https://doi.org/10.1038/ncomms7666

Molina, G., Vogt, A., Bakan, A., Dai, W., de Oliveira, P. Q., Znosko, W., Smithgall, T. E., Bahar, I., Lazo, J. S., Day, B. W., & Tsang, M. (2009). Zebrafish chemical screening reveals an inhibitor of Dusp6 that expands cardiac cell lineages. *Nature Chemical Biology*, *5*(9), 680–687. https://doi.org/10.1038/nchembio.190

Nakamura, S., Takino, H., & Kojima, M. K. (1987). Effect of lithium on flagellar length in Chlamydomonas reinhardtii. *Cell Structure and Function*, *12*(4), 369–374. https://doi.org/10.1247/csf.12.369

Nechipurenko, I. V. (2020). The Enigmatic Role of Lipids in Cilia Signaling. *Frontiers in Cell and Developmental Biology*, *8*, 777. https://doi.org/10.3389/fcell.2020.00777

Nikonova, A. S., Gaponova, A. V., Kudinov, A. E., & Golemis, E. A. (2014). CAS proteins in health and disease: An update: CAS Proteins: Recent Developments. *IUBMB Life*, *66*(6), 387–395. https://doi.org/10.1002/iub.1282

O'Hagan, R., Silva, M., Nguyen, K. C. Q., Zhang, W., Bellotti, S., Ramadan, Y. H., Hall, D. H., & Barr, M. M. (2017). Glutamylation Regulates Transport, Specializes Function, and Sculpts the Structure of Cilia. *Current Biology*, *27*(22), 3430-3441.e6. https://doi.org/10.1016/j.cub.2017.09.066

Omori, Y., Chaya, T., Katoh, K., Kajimura, N., Sato, S., Muraoka, K., Ueno, S., Koyasu, T., Kondo, M., & Furukawa, T. (2010). Negative regulation of ciliary length by ciliary male germ cell-associated kinase (Mak) is required for retinal photoreceptor survival. *Proceedings of the National Academy of Sciences*, *107*(52), 22671–22676. https://doi.org/10.1073/pnas.1009437108

O'Toole, E. T., & Dutcher, S. K. (2014). Site-specific basal body duplication in *Chlamydomonas*: *Chlamydomonas* Basal Body Duplication. *Cytoskeleton*, *71*(2), 108–118. https://doi.org/10.1002/cm.21155

O'Toole, E. T., Giddings, T. H., Porter, M. E., & Ostrowski, L. E. (2012). Computer-assisted image analysis of human cilia and Chlamydomonas flagella reveals both similarities and differences in axoneme structure. *Cytoskeleton*, *69*(8), 577–590. https://doi.org/10.1002/cm.21035

Overgaard, C. E., Sanzone, K. M., Spiczka, K. S., Sheff, D. R., Sandra, A., & Yeaman, C. (2009). Deciliation Is Associated with Dramatic Remodeling of Epithelial Cell Junctions and Surface Domains. *Molecular Biology of the Cell*, *20*(1), 102–113. https://doi.org/10.1091/mbc.e08-07-0741

Park, S. M., Jang, H. J., & Lee, J. H. (2019). Roles of Primary Cilia in the Developing Brain. *Frontiers in Cellular Neuroscience*, *13*, 218. https://doi.org/10.3389/fncel.2019.00218

Parker, A. L., Kavallaris, M., & McCarroll, J. A. (2014). Microtubules and Their Role in Cellular Stress in Cancer. *Frontiers in Oncology*, *4*. https://doi.org/10.3389/fonc.2014.00153

Parness, J., & Horwitz, S. (1981). Taxol binds to polymerized tubulin in vitro. *Journal of Cell Biology*, *91*(2), 479–487. https://doi.org/10.1083/jcb.91.2.479

Patel, M. M., & Tsiokas, L. (2021). Insights into the Regulation of Ciliary Disassembly. *Cells*, *10*(11), 2977. https://doi.org/10.3390/cells10112977

Patel-King, R. S., & King, S. M. (2016). A prefoldin-associated WD-repeat protein (WDR92) is required for the correct architectural assembly of motile cilia. *Molecular Biology of the Cell*, *27*(8), 1204–1209. https://doi.org/10.1091/mbc.E16-01-0040

Pazour, G. J., Agrin, N., Leszyk, J., & Witman, G. B. (2005). Proteomic analysis of a eukaryotic cilium. *Journal of Cell Biology*, *170*(1), 103–113. https://doi.org/10.1083/jcb.200504008

Pérez-Pérez, M. E., Mauriès, A., Maes, A., Tourasse, N. J., Hamon, M., Lemaire, S. D., & Marchand, C. H. (2017). The Deep Thioredoxome in Chlamydomonas reinhardtii: New Insights into Redox Regulation. *Molecular Plant*, *10*(8), 1107–1125. https://doi.org/10.1016/j.molp.2017.07.009

Pickart, C. M. (2001). Mechanisms Underlying Ubiquitination. *Annual Review of Biochemistry*, *70*(1), 503–533. https://doi.org/10.1146/annurev.biochem.70.1.503

Plotnikova, O. V., Nikonova, A. S., Loskutov, Y. V., Kozyulina, P. Y., Pugacheva, E. N., & Golemis, E. A. (2012). Calmodulin activation of Aurora-A kinase (AURKA) is required during ciliary disassembly and in mitosis. *Molecular Biology of the Cell*, *23*(14), 2658–2670. https://doi.org/10.1091/mbc.e11-12-1056

Prodromou, N. V., Thompson, C., Osborn, D. P. S., Cogger, K. F., Ashworth, R., Knight, M. M., Beales, P. L., & Chapple, J. P. (2012). Heat shock induces rapid resorption of primary cilia. *Journal of Cell Science*, jcs.100545. https://doi.org/10.1242/jcs.100545

Qin, H., Wang, Z., Diener, D., & Rosenbaum, J. (2007). Intraflagellar Transport Protein 27 Is a Small G Protein Involved in Cell-Cycle Control. *Current Biology*, *17*(3), 193–202. https://doi.org/10.1016/j.cub.2006.12.040

Quarmby, L., & Hartzell, H. (1994). Two distinct, calcium-mediated, signal transduction pathways can trigger deflagellation in Chlamydomonas reinhardtii. *Journal of Cell Biology*, *124*(5), 807–815. https://doi.org/10.1083/jcb.124.5.807

Quarmby, L. M., & Parker, J. D. K. (2005). Cilia and the cell cycle? *Journal of Cell Biology*, *169*(5), 707–710. https://doi.org/10.1083/jcb.200503053

Quarmby, L. M. (1996). Ca2+ influx activated by low pH in Chlamydomonas. *Journal of General Physiology*, *108*(4), 351–361. https://doi.org/10.1085/jgp.108.4.351

Quidwai, T., Wang, J., Hall, E. A., Petriman, N. A., Leng, W., Kiesel, P., Wells, J. N., Murphy, L. C., Keighren, M. A., Marsh, J. A., Lorentzen, E., Pigino, G., & Mill, P. (2021). A WDR35-dependent coat protein complex transports ciliary membrane cargo vesicles to cilia. *ELife*, *10*, e69786. https://doi.org/10.7554/eLife.69786

Ranjan, P., Awasthi, M., & Snell, W. J. (2019). Transient Internalization and Microtubule-Dependent Trafficking of a Ciliary Signaling Receptor from the Plasma Membrane to the Cilium. *Current Biology*, *29*(17), 2942-2947.e2. https://doi.org/10.1016/j.cub.2019.07.022

Rasmussen, C. G., Wright, A. J., & Müller, S. (2013). The role of the cytoskeleton and associated proteins in determination of the plant cell division plane. *The Plant Journal*, *75*(2), 258–269. https://doi.org/10.1111/tpj.12177

Reilly, M. L., & Benmerah, A. (2019). Ciliary kinesins beyond IFT: Cilium length, disassembly, cargo transport and signaling. *Biology of the Cell*, *111*(4), 79–94. https://doi.org/10.1111/boc.201800074

Reiter, J. F., Blacque, O. E., & Leroux, M. R. (2012). The base of the cilium: Roles for transition fibres and the transition zone in ciliary formation, maintenance and compartmentalization. *EMBO Reports*, *13*(7), 608–618. https://doi.org/10.1038/embor.2012.73

Reiter, J. F., & Leroux, M. R. (2017). Genes and molecular pathways underpinning ciliopathies. *Nature Reviews Molecular Cell Biology*, *18*(9), 533–547. https://doi.org/10.1038/nrm.2017.60

Reszka, A. A., Seger, R., Diltz, C. D., Krebs, E. G., & Fischer, E. H. (1995). Association of mitogen-activated protein kinase with the microtubule cytoskeleton. *Proceedings of the National Academy of Sciences*, *92*(19), 8881–8885. https://doi.org/10.1073/pnas.92.19.8881

Robertson, S. E., Setty, S. R. G., Sitaram, A., Marks, M. S., Lewis, R. E., & Chou, M. M. (2006). Extracellular Signal-regulated Kinase Regulates Clathrin- independent Endosomal Trafficking□D. *Molecular Biology of the Cell*, *17*.

Rosenbaum, J. L., & Carlson, K. (1969). Cilia regeneration in Tetrahymena and its inhibition by colchicine. *The Journal of Cell Biology*, *40*(2), 415–425. https://doi.org/10.1083/jcb.40.2.415

Rosenbaum, J. L., Moulder, J. E., & Ringo, D. L. (1969). Flagellar elongation and shortening in Chlamydomonas: The Use of Cycloheximide and Colchicine to Study the Synthesis and Assembly of Flagellar Proteins. *Journal of Cell Biology*, *41*(2), 600–619. https://doi.org/10.1083/jcb.41.2.600

Rosenbaum, J. L., & Witman, G. B. (2002). Intraflagellar transport. *Nature Reviews Molecular Cell Biology*, *3*(11), 813–825. https://doi.org/10.1038/nrm952

Sasso, S., Stibor, H., Mittag, M., & Grossman, A. R. (2018). From molecular manipulation of domesticated Chlamydomonas reinhardtii to survival in nature. *ELife*, *7*, e39233. https://doi.org/10.7554/eLife.39233

Schneider, L., Clement, C. A., Teilmann, S. C., Pazour, G. J., Hoffmann, E. K., Satir, P., & Christensen, S. T. (2005). PDGFRαα Signaling Is Regulated through the Primary Cilium in Fibroblasts. *Current Biology*, *15*(20), 1861–1866. https://doi.org/10.1016/j.cub.2005.09.012

Senatore, E., Iannucci, R., Chiuso, F., Delle Donne, R., Rinaldi, L., & Feliciello, A. (2022). Pathophysiology of Primary Cilia: Signaling and Proteostasis Regulation. *Frontiers in Cell and Developmental Biology*, *10*, 833086. https://doi.org/10.3389/fcell.2022.833086

Shah, A. S., Ben-Shahar, Y., Moninger, T. O., Kline, J. N., & Welsh, M. J. (2009). Motile Cilia of Human Airway Epithelia Are Chemosensory. *Science*, *325*(5944), 1131–1134. https://doi.org/10.1126/science.1173869

Sharma, N., Kosan, Z. A., Stallworth, J. E., Berbari, N. F., & Yoder, B. K. (2011). Soluble levels of cytosolic tubulin regulate ciliary length control. *Molecular Biology of the Cell*, *22*(6), 806–816. https://doi.org/10.1091/mbc.e10-03-0269

Sharp, P. M., & Li, W.-H. (1987). Ubiquitin genes as a paradigm of concerted evolution of tandem repeats. *Journal of Molecular Evolution*, *25*(1), 58–64. https://doi.org/10.1007/BF02100041

Shaul, Y. D., & Seger, R. (2007). The MEK/ERK cascade: From signaling specificity to diverse functions. *Biochimica et Biophysica Acta (BBA) - Molecular Cell Research*, *1773*(8), 1213–1226. https://doi.org/10.1016/j.bbamcr.2006.10.005

Shen, X.-L., Yuan, J.-F., Qin, X.-H., Song, G.-P., Hu, H.-B., Tu, H.-Q., Song, Z.-Q., Li, P.-Y., Xu, Y.-L., Li, S., Jian, X.-X., Li, J.-N., He, C.-Y., Yu, X.-P., Liang, L.-Y., Wu, M., Han, Q.-Y., Wang, K., Li, A.-L., … Li, H.-Y. (2022). LUBAC regulates ciliogenesis by promoting CP110 removal from the mother centriole. *Journal of Cell Biology*, *221*(1), e202105092. https://doi.org/10.1083/jcb.202105092

Shin, J., Kwon, S., Bak, Y., Lee, S., & Yoon, D. (2018). BCI induces apoptosis via generation of reactive oxygen species and activation of intrinsic mitochondrial pathway in H1299 lung cancer cells. *Science China Life Sciences*, *61*(10), 1243–1253.

Shin, L.-J., Lo, J.-C., & Yeh, K.-C. (2012). Copper Chaperone Antioxidant Protein1 Is Essential for Copper Homeostasis. *Plant Physiology*, *159*(3), 1099–1110. https://doi.org/10.1104/pp.112.195974

Shinde, S. R., Nager, A. R., & Nachury, M. V. (2020). Ubiquitin chains earmark GPCRs for BBSome-mediated removal from cilia. *Journal of Cell Biology*, *219*(12), e202003020. https://doi.org/10.1083/jcb.202003020

Shojaee, S., Caeser, R., Buchner, M., Park, E., Swaminathan, S., Hurtz, C., Geng, H., Chan, L. N., Klemm, L., Hofmann, W.-K., Qiu, Y. H., Zhang, N., Coombes, K. R., Paietta, E., Molkentin, J., Koeffler, H. P., Willman, C. L., Hunger, S. P., Melnick, A., … Müschen, M. (2015). Erk Negative Feedback Control Enables Pre-B Cell Transformation

and Represents a Therapeutic Target in Acute Lymphoblastic Leukemia. *Cancer Cell*, *28*(1), 114–128. https://doi.org/10.1016/j.ccell.2015.05.008

Solc, P., Baran, V., Mayer, A., Bohmova, T., Panenkova-Havlova, G., Saskova, A., Schultz, R. M., & Motlik, J. (2012). Aurora Kinase A Drives MTOC Biogenesis but Does Not Trigger Resumption of Meiosis in Mouse Oocytes Matured In Vivo1. *Biology of Reproduction*, *87*(4). https://doi.org/10.1095/biolreprod.112.101014

Solter, K. M. S., & Gibor, A. (1978). The relationship between tonicity and flagellar length. *Nature*, *275*(5681), 652–654. https://doi.org/10.1038/275652a0

Song, Y., Bi, Z., Liu, Y., Qin, F., Wei, Y., & Wei, X. (2023). Targeting RAS–RAF–MEK–ERK signaling pathway in human cancer: Current status in clinical trials. *Genes & Diseases*, *10*(1), 76–88. https://doi.org/10.1016/j.gendis.2022.05.006

Stargell, L. A., Heruth, D. P., Gaertig, J., & Gorovsky, M. A. (1992). Drugs affecting microtubule dynamics increase alpha-tubulin mRNA accumulation via transcription in Tetrahymena thermophila. *Molecular and Cellular Biology*, *12*(4), 1443–1450. https://doi.org/10.1128/mcb.12.4.1443-1450.1992

Stubblefield, E., & Brinkley, B. R. (1966). CILIA FORMATION IN CHINESE HAMSTER FIBROBLASTS IN VITRO AS A RESPONSE TO COLCEMID TREATMENT. *Journal of Cell Biology*, *30*(3), 645–652. https://doi.org/10.1083/jcb.30.3.645

Tereshko, L., Gao, Y., Cary, B. A., Turrigiano, G. G., & Sengupta, P. (2021). Ciliary neuropeptidergic signaling dynamically regulates excitatory synapses in postnatal neocortical pyramidal neurons. *ELife*, *10*, e65427. https://doi.org/10.7554/eLife.65427

Tisdale, E. J., Azizi, F., & Artalejo, C. R. (2009). Rab2 Utilizes Glyceraldehyde-3-phosphate Dehydrogenase and Protein Kinase Cι to Associate with Microtubules and to Recruit Dynein. *Journal of Biological Chemistry*, *284*(9), 5876–5884. https://doi.org/10.1074/jbc.M807756200

Tripathi, P., Zhu, Z., Qin, H., Elsherbini, A., Crivelli, S. M., Roush, E., Wang, G., Spassieva, S. D., & Bieberich, E. (2021). Palmitoylation of acetylated tubulin and

association with ceramide-rich platforms is critical for ciliogenesis. *Journal of Lipid Research*, *62*, 100021. https://doi.org/10.1194/jlr.RA120001190

Tucker, R. W., Pardee, A. B., & Fujiwara, K. (1979). Centriole ciliation is related to quiescence and DNA synthesis in 3T3 cells. *Cell*, *17*(3), 527–535. https://doi.org/10.1016/0092-8674(79)90261-7

Tucker, R. W., Scher, C. D., & Stiles, C. D. (1979). Centriole deciliation associated with the early response of 3T3 cells to growth factors but not to SV40. *Cell*, *18*(4), 1065–1072. https://doi.org/10.1016/0092-8674(79)90219-8

Tulin, F. (2019). Mating and Tetrad Dissection in Chlamydomonas. *BIO-PROTOCOL*, *9*(7). https://doi.org/10.21769/BioProtoc.3207

Van Den Hoek, H., Klena, N., Jordan, M. A., Alvarez Viar, G., Righetto, R. D., Schaffer, M., Erdmann, P. S., Wan, W., Geimer, S., Plitzko, J. M., Baumeister, W., Pigino, G., Hamel, V., Guichard, P., & Engel, B. D. (2022). In situ architecture of the ciliary base reveals the stepwise assembly of intraflagellar transport trains. *Science*, *377*(6605), 543–548. https://doi.org/10.1126/science.abm6704

van der Vaart, A., Rademakers, S., & Jansen, G. (2015). DLK-1/p38 MAP Kinase Signaling Controls Cilium Length by Regulating RAB-5 Mediated Endocytosis in Caenorhabditis elegans. *PLOS Genetics*, *11*(12), e1005733–e1005733. https://doi.org/10.1371/journal.pgen.1005733

Veland, I. R., Lindbæk, L., & Christensen, S. T. (2014). Linking the Primary Cilium to Cell Migration in Tissue Repair and Brain Development. *BioScience*, *64*(12), 1115–1125. https://doi.org/10.1093/biosci/biu179

Viswanadha, R., Hunter, E. L., Yamamoto, R., Wirschell, M., Alford, L. M., Dutcher, S. K., & Sale, W. S. (2014). The ciliary inner dynein arm, I1 dynein, is assembled in the cytoplasm and transported by IFT before axonemal docking: Assembly of Ciliary Inner Dynein Arms. *Cytoskeleton*, *71*(10), 573–586. https://doi.org/10.1002/cm.21192

Vladar, E. K., Stratton, M. B., Saal, M. L., Salazar-De Simone, G., Wang, X., Wolgemuth, D., Stearns, T., & Axelrod, J. D. (2018). Cyclin-dependent kinase control of motile ciliogenesis. *ELife*, *7*, e36375. https://doi.org/10.7554/eLife.36375

Wang, G., Hu, H.-B., Chang, Y., Huang, Y., Song, Z.-Q., Zhou, S.-B., Chen, L., Zhang, Y.-C., Wu, M., Tu, H.-Q., Yuan, J.-F., Wang, N., Pan, X., Li, A.-L., Zhou, T., Zhang, X.-M., He, K., & Li, H.-Y. (2019). Rab7 regulates primary cilia disassembly through cilia excision. *Journal of Cell Biology*, *218*(12), 4030–4041. https://doi.org/10.1083/jcb.201811136

Wang, L., & Dynlacht, B. D. (2018). The regulation of cilium assembly and disassembly in development and disease. *Development (Cambridge)*, *145*(18). https://doi.org/10.1242/dev.151407

Wang, L., Piao, T., Cao, M., Qin, T., Huang, L., Deng, H., Mao, T., & Pan, J. (2013). Flagellar regeneration requires cytoplasmic microtubule depolymerization and kinesin-13. *Journal of Cell Science*, *126*(6), 1531–1540. https://doi.org/10.1242/jcs.124255

Wang, L., Wen, X., Wang, Z., Lin, Z., Li, C., Zhou, H., Yu, H., Li, Y., Cheng, Y., Chen, Y., Lou, G., Pan, J., & Cao, M. (2022). Ciliary transition zone proteins coordinate ciliary protein composition and ectosome shedding. *Nature Communications*, *13*(1), 3997. https://doi.org/10.1038/s41467-022-31751-0

Wang, L., Yang, L., Wen, X., Chen, Z., Liang, Q., Li, J., & Wang, W. (2019). Rapid and high efficiency transformation of Chlamydomonas reinhardtii by square-wave electroporation. *Bioscience Reports*, *39*(1), 1–8. https://doi.org/10.1042/BSR20181210

Wang, Q., Peng, Z., Long, H., Deng, X., & Huang, K. (2019). Polyubiquitylation of α-tubulin at K304 is required for flagellar disassembly in Chlamydomonas. *Journal of Cell Science*, *132*(6). https://doi.org/10.1242/jcs.229047

Wang, S., Wei, Q., Dong, G., & Dong, Z. (2013). ERK-mediated suppression of cilia in cisplatin-induced tubular cell apoptosis and acute kidney injury. *Biochimica et Biophysica Acta (BBA) - Molecular Basis of Disease*, *1832*(10), 1582–1590. https://doi.org/10.1016/j.bbadis.2013.05.023

Wang, W., Wu, T., & Kirschner, M. W. (2014). The master cell cycle regulator APC-Cdc20 regulates ciliary length and disassembly of the primary cilium. *ELife*, *3*, e03083. https://doi.org/10.7554/eLife.03083

Wang, Y., Zhou, Z., Walsh, C. T., & McMahon, A. P. (2009). Selective translocation of intracellular Smoothened to the primary cilium in response to Hedgehog pathway modulation. *Proceedings of the National Academy of Sciences*, *106*(8), 2623–2628. https://doi.org/10.1073/pnas.0812110106

Wang, Z., Fan, Z.-C., Williamson, S. M., & Qin, H. (2009). Intraflagellar Transport (IFT) Protein IFT25 Is a Phosphoprotein Component of IFT Complex B and Physically Interacts with IFT27 in Chlamydomonas. *PLoS ONE*, *4*(5), e5384. https://doi.org/10.1371/journal.pone.0005384

Wax, M. B., Saito, I., Tenkova, T., Krupin, T., Becker, B., Nelson, N., Brown, D., & Gluck, S. L. (1997). Vacuolar H^+-ATPase in ocular ciliary epithelium. *Proceedings of the National Academy of Sciences*, *94*(13), 6752–6757. https://doi.org/10.1073/pnas.94.13.6752

Wheeler, G. L., Joint, I., & Brownlee, C. (2007). Rapid spatiotemporal patterning of cytosolic Ca2+ underlies flagellar excision in Chlamydomonas reinhardtii: Calcium signalling in Chlamydomonas. *The Plant Journal*, *53*(3), 401–413. https://doi.org/10.1111/j.1365-313X.2007.03349.x

Wheway, G., Nazlamova, L., & Hancock, J. T. (2018). Signaling through the Primary Cilium. *Frontiers in Cell and Developmental Biology*, *6*, 8. https://doi.org/10.3389/fcell.2018.00008

White, M. C., & Quarmby, L. M. (2008). The NIMA-family kinase, Nek1 affects the stability of centrosomes and ciliogenesis. *BMC Cell Biology*, *9*(1), 29. https://doi.org/10.1186/1471-2121-9-29

Wingfield, J. L., Mekonnen, B., Mengoni, I., Liu, P., Jordan, M., Diener, D., Pigino, G., & Lechtreck, K. (2021). *In vivo* imaging shows continued association of several IFT-A,

IFT-B and dynein complexes while IFT trains U-turn at the tip. *Journal of Cell Science*, *134*(18), jcs259010. https://doi.org/10.1242/jcs.259010

Witman, G. B., Carlson, K., Berliner, J., & Rosenbaum, L. (1972). I. Isolation and Electrophoretic Analysis of Microtubules, Matrix, Membranes, and Mastigonemes. *The Journal of Cell Biology*, *54*, 507–539. https://doi.org/10.1083/jcb.54.3.507

Witman, G. B., Plummer, J., & Sander, G. (1978). Chlamydomonas flagellar mutants lacking radial spokes and central tubules. Structure, composition, and function of specific axonemal components. *Journal of Cell Biology*, *76*(3), 729–747. https://doi.org/10.1083/jcb.76.3.729

Wortzel, I., & Seger, R. (2011). The ERK Cascade: Distinct Functions within Various Subcellular Organelles. *Genes & Cancer*, *2*(3), 195–209. https://doi.org/10.1177/1947601911407328

Yeh, C., Li, A., Chuang, J.-Z., Saito, M., Cáceres, A., & Sung, C.-H. (2013). IGF-1 Activates a Cilium-Localized Noncanonical Gβγ Signaling Pathway that Regulates Cell-Cycle Progression. *Developmental Cell*, *26*(4), 358–368. https://doi.org/10.1016/j.devcel.2013.07.014

Yoder, B. K. (2007). Role of Primary Cilia in the Pathogenesis of Polycystic Kidney Disease. *Journal of the American Society of Nephrology*, *18*(5), 1381–1388. https://doi.org/10.1681/ASN.2006111215

Yuan, S., Wang, Z., Peng, H., Ward, S. M., Hennig, G. W., Zheng, H., & Yan, W. (2021). Oviductal motile cilia are essential for oocyte pickup but dispensable for sperm and embryo transport. *Proceedings of the National Academy of Sciences*, *118*(22), e2102940118. https://doi.org/10.1073/pnas.2102940118

Zalli, D., Bayliss, R., & Fry, A. M. (2012). The Nek8 protein kinase, mutated in the human cystic kidney disease nephronophthisis, is both activated and degraded during ciliogenesis. *Human Molecular Genetics*, *21*(5), 1155–1171. https://doi.org/10.1093/hmg/ddr544

Zhang, R., Tang, J., Li, T., Zhou, J., & Pan, W. (2022). INPP5E and Coordination of Signaling Networks in Cilia. *Frontiers in Molecular Biosciences*, *9*, 885592. https://doi.org/10.3389/fmolb.2022.885592

Zhang, W., & Liu, H. T. (2002). MAPK signal pathways in the regulation of cell proliferation in mammalian cells. *Cell Research*, *12*(1), 9–18. https://doi.org/10.1038/sj.cr.7290105

Zhang, X. M., Ramalho-Santos, M., & McMahon, A. P. (2001). Smoothened Mutants Reveal Redundant Roles for Shh and Ihh Signaling Including Regulation of L/R Asymmetry by the Mouse Node. *Cell*, *105*(6), 781–792. https://doi.org/10.1016/S0092-8674(01)00385-3

Zhu, Iwano, & Takeda. (2019). Estrogen and EGFR Pathways Regulate Notch Signaling in Opposing Directions for Multi-Ciliogenesis in the Fallopian Tube. *Cells*, *8*(8), 933. https://doi.org/10.3390/cells8080933